

**Molecular Modelling and Experimental  
Studies of the Interactions between  
Biomolecules and Nanostructured  
Inorganic Materials**

Inaugural Dissertation

zur Erlangung des Grades eines  
Doktors der Naturwissenschaften  
des Fachbereichs Chemie  
der Universität Duisburg-Essen

von

**Maria Tsoli**

aus Serres, Griechenland

Essen 2004

Die vorliegende Arbeit wurde am Institut für Anorganische Chemie des Fachbereichs Chemie der Universität Duisburg-Essen unter der Leitung von Prof. Dr. G. Schmid angefertigt.

Tag der mündlichen Prüfung: 28.04.2004

Gutachter: Prof. Dr. G. Schmid  
Prof. Dr. H. Esche

Prüfungsvorsitzender:

I would like to sincerely thank my Doctorate Father, Prof. Dr. G. Schmid for agreeing to supervise this project and for the freedom granted in the course of the research. I would like to deeply thank Prof. Dr. H. Esche for his very useful comments and for allowing me to work at his laboratory.

I would like to thank 'Dr.' H. Kuhn not only for teaching me molecular modelling but also for taking care of me during my doctorate study. Your help is deeply appreciated.

My sincerest thanks goes to Prof. Dr. B. Brandau and Prof Dr. G. Iliakis for their advices during this study.

I am very grateful to my colleagues from the Departments of Molecular Biology, Physical Chemistry and Inorganic Chemistry. I would also like to thank Olivia Vidoni, Birgit Wöstefeld and the students of the Graduate School.

My very good friends Anke Besselin, Uli Weber, Beate Kirstein, Ulf and Verena Frieske thank you very much for the funny and relaxing moments in Germany. Please make me a Godmother soon.

My sincerest thanks and love goes to my adopted Greek-Polish family: Maria Chatzinikolaidou, Anastasia Karakesisoglou and Anna Runiewicz. You are simply the best. Thank you for taking care of me.

I would also like to thank an old simple man that during his visit at the ACHEMA exhibition brought me back to the cruel reality of cancer treatment and reminded me that science is something more than simply fighting for another publication or a patent.

Dad, Mum and Kiki, you have been hearing about my doctorate study every Sunday for the last three years. Thank you for your support and encouragement. Thank you for listening about every single experiment I have done. Thank you for being a shoulder to cry when I couldn't see the light at the end of the tunnel. Thank you for sharing my enthusiasm after each conference. Thank you for believing in me and for bringing me up in such a way that no matter what I decently do in life to put my whole soul into it.

*Στον Λαμπρουκο*

*Στην Εφη*

*Στην Κικιτσα*

*'Give me any word and I will prove to you that the root of this word is Greek'*

*Mr Portokalos (My Big Fat Greek Wedding)*

# Contents

<i>Abbreviations and units</i>	IV
<i>List of Figures</i>	VI
<i>List of Tables</i>	VIII
<b>1 Introduction</b>	<b>1</b>
1.1 Applications in nanotechnology	1
1.2 Applications in medicine	5
1.3 Applications in biotechnology	9
1.4 Aims of this study	10
<i>1.4.1 Aims with applications in nanotechnology</i>	10
<i>1.4.2 Aims with applications in medicine</i>	12
<i>1.4.3 Aims with applications in biotechnology</i>	12
<b>2 Theory</b>	<b>13</b>
2.1 What is molecular modelling	13
2.2 Useful concepts in molecular modelling	13
2.3 Some general features of a molecular mechanics forcefield	14
2.3.1 <i>Bond stretching: <math>E_{str}</math></i>	16
2.3.2 <i>Angle bending: <math>E_{bend}</math></i>	18
2.3.3 <i>Torsion angle: <math>E_{tors}</math></i>	18
2.3.4 <i>Cross terms: <math>E_{cross}</math></i>	18
2.3.5 <i>van der Waals interactions: <math>E_{vdw}</math></i>	19
2.3.6 <i>Electrostatic interactions: <math>E_{el}</math></i>	20
2.3.7 <i>Hydrogen bonding interactions: <math>E_{hb}</math></i>	21
2.4 Molecular mechanics simulations-Energy minimisations	21
2.4.1 <i>The gradient methods</i>	22
2.4.2 <i>The second derivative method</i>	23
2.4.3 <i>Choice of the method</i>	24
2.4.4 <i>The problem of local minima</i>	25
2.5 Molecular dynamics simulations	25
2.5.1 <i>Periodic boundary conditions</i>	29

2.5.2	<i>The cut-offs of non-bonded energy terms</i>	30
<b>3</b>	<b>Materials</b>	<b>32</b>
3.1	Chemicals	32
3.2	Proteins, enzymes and plasmids	32
3.3	Cell culture media, sera and culture plates	33
3.4	Molecular weight standard	33
3.5	Kits	33
3.6	Laboratory instruments	33
3.7	Buffers and solutions	34
3.8	Cell lines	35
<b>4</b>	<b>Methods</b>	<b>36</b>
4.1	Computational methods	36
4.1.1	<i>Molecular structures</i>	36
4.1.2	<i>Molecular mechanics simulations</i>	37
4.1.3	<i>Molecular dynamics simulation of Au<sub>13</sub> clusters with A-DNA molecules</i>	39
4.1.4	<i>Molecular dynamics simulations of zeolite beta with various amino acids</i>	39
4.1.5	<i>Molecular docking simulations</i>	41
4.1.6	<i>Molecular modelling flowchart</i>	44
4.2	Experimental methods	45
4.2.1	<i>Synthesis of Au<sub>55</sub> cluster</i>	45
4.2.2	<i>Cell culturing and maintenance</i>	45
4.2.3	<i>In vitro cytotoxicity assays MTT</i>	46
4.2.4	<i>Apoptosis/necrosis assays</i>	47
4.2.5	<i>Interaction of Au<sub>55</sub> with plasmid DNA analysed by agarose gel electrophoresis</i>	47
4.2.6	<i>Cellular fractionation</i>	47
<b>5.</b>	<b>Results</b>	<b>49</b>
5.1	Interactions between Au clusters and DNAs: formation of nanowires	49
5.1.1	<i>Characterisation of naked A- and B-DNA after minimisation</i>	49
5.1.2	<i>Characterisation of A- and B-DNA with gold clusters</i>	50
5.1.3	<i>Formation of Au<sub>13</sub> nanowires</i>	52

5.2	Anticancer properties of gold cluster Au <sub>55</sub>	54
5.2.1	<i>In vitro cytotoxicity assays</i>	54
5.2.2	<i>Apoptosis/ Necrosis assays</i>	57
5.2.3	<i>Interaction of Au<sub>55</sub> with plasmid DNA analysed by agarose gel electrophoresis</i>	59
5.2.4	<i>Cellular fractionation</i>	61
5.2.5	<i>Molecular docking simulations of the interactions between different DNA structures and Au<sub>55</sub></i>	63
5.2.6	<i>Interactions between albumin and Au<sub>55</sub></i>	66
5.3	Interactions between amino acids and zeolite beta	69
<b>6.</b>	<b>Discussion</b>	<b>80</b>
6.1	Interactions between Au clusters and DNAs: formation of nanowires	80
6.2	Anticancer properties of gold cluster Au <sub>55</sub>	82
6.3	Interactions between amino acids and zeolite beta	90
<b>7.</b>	<b>Summary</b>	<b>93</b>
<b>8.</b>	<b>Outlook</b>	<b>95</b>
<b>9.</b>	<b>References</b>	<b>99</b>
<b>10.</b>	<b>Appendix</b>	<b>109</b>
10.1	Additional <i>in vitro</i> cytotoxicity assays	109
10.2	Additional caspase 3/7 assays	119
10.3	Additional results obtained from cellular fractionation experiments	120
10.4	Additional molecular modelling structures	122
<b>11.</b>	<b>Curriculum Vitae</b>	<b>123</b>

## ***Abbreviations and units***

A	Adenine (purine nitrogenous base)
A-DNA	A-form of DNA (dehydrated form)
ATP	Adenosine 5'-triphosphate
ATPase	ATP synthase
Au <sub>13</sub>	Cluster made of 13 gold atoms
Au <sub>55</sub>	Cluster made of 55 gold atoms
B-DNA	B-form of DNA (hydrated form found in living organisms)
BEA	Zeolite beta
bp	Base pair
C	Cytosine (pyrimidine nitrogenous base)
°C	Degrees of Celsius
caspases	Cysteine aspartate-specific proteases
CG	Conjugate gradient (minimisation algorithm)
cisplatin	cis-Diamminedichloroplatinum (II)
DNA	Deoxyribonucleic acid
DMEM	Dulbecco's modification of Eagle's medium
FCS	Fetal calf serum
FFT	Fourier transform algorithm
g	Gram
G	Guanine (purine nitrogenous base)
h	Hour
°K	Degrees of Kelvin
l	Liter
l	linear form of plasmid
M	Molarity (mol/l)
min	Minutes
MC	Monte Carlo
MD	Molecular Dynamics
MEM	Modified Eagle's medium
mRNA	Messenger RNA
MTT	<i>In vitro</i> cytotoxicity assay

NAD <sup>+</sup>	Nicotine adenine dinucleotide
NPT	Constant number of particles, constant pressure and constant temperature
NVE	Constant number of particles, constant volume and constant energy.
NVT	Constant number of particles, constant volume and constant temperature
oc	Open circular form of plasmid DNA which is nicked at one strand
PARP	poly (ADP-ribose) polymerase
PBS	Phosphate buffered saline
PDB	Protein data bank ( <a href="http://www.rcsb.org/pdb">www.rcsb.org/pdb</a> )
pI	Isoelectric point of proteins
PNA	Peptide nucleic acid
PME	Particle-mesh Ewald
RMS	Root mean square
RNA	Ribonucleic acid
SAMs	Self-assembled monolayers
s	Seconds
s	Supercoiled form of plasmid DNA
SD	Steepest descent (minimisation algorithm)
Si/Al	Silicon to aluminium ratio
T	Thymine (pyrimidine nitrogenous base)
TEM	Transmission electron microscopy
UV	Ultra-violet light

#### Prefixes that describe sizes of things

Prefix	Symbol	Power
Unity		10 <sup>0</sup>
Centi	c	10 <sup>-2</sup>
Milli	m	10 <sup>-3</sup>
Micro	μ	10 <sup>-6</sup>
Nano	n	10 <sup>-9</sup>
Pico	p	10 <sup>-12</sup>
Femto	f	10 <sup>-15</sup>
Atto	a	10 <sup>-18</sup>



## *List of Figures*

<b>Figure 1.1</b>	Overview of the mechanisms of action of chemotherapeutic agents used in cancer treatment.	6
<b>Figure 1.2</b>	Transmission electron micrographs of B-DNA with gold cluster Au <sub>55</sub> .	11
<b>Figure 2.1</b>	The molecular mechanics method.	15
<b>Figure 2.2</b>	Hooke's law describing a simple harmonic potential.	16
<b>Figure 2.3</b>	Comparison of the Morse and Taylor potential curves.	17
<b>Figure 2.4</b>	Various cross terms present in some force fields.	19
<b>Figure 2.5</b>	A contour plot of the energy E in the (x,y) plane.	22
<b>Figure 2.6</b>	Steepest descent minimisation.	23
<b>Figure 2.7</b>	The Newton –Raphson method.	24
<b>Figure 2.8</b>	One dimensional function with multiple minima.	25
<b>Figure 2.9</b>	Periodic boundary conditions.	29
<b>Figure 2.10</b>	Separation of an amino acid residue of a protein into charge groups.	30
<b>Figure 4.1</b>	Molecular models of the amino acids glutamic acid, lysine and phenylalanine.	39
<b>Figure 4.2</b>	Construction of a plane on the zeolite surface.	40
<b>Figure 4.3</b>	Schematic representation at one dimension of the different positions of an amino acid being placed around the zeolite structure.	40
<b>Figure 4.4</b>	Representation of the docking procedure in the form of a flowchart.	42
<b>Figure 4.5</b>	Schematic representation of gold cluster Au <sub>55</sub> .	45
<b>Figure 5.1</b>	Model structures of energy-minimised A-, and B-DNA molecules.	50
<b>Figure 5.2</b>	Energy minimised structure of A-DNA with Au <sub>13</sub> clusters located along the phosphate backbone of the DNA major grooves.	52
<b>Figure 5.3</b>	Different orientations of A-DNA structures decorated each with Au <sub>13</sub> clusters generated by the molecular dynamics simulation.	53
<b>Figure 5.4</b>	<i>In vitro</i> cytotoxicity assay of metastatic melanoma cells BLM, exposed to Au <sub>55</sub> or cisplatin for various periods of time.	55
<b>Figure 5.5</b>	<i>In vitro</i> cytotoxicity assay of metastatic melanoma cells BLM, exposed for 24 hours with various concentrations of the	

	triphenylphosphane ligand	57
<b>Figure 5.6</b>	Apoptosis assay performed for the osteosarcoma cell line U-2OS in the presence of cluster Au <sub>55</sub> and cisplatin.	58
<b>Figure 5.7</b>	Apoptosis assay performed for the melanoma cell line BLM in the presence of cluster Au <sub>55</sub> and cisplatin.	59
<b>Figure 5.8</b>	Agarose gel electrophoresis of DNA plasmid with increasing concentrations of Au <sub>55</sub> .	60
<b>Figure 5.9</b>	Cellular fractionation of BLM cells being exposed to various concentrations of radioactive <sup>198</sup> Au <sub>55</sub> for different periods of time	62
<b>Figure 5.10</b>	Different structures obtained by the docking of 1BNA molecule with Au <sub>55</sub> and their respective intermolecular interactions.	64
<b>Figure 5.11</b>	Conolly surface representations of the docked structures of 1BNA molecule with their respective intermolecular interactions.	65
<b>Figure 5.12</b>	Drug sensitivity profile of BLM towards various concentrations of Au <sub>55</sub> in the presence of additional FCS and albumin protein.	66
<b>Figure 5.13</b>	Structures obtained from the docking simulations of albumin and Au <sub>55</sub> with respective intermolecular interactions given in Kcal/mol Å.	68
<b>Figure 5.14</b>	Enlarged images of the binding sites of Au <sub>55</sub> in docked structures visualised as CPK models.	69
<b>Figure 5.15</b>	MD simulation of glutamic acid with zeolite beta.	72
<b>Figure 5.16</b>	Distances between the centre of the mass of the glutamic acid and the surface of the zeolite.	73
<b>Figure 5.17</b>	Distances between the amino group of the glutamic acid and the surface of the zeolite.	74
<b>Figure 5.18</b>	Distances between the carboxyl group of the glutamic acid and the surface of the zeolite.	74
<b>Figure 5.19</b>	MD simulation of lysine with zeolite beta.	75
<b>Figure 5.20</b>	Distances between the centre of the mass of the lysine and the surface of the zeolite beta.	76
<b>Figure 5.21</b>	Distances between the amino group of the lysine and the surface of the zeolite.	76
<b>Figure 5.22</b>	Distances between the carboxyl group of the lysine and the surface of the zeolite.	77
<b>Figure 5.23</b>	MD simulation of phenylalanine with zeolite beta.	78

<b>Figure 5.24</b>	Distances between the centre of the mass of phenylalanine and the surface of the zeolite beta.	79
<b>Figure 5.25</b>	Distances between the amino group of the phenylalanine and the surface of the zeolite.	79
<b>Figure 5.26</b>	Distances between the carboxyl group of the phenylalanine and the surface of the zeolite.	79
<b>Figure 8.1</b>	Schematic representation of a mammalian cell.	97

### *List of Tables*

<b>Table 5.1</b>	Stabilisation energies calculated by energy-minimisation of the two forms of DNA with and without the gold clusters.	51
<b>Table 5.2</b>	Inhibitory concentrations (IC <sub>50</sub> ) of cisplatin and Au <sub>55</sub> incubated with various human cancer and healthy cell lines for 72 and 24 hours respectively.	56
<b>Table 5.3</b>	Summary of the molecular docking simulations.	66
<b>Table 5.4</b>	Average Total Energies (TotE) in kcal of the structures obtained from the MD simulations.	70

# 1. Introduction

---

Interactions between metals and biomacromolecules including proteins, polysaccharides, and nucleic acids are important and in many cases essential for a number of natural and technical phenomena. These range from interactions of highly specific metal cofactors with particular proteins (1) biosorption of heavy metals by polysaccharide hydrogels (101) and adsorption of amino acids in aluminosilicate surfaces (83). Nucleic acids have many advantages over other classes of biomolecules for many applications, since it is possible to tailor specific lengths, sequences and conformations. These unique features of DNA have been exploited in the development of novel materials, especially in the areas of medicine and nanotechnology. Classical research concerning antitumour drugs has focussed on the interactions of platinum-, ruthenium-, or gold-containing compounds with the major or minor grooves of polynucleotides (51, 56, 89, 123). There is a tremendous interest in the use of DNA in nanotechnology as a positioning template or “scaffold” for the immobilisation of metal nanoclusters (platinum, silver or gold) with a view towards future applications in the construction of nanoelectronic devices (3, 47). In the following sections will be reviewed the interactions of biomolecules with inorganic nanostructured materials which have main applications in the fields of nanotechnology, medicine and biotechnology.

## 1.1 Applications in nanotechnology

Nanotechnology is a very important scientific advance which is involved in the manufacturing of structured matter by working with atoms. Such a technology has the advantage of being easily controlled without causing environmental problems since it does not involve the breaking of natural material but leads to the building of structures and therefore to the production of nanodevices or nanomachines by specifically manoeuvring atoms (120). Since we know its structure, a nanoscale object can be disabled or disconnected.

Nanotechnology can be used in nanoelectronics and medicine nevertheless, nanomaterials have been found to have applications as insulators, batteries as well as magnets(120). The input from physicists, chemists and biologists is highly required for the generation of

molecular switches, or nanoassemblies for nanomachines or nanorobots. A great amount of knowledge and some degree of imagination is demanded for the chemical synthesis, visualisation, manipulation and assembling of building blocks into a nanostructure. Regarding imagination, one needs to admit that nature can provide millions of examples that can be mimicked and used in nanotechnology. Every component of life is built upon nanomachines which in reality are much more sophisticated than the human nanomachines made so far, since, they are capable of self maintenance. The basic structural units found in biology such as lipids, proteins and DNA can be used in nanotechnology since they have the property of self-assembly.

Lipids are very interesting molecules because they are capable of forming various highly-ordered structures such as spherical, globular or cylindrical micelles as well as bilayer membranes by simply adjusting the size of the head group and hydrocarbon chain. Such nanoarchitectures are precisely defined leading thus to the development of well organised supramolecular structures that can be used as templates for the incorporation of other molecules of interest which can be either biological or non-biological. Nanorods have been developed using properties of lipids that can form inverted hexagonal water in oil structures. If a water soluble salt e.g. Cu salt is mixed with a lipid then a metal nanoparticle will occur in the water tubules formed by the lipids. It is the structure-property of the lipid that forces the metal nanoparticle to be grown inside the water tubule thus forming nanorods (84, 88).

It is also worth mentioning the self-assembled monolayers (SAMs) which are monolayers that are formed on surfaces by a self-assembly process which is not driven by hydrophobic/hydrophilic groups but is based on the strong electrostatic interaction between a solid surface and a specific functional group built into a molecule. One of the most studied examples is the monolayer formation of alkane thiols on gold surfaces. Often the alkane thiols contain additional active groups generating thus a nanostructure material whose surface properties can be controlled (88).

Proteins are another important class of biomolecules which, in living organisms, may have variety of functions such as synthesis of DNA, transcription, translation, cell cycle control as well as production of energy, conversion of sunlight to sugar and so on. Proteins are biopolymers made up from 20 amino acids which are linked by amide bonds. Each amino

acid has different functional groups which can provide the amino acids with hydrophobic, hydrophilic, basic or acidic characteristics. It is the variability in the amino acid sequence that makes these biopolymers adopt different three dimensional structures. Given a specific sequence of amino acids, it is not possible to predict what structure the peptide will adopt even if we use the most sophisticated computational approaches.

One of the most well studied protein is the ATP synthase which is found in all living organisms. This protein is important for the hydrolysis or generation of ATP upon the influence of the protonmotive force. What makes these proteins important for nanotechnology is their ability to rotate as they are embedded in a lipid membrane. When there is an excess of protons at one side of the membrane then protons flow through the ATPase which also leads to the rotation of a domain of this protein. This ability to rotate can characterise the ATPase as a nanomotor capable of performing 17 rotations per second. The ability to use this biomolecule as a nanomotor has been proven by the Montemagno group which succeeded in isolating individual ATPases and transferred them into a solid substrate. Then they attached micron-sized polystyrene beads into the ATPase which is only 12 nm in diameter and observed the rotation of the polystyrene bead tail (80).

An additional interesting example of a protein being exploited for nanotechnology is of prokaryotic origin and is called S-layer. This protein is characterised by its tremendous ability to self assemble into a monolayer composed of identical sub-units. S-layer lattices have been used as matrices for the scaffolding of nanoparticles. The S-layer of *Sulfolobus acidocaldarius* has been used as a template for the positioning of tantalum-tungsten nanoarrays (34).

Another important biomolecule that has attracted a lot of scientists is the DNA. Even though it is considered to be chemically simple it may be however one of the most important biomolecules, since due to its sequence variability it carries a lot of information that is essential for any living organism.

In a general sense, DNA typically consists of two strands that coil each other to make a helix. Each strand comprises a series of phosphodiester-linked nucleotide units that contain a 2' -deoxy-D-ribose and a nucleobase. There are four nucleobases in DNA; the purines, adenine and guanine and the pyrimidines, thymine and cytosine. The two strands of DNA

are connected with each other by hydrogen bonding between the nucleobases. DNA can adopt different conformations depending on its particular nucleotide sequence and on factors such as ionic strength and type of ions, as well as solvents (30). The B-form of DNA has been considered to be the DNA present under physiological conditions, i.e. in aqueous solution with typical counterions. The overall structure of B-DNA forms two distinct helical grooves: the major and the minor groove. The major groove is wide, while the minor groove is narrow with both grooves having almost equivalent depth. The A-form is adopted by both RNA and DNA molecules, and in the case of DNA, it is considered to be the dehydrated form (75 % relative humidity) of DNA (30). The groove geometry of A-DNA is different from that of B-DNA. It consists of deep and narrow major grooves and very shallow and wide minor grooves. It is still unknown whether A-DNA is present under certain physiological conditions; however, it is believed to occur upon binding of some proteins (64). Generally, at low relative humidity or in the presence of 75 % ethanol, the transition from B-DNA to A-DNA can take place (30).

Studies performed so far have indicated that DNA can be used as a template for the scaffolding of metal clusters. One study performed by Mirkin and his group has shown the ability of DNA to act as a smart glue by using the ability of DNA sequences to complement with each other (108). More specifically, gold clusters were functionalised with single stranded DNA sequences which had thiol groups at each end. DNA sequences which were complementary, cross linked leading to nanoarrays where the gold clusters were located close to each other. Depending on how close the gold clusters were located the optical properties of the gold also changed (108).

Another pioneering study has shown that DNA can be used to form electrically conductive nanosized wires (8). According to this study, a silver wire of 12  $\mu\text{m}$  long and 100 nm wide was constructed between two gold electrodes. One interesting aspect of this approach for making nanowires is that the researchers took advantage of the recognition capabilities of DNA for linking it between the gold electrodes. More specifically 12 base oligonucleotides derivatised with a disulfide group were linked in gold surface via sulfur-gold interactions. The connection between the two electrodes occurred with a 16  $\mu\text{m}$  long DNA which consisted of two 12 base 'sticky ends' that were complementary to the surface bound DNA sequences. This long DNA strand was used to deposit silver metal using standard silver deposition techniques. Since DNA is negatively charged due to the phosphate backbone, it

is possible to exchange the counterions with silver ions. The silver ions can be reduced chemically into silver metal (8). DNA is a very sophisticated biomaterial for the targeted growth of metal nanowires based on its recognition capability. This versatility allows also the arrangement of the nanowires as squares, cubes and movable hinges, which allows the researchers to control the shapes and sizes of the organised nanoassemblies (120).

## **1.2 Applications in medicine**

There has been a significant advance in the past four decades in medicine, and more specifically in the field of medical oncology, with a large amount of new drugs being developed and used clinically for the treatment of many fatal malignancies. The basic approaches for the treatment of cancer are constantly changing, leading to a large variety of anticancer drugs which have succeeded in treating neoplastic diseases that previously were considered impossible to cure by surgery or irradiation. Nevertheless, still most of the anticancer drugs have a rather narrow therapeutic index and a great potential to cause harmful side effects. Thus a better understanding on the interactions between biomolecules and drugs is required for safe and effective use in human beings. In Figure 1.1 is listed a synopsis of different categories of existing anticancer drugs or drugs being currently investigated by clinical studies. It is clearly indicated that among the different classes of antineoplastic agents, metal-based drugs, are also used for the treatment of cancer by exhibiting a variation on mechanism of action.



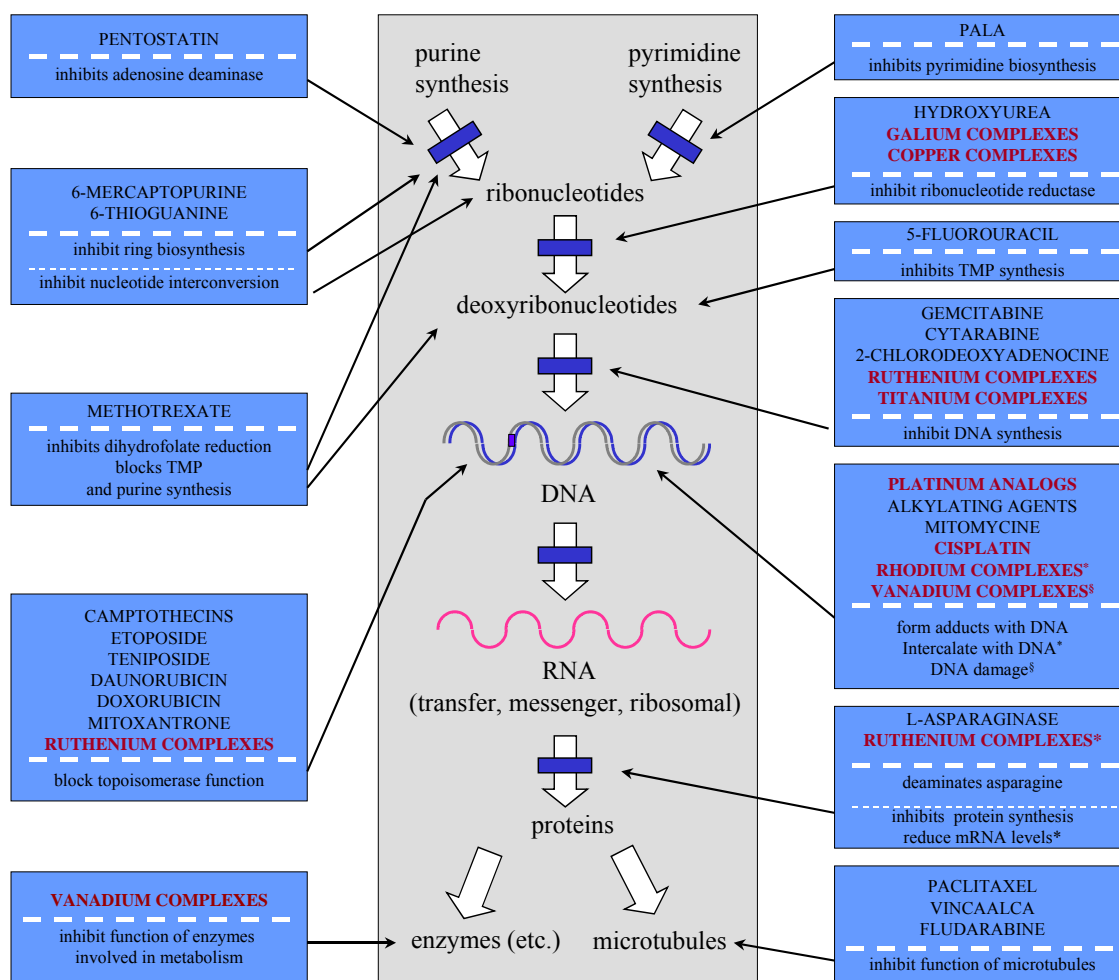


**Figure 1.1 Overview of the mechanisms of action of chemotherapeutic agents used in cancer treatment.** Metal-based complexes are given in bold characters in dark pink colour. This is a rather simplified summary of many anticancer drugs which are currently used in the treatment of malignant tumours or are still under development. Among the different drugs metal-based compounds are also exploited for their antitumor potential with their mechanism of action being considered as relatively diverse. They can react with DNA by forming adducts or by intercalating. Damage through strand-breaks also may occur. Nevertheless their association with the DNA structure may lead to blockage of the function of DNA associating proteins. Direct association with proteins and inhibition of their function is also observed (14, 20, 123).

DNA has been considered for many years as one of the most important biomolecules apart from RNA and proteins, as a pharmacological target for the action of many anticancer compounds. There are almost more than a thousand platinum-based complexes with each study contributing significant knowledge on the mechanism of action of this class of metal-based compound and leading to new generation of platinum complexes like oxaliplatin and carboplatin with reduced side effects (13). DNA has been mainly considered as the target of platinum-based compounds leading to the formation of intrastrand, and interstrand

adducts. Nevertheless, the interaction of these molecules with the exposed sulfohydryl groups of proteins cannot be ruled out and has been experimentally shown (122). The intrastrand adducts form through the crosslinking of adjacent guanine bases (influenced by the N7 of guanine) on the same strand, however guanine-adenine cross-links may also occur. Interstrand cross links are formed slower and occur at a lower extent. These intra- and interstrand adducts formed by the platinum-based compounds lead to DNA breaks, DNA bending and subsequent miscoding, which can inhibit DNA replication and transcription. It should be considered though, that no conclusive association between platinum adduct formation and efficacy has been documented, however preclinical studies suggest that platinum-DNA adducts may be important in terms for cytotoxicity (117).

DNA structure alone or with ligands has been well characterised either experimentally, by X-ray crystallography, or by computer simulations; however it still attracts much interest because the way ligands interact with DNA is very important for drug design.

Molecular modelling studies of the interactions of DNA molecules and metal ions or anticancer compounds have provided much useful information concerning the specific and nonspecific binding sites for metal ions/ligands on DNA, structural changes of DNA upon binding, and the overall distribution of metal ions along the DNA helix. In addition to the classical anticancer compounds, various monovalent and bivalent metal ions such as  $\text{Na}^+$ ,  $\text{K}^+$ ,  $\text{Au}^+$ ,  $\text{Mg}^{2+}$  and  $\text{Zn}^{2+}$  can interact with either the phosphate groups of the backbone or with the N7 atoms of the purine bases, either directly or via bridging of water molecules (10, 67, 90).

Apart from platinum complexes, gold-based compounds have also attracted a lot of interest in the recent years. Originally gold-based compounds like auranofin have been employed clinically for the treatment of rheumatoid arthritis (58). Nevertheless, some of them have shown a great potency against various tumors. Particularly triphenyl phosphine gold (I) complexes have indicated a significant antitumor activity (110).

The mechanism of action of gold-based compounds is not understood yet. There are rather contradicting views, about how gold-based drugs interact with biomolecules such as DNA. Some studies have shown that particular gold (III) compounds can damage DNA in a manner similar to that of cisplatin, through the formation of interstrand crosslinks and single strand breaks (116) while others have shown that gold drugs have a low binding affinity for the DNA double helix (78).

Understanding the molecular mechanism of action of chemotherapeutic drugs has been considered of great importance. Nevertheless the mechanism that triggers the cells to die as a result of the cytotoxic action of a chemotherapeutic agent has also started to attract a significant amount of interest. The purpose of cell death is to kill unwanted cells during important physiological situations like maintenance of homeostasis and development, defence and aging (107). Specific stimuli like the lack of growth factors as well as drugs, toxins and viral infections can provoke cell death (114). There are two ways by which cells die. There is death by injury which is termed as 'necrosis' and physiological death or death by suicide which is called 'apoptosis'. Necrosis is characterised by external damage and exhibits swollen morphology, plasma membrane lysis, release of cytoplasmic components in the surrounding tissue spaces leading to an inflammatory response. Necrosis can occur very rapidly in a matter of seconds and it could be considered as analogous to 'cell murder'(21, 29). Apoptosis is a controlled type of cell death that is energy-dependent and is characterised by cell shrinkage, chromatin condensation, membrane budding, phosphatidylserine externalisation and activation of a family of cysteine proteases called caspases. Apoptosis involves a slower series of events, therefore it could take few hours to several days (95). Apart from the kind of cells and type of genetic changes that occur in cancer cells there are several other factors that may determine which mode of death will be induced like dosage of anticancer agent as well as the availability of energy and the metabolic condition of the cell (45).

There are still many questions that need to be answered regarding how cells sense damage and trigger apoptosis. Even in the case of cisplatin, that has been used for almost 30 years in chemotherapy, is still not clear after DNA adduct formation, what are the downstream events that lead to cell death. Several studies have indicated that DNA damage is recognised by almost 20 proteins that bind to the distorted DNA (4). Some of these proteins include components of the mismatch repair system and transcriptional factors that can lead to the induction of p53 (102). p53, is a transcriptional activator of many genes that result to cell arrest or apoptosis (33). If the dosage of cisplatin is high enough to overwhelm the cellular repair, then a cascade of events takes place which involves the release of cytochrome c from the mitochondria and the activation of the caspase 9-3 pathway subsequently leading to apoptosis (115). It has also been found that apoptosis can be mediated through an alternative pathway which involves the activation of the caspases - 8 and -3 through Fas/FasL which are mediated by p53 (79). However this pathway is still not fully understood since caspases -8 and -3 are in some systems activated independently

by Fas/FasL (41). Apparently cisplatin may also induce the necrotic pathway through the activation of a polymerase (PARP) which recognises the DNA adducts caused by cisplatin. PARP cleaves the glycolytic enzyme NAD<sup>+</sup> leading to the formation of poly(ADP-ribose) moieties instead of NAD<sup>+</sup>. A decrease in NAD<sup>+</sup> inhibits the glycolytic production of ATP. ATP depletion subsequently leads to cell death by necrosis (17). Apparently inactivation of PARP may occur by caspases -3, -6 and -7. This indicates that the biochemical pathways that involve necrosis and apoptosis are interconnected (37, 45).

Tumor resistance to chemotherapeutic agents has emerged as an obstacle for the treatment of malignancies leading to the administration of more than one chemotherapeutic agent or to the combination of chemotherapy and radiotherapy. Some of the mechanisms of drug resistance include reduced drug uptake, increased drug metabolism and enhanced repair of DNA damage(114). Apart from these factors susceptibility to activation of apoptosis has also started to be considered as determinant factor of tumor resistance. Therefore new therapeutic agents that can modulate the response to apoptosis are now considered as a new strategy for the treatment of malignancies which are resistant to existing anticancer drugs.

### **1.3 Applications in biotechnology**

Synthesis of biocompatible surfaces is an area with significant interest in biotechnology. The immobilisation of proteins and enzymes as well as the purification of amino acids have been considered as some of the main applications. Recently zeolites have attracted a lot of interest as inorganic structures with abilities to conjugate biopolymers.

Zeolite is a naturally occurring mineral group consisting of three-dimensional, crystalline structures. It is composed mainly of silicon and aluminium atoms tetrahedrally coordinated with each other through shared oxygen atoms. Most of the zeolites contain water and exchangeable cations in their channels and cavities that can play an important role in balancing the anionic charge of these structures (44). Apart from their recent application in amino acid purification they have been also considered important in odor control (76), water filtration (66), heavy metal (62) and ammonia removal (19, 76), oil absorbance and gas separations (24). Physicochemical characteristics of these structures such as Si/Al ratios and therefore degree of hydrophobicity as well as pore sizes and structure morphology can strongly influence the adsorption of biopolymers. In addition zeolites are resistant to extreme pHs, as well as stable at high and low temperatures (59).

Immobilisation of proteins or enzymes is very important in the field of biosensing and it has been proven to be a rather difficult task since biological activity can be easily affected. Nevertheless, recent studies have successfully achieved the conjugation of various enzymes with gold nanoparticles which were bound to functionalised zeolite-Y (82). The enzymes showed increased activity comparing to the free enzymes in solution as well as higher stability at various temperatures and pHs. Interestingly this new type of bioconjugate could be easily removed by the reaction medium by simple centrifugation and exhibited excellent reuse characteristics (82).

Apart from the commonly used chromatographic techniques which include organic ion exchange resins, zeolites, have been recently examined for the purification of proteins. It has been demonstrated that various proteins with different pIs and molecular weights can adsorb different zeolites with maximum adsorbance occurring at their pI (16, 74). Desorption of each protein has been achieved at pI only with polyethylene glycol rather than with conventional eluents. The eluted proteins were proven to retain their activities (16).

Finally adsorption and separation of amino acids has also been proven to be possible in the presence of zeolites. Separation of the amino acids lysine, phenylalanine and glutamic acid was achieved at different pHs at zeolite-beta. In addition to this zeolite other zeolite structures were also tested indicating that pore sizes as well as aluminium content can influence the adsorption of the above amino acids (83).

## **1.4 Aims of this study**

The general aim of this study is to investigate by computational and experimental methods how biomolecules such as DNA, proteins and small amino acids are influenced when they come into contact with inorganic nanostructured materials. For reasons of clarity more specific aims will be discussed separately in the following sections.

### **1.4.1 Aims with applications in nanotechnology**

The majority of experimental or theoretical studies reported in the literature have concerned the interactions of nucleic acids with single-atom metal ions or organometal

compounds, rather than metal clusters. Such clusters are well suited to the fabrication of nanoscale conducting devices (121). Transmission electron microscopy (TEM) studies (Figure 1.2a and 1.2b) performed in the laboratory of Prof. Schmid (Department of Inorganic Chemistry, University of Duisburg-Essen) have suggested that the incubation of B-DNA molecules with  $\text{Au}_{55}$  clusters results in the formation of many gold “nanowires” arranged in the form of a number of electron-dense columns. The respective widths of the wires are consistent with the width of a  $\text{Au}_{13}$  cluster. The distance separating each wire is approximately 0.5 nm.

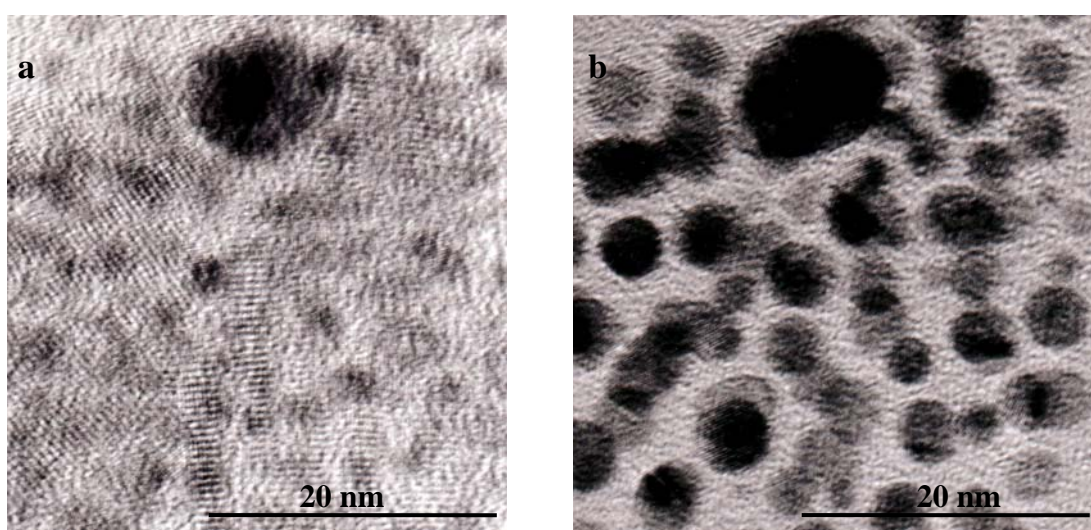


**Figure 1.2 Transmission electron micrographs of B-DNA with gold cluster  $\text{Au}_{55}$ ;** (a) Initial micrograph indicating the formation of nanowires. Each nanowire has the same diameter as if it was composed of only 13 gold atoms rather than 55. Each gold wire is separated from each other by 0.5 nm; (b) Micrograph obtained after further exposure in vacuo. In TEM micrographs, the DNA molecules are not visualised.

In the present work, molecular mechanics simulations have been employed to investigate the interactions of two different DNA conformations, the A- and the B-form, with gold clusters comprising either 13 or 55 atoms ( $\text{Au}_{13}$  and  $\text{Au}_{55}$ , respectively). These simulations were aimed at understanding the fundamental interactions between a single gold cluster and a DNA molecule. Molecular dynamics simulations of many DNA molecules in the presence of  $\text{Au}_{13}$  clusters have been performed in order to provide further information on the mechanism by which gold wires form, and evidence to explain the proposed interwire separation distance of 0.5 nm. This work has been performed with the assumption that the TEM observations represent the dehydrated form of the DNA (A-DNA).

### **1.4.2 Aims with applications in medicine**

Based on observations obtained from TEM and molecular modelling studies which suggest that gold clusters can interact with important biomolecules such as DNA one could therefore logically think that Au<sub>55</sub> cluster could exhibit anticancer or antimicrobial properties. In this study the anticancer potential of Au<sub>55</sub> cluster has been investigated against a variety of human cancer cell lines. Based on experimental methods, basic, but rather important questions were attempted to be answered eg., how cytotoxic is Au<sub>55</sub> on various cancer cell lines?; what influence might Au<sub>55</sub> have on the structure of plasmid DNA?; whether inside a cell Au<sub>55</sub> molecules reach the ultimate goal i.e the DNA and once they are inside the cells are the gold cluster influencing the apoptotic or necrotic death? Apart from DNA as the target biomolecule, proteins perhaps could influence the anticancer potential of Au<sub>55</sub> thus, using albumin as a model protein the sequestering capability of this protein was investigated. Based on molecular modelling techniques, molecular docking simulations were performed in order to understand how Au<sub>55</sub> interacts with the structure of DNA molecules. More specifically the main interest was focused in understanding where Au<sub>55</sub> interacts with the structure of DNA i.e. in the major grooves or minor grooves and whether specific sequences are energetically preferred. In addition molecular docking simulations have been performed with human albumin protein and Au<sub>55</sub>. All this information will provide further understanding in the mechanism of action of this potentially new anticancer drug.

### **1.4.3 Aims with applications in biotechnology**

In order to design tailor-made adsorbents for the separations of amino acids and proteins we need to understand the fundamentals of the interactions that occur between different amino acids and zeolite structures. Based on the experimental work performed by the group of Ernst and co-workers who investigated the adsorption of amino acids, lysine, phenylalanine and glutamic acid on various zeolites, molecular dynamics simulations have been performed in order to examine at the molecular level the decisive interactions occurring between a zeolite beta structure which is free of aluminum with the amino acids listed above (83).

## **2. Theory**

---

### **2.1 What is molecular modelling ?**

Chemistry is a science which deals with the properties of molecules, their construction and transformation from one stable form to another. Theoretical chemistry is rather a subfield of chemistry where mathematical calculations are combined with the laws of physics in order to study chemical processes. There is a confusion with the meaning of the terms ‘theoretical chemistry’ and ‘molecular modelling’. Theoretical chemistry often involves quantum mechanics methods which calculate the properties of molecules by explicitly including electrons in the calculations. Molecular modelling which is synonymous to ‘computational chemistry’ includes any method, i.e. quantum mechanics or molecular mechanics methods or any other method that gives insight into the behaviour and properties of molecules. It should be noted that molecular modelling simulations are not a replacement for experimental work. Instead, both approaches may be used to complement one another. Simulations may be used to aid in the interpretation of experimental results and computational experiments may be used to provide supplementary information (96).

### **2.2 Useful concepts in molecular modelling**

Molecular modelling is highly dependent on the computational resources available. For a long time workstations were the primary and only use for single task calculations. Fortunately the fast development of processors has allowed researchers to perform advanced calculations on computers. Of course to perform molecular modelling calculations the appropriate programs are required. A significant effort is required to convert existing programs to run efficiently in parallel.

There are various programs which are used to perform computational simulations. They can range from simple to very complex packages that allow a researcher to use many different modelling methods. Today modelling packages are commercially available and while some programs are widely used others are still in the process of being tested and compared to the standard ones. It is not in the scope of this study to discuss in detail the programs used since they become rapidly outdated, however, each program used will be



noted later on. For general information the programs mainly used in this thesis are by Accelrys which offer a wide range of products that can be used either for researchers that are interested in life sciences or material sciences. Generally they allow one to create a molecule on the screen, change it, or import molecules from databases on the internet. They often have computer graphics which allow better visualisation and presentation of molecules. It should be remembered though that there is more than just molecular graphics. Such programs should be capable of performing energy minimisations and molecular dynamics simulations and predict structure, properties and energetics of organic, inorganic, organometallic molecules, surfaces or of large biological systems. Together the interaction of good molecular graphics and computational methods can aid in the analysis and interpretation of results after molecular modelling calculations (96).

It has been considered that computer power and the use of parallelised programs is not one of the main advances in molecular modelling. The development of forcefields that can accurately characterise the molecule of interest and calculate the potential energy is really significant. Usually modelling programs contain many forcefields for calculations. Some of them have been widely tested and others not. It is really important that a molecular modeller really carefully evaluates whether the forcefield used for the particular molecule of interest is really appropriate. It should never be assumed that the forcefields and the methods included in the programs are always appropriate for all the molecular systems to be investigated. A good understanding of the forcefields provided and the methods used by the programs to calculate, create structures, properties and energies is really important.

### **2.3 Some general features of a molecular mechanics force field.**

A molecular mechanics forcefield is based on the assumption that atoms are presented as balls and the bonds are modelled as springs that obey Hooke's law. The position of the atoms is dependent on the forces between pairs of atoms (e.g. bond stretching, van der Waals and electrostatic interactions), and groups of atoms (e.g. torsional angles) as shown in Figure 2.1 (22).

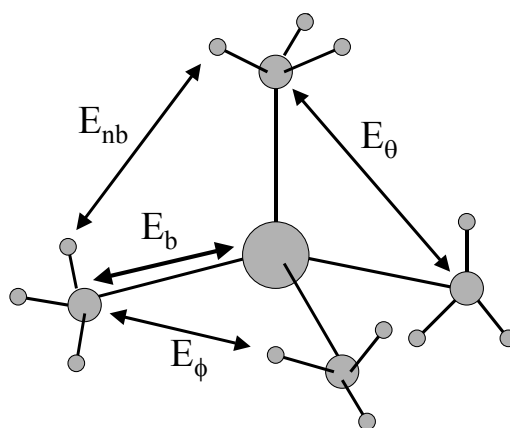


**Figure 2.1 The molecular mechanics method.** Typical forces acting between atoms are the bonding interactions such as bond stretching ( $E_b$ ), torsions ( $E_\phi$ ), angle bending ( $E_\theta$ ) and the non-bonding interactions like van der Waals and electrostatic forces ( $E_{nb}$ ).

The energies that result by these forces are also dependent on the positions of the nuclei in the molecule. When the atoms move away from their ideal positions then the energy lost is related to the strain, steric or potential energy  $E_{FF}$ . The optimisation of the potential energy which results in the rearrangement of the nuclear geometry leads to the optimised structure of a molecule. A general mathematical description of the interaction energy between all pairs of atoms is given below.

$$E_{FF} = E_{str} + E_{bend} + E_{tors} + E_{cross} + E_{vdw} + E_{el} \quad \text{Eq. 2.1}$$

$E_{FF}$  is the sum of the terms describing the potential energy of a molecule.  $E_{str}$  is the energy required to stretch a bond between two atoms.  $E_{bend}$  represents the energy required to bend an angle.  $E_{tors}$  is the energy required to rotate around a bond. The non-bonded interactions such as the van der Waals and electrostatic interactions are represented by the terms  $E_{vdw}$  and the  $E_{el}$  respectively. The coupling of the first three terms is described as  $E_{cross}$  and is present mainly in recent forcefields (22).

It should be noted that each functional term calculated is composed of mathematical forms which can range from simple quadratic forms to complex forms such as Morse functions, Fourier expansions and Lennard-Jones potentials. The energy is not only described as functional terms (bond distances, torsions) but also in relation to internal coordinates. In addition a forcefield contains all the information required for registering all the atoms in a

molecule according to their atomic number and the type of chemical bond they are involved in (atom typing). Force fields also include information on atomic charges (partial and formal charges). Finally parameters which are important for the functional forms that calculate the  $E_{FF}$  are also present (54).

Usually a force field is generated to describe a specific class of molecules with reasonable accuracy. Its functional forms and parameter values cannot be applied for calculating the potential energy of all existing molecules. Ideally the new molecules to be investigated by molecular modelling should be similar to those used for the parameterisation of the force field. The parameters for the functional forms included in a force field are mainly obtained by experimental data such as crystal structures or vibrational spectra, and by computational methods such as quantum mechanics (54).

Now will be discussed in some more detail the various functional forms that are in common use in molecular mechanics force fields.

### 2.3.1 Bond stretching: $E_{str}$

The first component of the potential energy to be considered is the functional form that contributes to the calculation of the energy of bond stretching. The simplest way is to treat the bond between two atoms as a spring which according to Hooke's law gives a harmonic energy curve (Figure 2.2) (60, 70).

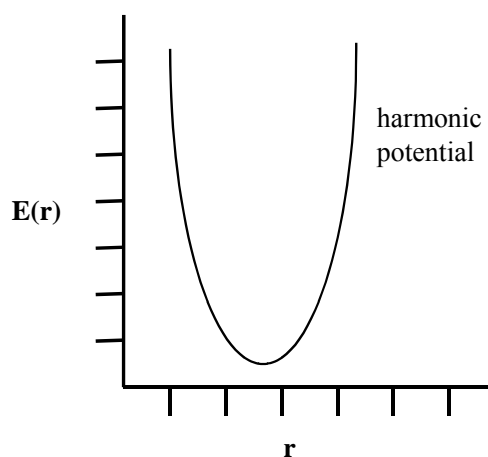


**Figure 2.2 Hooke's law describing a simple harmonic potential.**

$$E(r) = \frac{k}{2}(r - r_0)^2 \quad \text{Eq. 2.2}$$

Where  $k$  is the stretching constant and  $r_0$  is the ideal bond distance.

The ideal bond distance or ‘natural’ bond length is the value that the bond adopts when all other terms are set to zero. A true bond stretching potential curve is not harmonic but rather of the shape presented on Figure 2.3 .

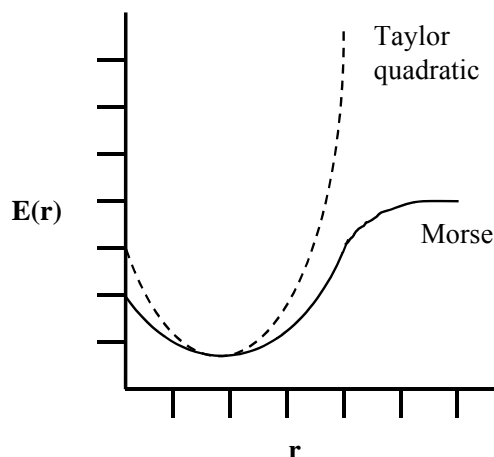


**Figure 2.3 Comparison of the Morse and Taylor potential curves.**

This curve can be properly described by the Morse function, however, there are difficulties in using it for computational calculations due to the exponential term and the square function which can lead to longer computational effort and complexity in the parameterisation of the forcefield (Equation 2.3). Such a functional form can be mimicked by the Taylor expansion on which higher terms are included (Equation 2.4) (60).

$$E_{\text{str}}(r^{AB} - r_0^{AB}) = D(1 - e^{-\alpha(r-r_0)^2}) \quad \text{Eq. 2.3}$$

Where  $D$  is the depth of the potential minimum and  $\alpha = \beta\sqrt{\mu/2D}$ ,  $\mu$  is the reduced mass and  $\beta$  is related to the stretching constant  $k$  of the A-B bond.

$$E_{\text{str}}(r^{AB} - r_0^{AB}) = k_2^{AB}(r^{AB} - r_0^{AB})^2 + k_3^{AB}(r^{AB} - r_0^{AB})^3 + \dots \quad \text{Eq. 2.4}$$

Where  $k_2^{AB}$  and  $k_3^{AB}$  are the force constants for the A-B bond and  $r_0^{AB}$  is the ideal bond distance between the two atoms A and B (60).

### 2.3.2 Angle bending: $E_{\text{bend}}$

$E_{\text{bend}}$  is the energy required to bend an angle between three atoms  $A$ - $B$ - $C$ , where  $A$ - $B$  and  $B$ - $C$  are connected by a bond. It is similar to the  $E_{\text{str}}$ , by being simply described using Hooke's law (Equation 2.5). In most applications a simple harmonic term is adequate since molecules deviate only slightly from their natural bond angle. Refinements do occur in some cases where higher accuracy is needed, by incorporating higher terms such as those described by the Taylor series.

$$E_{\text{bend}}(\theta^{ABC} - \theta_0^{ABC}) = \frac{k}{2}(\theta^{ABC} - \theta_0^{ABC})^2 \quad \text{Eq. 2.5}$$

where  $\theta_0$  is the ideal angle and  $k$  is the force constant for the angle between three atoms (22, 70).

### 2.3.3 Torsion angle: $E_{\text{tors}}$

$E_{\text{tors}}$  is the energy required to rotate a bond  $B$ - $C$  in a four-atom molecule  $A$ - $B$ - $C$ - $D$  where  $A$ - $B$ ,  $B$ - $C$  and  $C$ - $D$  are connected by a bond. Torsional changes together with non-bonded interactions play a very important role for determining variations in molecular structures and energies. In the case of bond and angle stretching, a substantial amount of energy is required in order to cause a significant change in a structure.  $E_{\text{tors}}$  is expressed differently to that of  $E_{\text{bend}}$  and  $E_{\text{str}}$ . It is expressed as a Fourier expansion which contributes to the periodicity of the angle instead of a Taylor expansion (Equation 2.6).

$$E_{\text{tors}}(\omega) = \frac{V_1}{2}(1 + \cos \omega) + \frac{V_2}{2}(1 - \cos 2\omega) + \frac{V_3}{2}(1 + \cos 3\omega) \quad \text{Eq. 2.6}$$

Where  $\omega$  is the torsional angle in a four-atom molecule  $A$ - $B$ - $C$ - $D$ . The constants  $V_1$ ,  $V_2$  and  $V_3$  determine the barrier for rotation around the  $B$ - $C$  bond (63, 70).

### 2.3.4 Cross terms: $E_{\text{cross}}$

The first five terms in the potential energy expression (Eq 2.1) are common in all forcefields. The last term  $E_{\text{cross}}$  represents a coupling of the internal coordinates. Consider for example a molecule composed of three atoms  $A$ - $B$ - $C$  where  $A$ - $B$  and  $B$ - $C$  are connected

by a bond. If the bond angle between  $A-B-C$  is decreased then the length of the  $A-B$  and  $B-C$  bonds will increase due to the repulsions between the atoms.

The components of the  $E_{\text{cross}}$  are written as Taylor-like expansions as shown in equations 2.7 and 2.8. The most important cross terms present in force fields are shown on Figure 2.4 (63, 70)

$$E_{\text{str/str}} = k^{ABC} (r^{AB} - r_0^{AB}) \times (r^{BC} - r_0^{BC}) \quad \text{Eq. 2.7}$$

$$E_{\text{str/bend}} = k^{ABC} (\theta^{AB} - \theta_0^{AB}) \times [(r^{AB} - r_0^{AB}) + (r^{BC} - r_0^{BC})] \quad \text{Eq. 2.8}$$

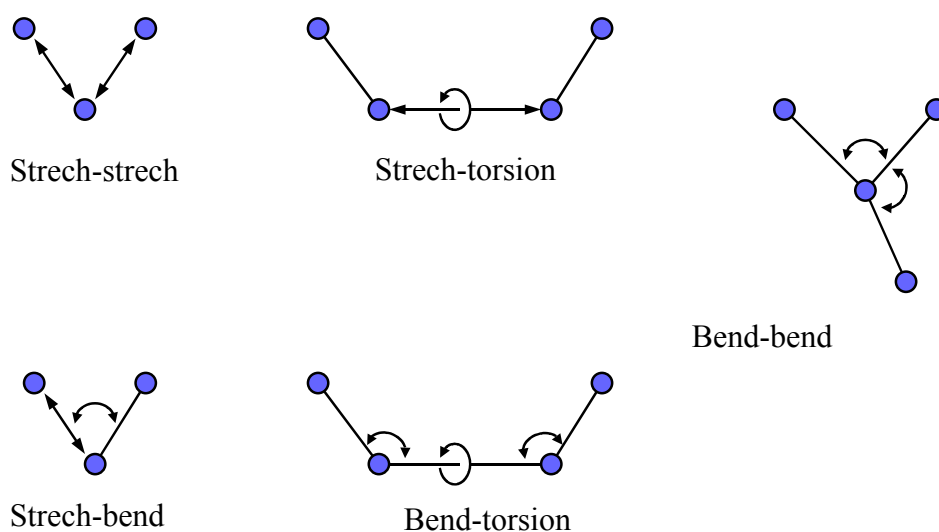


**Figure 2.4** Various cross terms present in some force fields.

### 2.3.5 van der Waals interactions: $E_{\text{vdw}}$

The term  $E_{\text{vdw}}$  describes the repulsion or attraction between atoms that are not bonded. At long interatomic distances the  $E_{\text{vdw}}$  is zero whereas at short distances it becomes repulsive. The attraction is due to induced dipole-dipole interactions. This may also occur even when a molecule (or part of a molecule) does not have a permanent dipole moment, however due to an uneven distribution of electrons around the nucleus they can cause an instantaneous dipole to exist. This will induce a dipole moment in the neighbouring molecule (or another part of the same molecule) creating an attraction. This attraction is often called *London force* or *dispersive interaction*. The short-ranged repulsive interactions are often called

*exchange forces* and they occur due to the electrostatic repulsion between pairs of electrons which inhibits them to occupy the same internuclear region (70).

A general form that can fit the above consideration is the *Lennard-Jones* function, where the attractive and repulsive forces are modelled by an  $1/r^6$  and  $1/r^{12}$  term respectively (Eq 2.9). There are also other equations that describe the short-ranged interactions differently e.g. the *Morse* function which gives a better description of the repulsive interactions than the *Lennard-Jones*. It has been considered that for chemical purposes the attractive forces are much more important for intermolecular interactions. In addition the *Morse* function requires more computational effort. For these reasons the *Lennard-Jones* potential is more often used than any other function (22).

$$E_{\text{vdw}}^{\text{LJ}}(r) = \delta \left[ \left( \frac{r_0}{r} \right)^{12} - 2 \left( \frac{r_0}{r} \right)^6 \right] \quad \text{Eq 2.9}$$

Where  $\delta$  is the depth of the minimum and  $r_0$  is the minimum energy distance.

### 2.3.6 Electrostatic interactions: $E_{\text{el}}$

The second group of the non-bonded interactions is the electrostatic interaction which is due to the unequal distribution of the electrons creating a positive and negative charge in a molecule. The electrostatic interactions can be determined in two ways i.e. by assigning charges at each atom, or, bonds are assigned with a dipole moment (70).

Using *Coulomb's law* the electrostatic interaction between point charges can be calculated as a sum of the interactions between all pairs of atoms (70).

$$E_{\text{el}} = \frac{q_A \times q_B}{4 \times \pi \times \varepsilon \times r_{AB}} \quad \text{charge-charge interaction} \quad \text{Eq. 2.10}$$

Where  $\varepsilon$  is the dielectric constant which is included to model the surrounding solvent molecules.

The interaction energy between two dipoles  $p_1$  and  $p_2$  separated by a distance  $r$  can be calculated as following:

$$E_{\text{el}} = \frac{K \times p_1 \times p_2}{4 \times \pi \times \varepsilon \times r^3} \quad \text{dipole-dipole interaction} \quad \text{Eq. 2.11}$$

Where  $K = \sin \theta_1 \times \sin \theta_2 \times \cos(\phi_1 - \phi_2) - 2 \times \cos \theta_1 \times \cos \theta_2$

### 2.3.7 Hydrogen bonding interactions: $E_{hb}$

Except the van der Waals and the electrostatic interactions also the hydrogen bond is considered in some forcefields for the calculation of the  $E_{FF}$ . The hydrogen bond occurs between a proton donor such as the strongly polar molecules OH, NH and SH and a proton acceptor atom like the electronegative O and N atoms.

Some forcefields use the Lennard-Jones function to calculate such an interaction which is described by the Eq 2.12.

$$E_H(r) = \delta \left[ \left( \frac{r_0}{r} \right)^{12} - 2 \left( \frac{r_0}{r} \right)^{10} \right] \quad \text{Eq. 2.12}$$

Where  $\delta$  is the depth of the minimum and  $r_0$  is the minimum energy distance.

Some forcefields incorporate much more complicated functions for determining the  $E_{hb}$ , however, the current trend is that complex functions and extra parameters are avoided and instead hydrogen bonding is calculated in terms of electrostatic interactions. The hydrogen bonding terms are usually included with the van der Waals terms (63, 70).

## 2.4 Molecular Mechanics Simulations – Energy Minimisation

Molecular mechanics simulation or the synonymous energy minimisation and energy optimisation are performed in order to calculate the molecular structure and the corresponding potential energy using the internal coordinates, parameters and functional forms. Usually the structure is modified to make it more consistent with the parameter information within the molecular mechanics force field. Various mathematical procedures are used to determine how the geometry will change from one step to the next (63).

Energy-minimisation is mainly performed in order to optimise structures that result from building them with a molecular graphics program. Other examples include the optimisation of protein structures which are generated by homology methods. In addition molecular mechanics simulations are used in docking simulations where the conformation of a ligand on a respective binding site is investigated .

The most common methods used to energy-minimise structures are the gradient methods which utilise only the first derivative, and the second derivative methods.



### 2.4.1 The gradient methods

Two common gradient methods are the *Steepest Descent* (SD) and *Conjugate Gradient* (CG). In order to understand how minimisation algorithms operate we need to consider first a simple function where the energy of a molecular system is described as a function of its coordinates (either cartesian or internal) e.g.  $E(x,y) = x^2 + 5y^2$ . This function is represented as a diagram in Figure 2.5 (81).

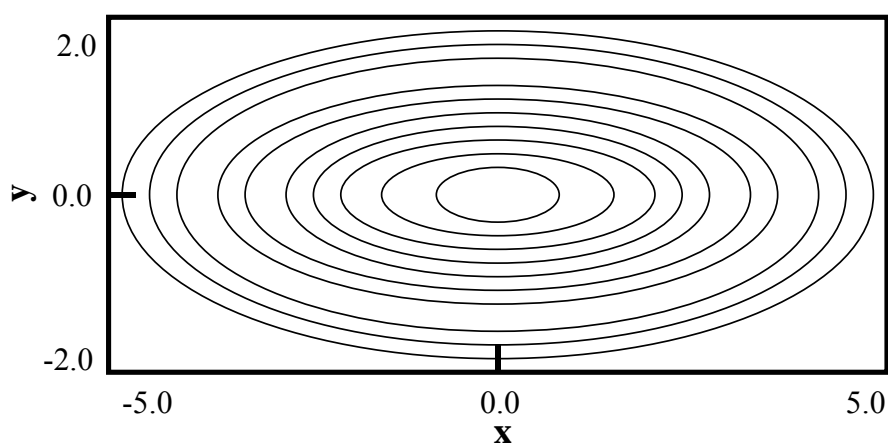


**Figure 2.5** A contour plot of the energy  $E$  in the  $(x,y)$  plane

The minimum of this function can be considered at the point 0.0 where the first derivative of the energy function is equal to zero and the second derivative is positive. A minimisation algorithm must find from its starting point, the direction towards the minimum, as well its distance from it (81).

The SD is known as one of the simplest minimisation methods. It performs a straight line search in order to find the minimum point by using the vector of the first derivative of the potential function. Once a local minimum is found the next gradient direction will be perpendicular to the first vector. It has been found that SD is very rapid at points that are away from the minimum. When the line search is close to the minimum it slows down leading to a simple oscillation around the minimum path. For this reason SD is useful when performed for starting geometries that are far from the minimum i.e very distorted (60).

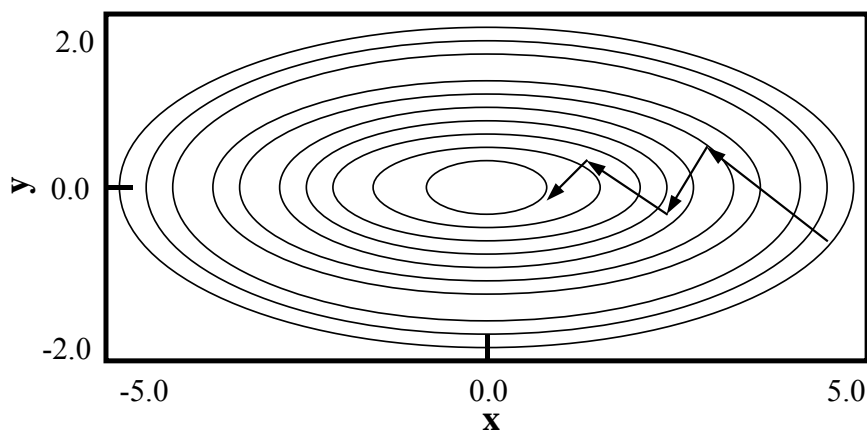


**Figure 2.6 Steepest descent minimisation**

The CG method is a more efficient method than SD. It uses information from the previous first derivative to find the direction of the line search. CG methods produce a set of directions that can overcome the oscillatory behaviour of the SD, for this reason the successive directions are not perpendicular to each other (81).

#### **2.4.2 The second derivative method**

Second derivative methods use both first and second derivative vectors to calculate the energy in relation to the atomic coordinates. Second derivative methods are mainly performed in small molecular systems composed of about 300 atoms, otherwise the method is computationally intensive. One commonly used method is the Newton Raphson and its derivatives which use not only the gradient but also the hessian to locate a minimum (54).

This method will not be described extensively however a few points are worth noting. Newton-Raphson method works quite well in the ideal case, that is, when  $x_0$  is close to  $x^*$ , however when  $f(x)$  is close to zero or at zero then this method exhibits poor numerical behaviour leading to worsen performance and accuracy (96).

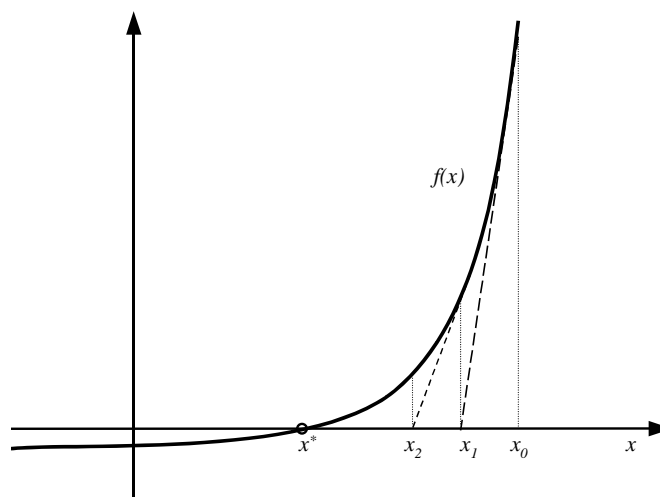


**Figure 2.7: The Newton –Raphson method.** It uses the first derivative to find the next point.

This method is described generally by the following equation:

$$r_{\min} = r_0 - \frac{1}{A(r_0)} \nabla E(r_0) \quad \text{Eq 2.13}$$

Where  $r_{\min}$  is the predicted minimum,  $r_0$  is described as an arbitrary point, the Hessian matrix ( i.e. matrix of the second derivative of the potential energy function in respect to the atomic coordinates) is  $A(r_0)$ , the gradient of the potential energy at  $r_0$  is  $\nabla E(r_0)$ . Since the low energy structure cannot be obtained by one step thus it can be written iteratively as following. The  $i$  th position can be determined just like in CG by the previous position  $i-1$  (54).

$$r_i = r_{i-1} - \frac{1}{A(r_{i-1})} \nabla E(r_{i-1}) \quad \text{Eq 2.14}$$

### 2.4.3 Choice of the method

The choice of the algorithm to be used to optimise a structure depends on many factors including computer requirements. Generally molecular mechanics calculations of large systems are often performed using the SD or CG methods. The Newton-Raphson methods are mostly popular for smaller systems and usually for structures that are close to the minimum. Very often molecular mechanics simulations are performed by combining the above minimisation algorithms i.e. if the starting structure is far away from the minimum

then SD is applied first. When a low energy structure is obtained then a method which gives better convergence is then used like CG or a variant of the Newton–Raphson method (26, 96).

#### 2.4.4 The problem of local minima

The major problem with molecular mechanics calculations is that they converge on the nearest local minimum which is not necessarily the global minimum. The local minimum can be described as the nearest minimum on the potential energy surface located by the minimisation algorithms previously described. The global minimum is the lowest energy point on the potential energy surface (Figure 2.8) (96).

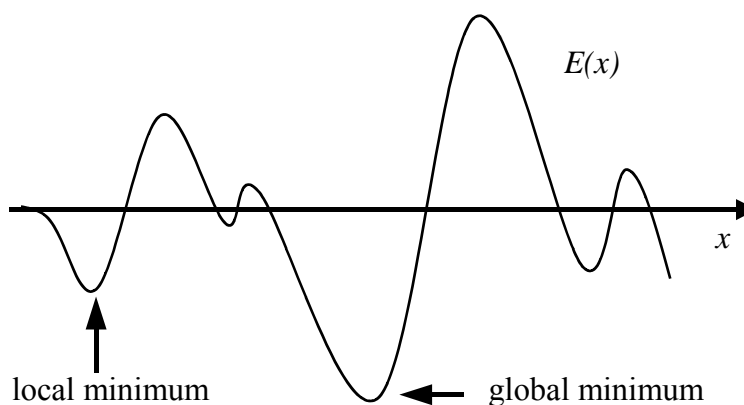


**Figure 2.8 One dimensional function with multiple minima.**

When there are only a few rotatable torsion angles then it is possible to systematically rotate the torsion angles and locate the global minimum. When there are multiple torsion angles then it is very hard to locate the global minimum. It is advised that an unoptimized structure is usually subjected to other computer simulation methods such as *Molecular Dynamics* to find low energy conformations (96).

### 2.5 Molecular dynamics simulations

There are many computational simulation methods used for determining structures of molecules at a global minimum. One of the most common simulation methods is the molecular dynamics (M) method.

A molecular dynamics simulation uses the Newtonian equations of motion, a potential energy function  $E_{FF}$  and associated force field to follow the displacement of atoms in a molecule over a certain period of time (ps to ns range), at a certain temperature and a certain pressure.

$$E = m \times a = \frac{dE}{dr} = m \frac{d^2 r_i}{dt^2} \quad \text{Eq 2.15}$$

$$\frac{d^2 r_i}{dt^2} = a_i = \frac{F_i}{m_i}; F = \frac{\delta E}{\delta r_i} \quad \text{Eq 2.16}$$

Where  $F$  is the force,  $m$  is the mass, and  $a$  is the acceleration of the atom. The force acting on an atom  $i$  can also be calculated as a function of the nuclear coordinates  $r_i$  (54).

There are many integration algorithms that have been developed to solve Newton's law numerically. All the integration algorithms approximate the positions of atoms, the velocities and accelerations by a Taylor series of expansion. One of those algorithms that has been used in this study is the Verlet algorithm (54).

$$r_i(t + \Delta t) = 2r_i(t) - r_i(t - \Delta t) + \left( \frac{d^2 r_i}{dt^2} \right)_t (\Delta t)^2 \quad \text{Eq 2.17}$$

This algorithm uses the position at time  $t - \Delta t$  and the position and acceleration of an atom  $i$  at time  $t$  in order to calculate the new position at time  $t + \Delta t$ .

The velocity of the atom  $i$  does not appear in the expression but it can be obtained by the following equation:

$$v_i(t) = \frac{r_i(t + \Delta t) - r_i(t - \Delta t)}{2\Delta t} \quad \text{Eq 2.18}$$

A variant of this algorithm is the velocity Verlet algorithm and it requires only the positions, velocities and accelerations of atoms that correspond at the same time step i.e. only at  $t$  (54). Then the equations take the form:

$$r_i(t + \Delta t) = r_i(t) + \left( \frac{dr_i}{dt} \right)_t \Delta t + \frac{1}{2} \left( \frac{d^2 r_i}{dt^2} \right)_t (\Delta t)^2 \quad \text{Eq 2.19}$$

$$v_i(t + \Delta t) = \left( \frac{dr_i}{dt} \right)_t + \frac{1}{2} \left( \left( \frac{d^2 r_i}{dt^2} \right)_t + \left( \frac{d^2 r_i}{dt^2} \right)_{t+\Delta t} \right) \Delta t \quad \text{Eq 2.20}$$

During MD simulations the calculation is broken into short time steps usually of 1 fs. At each step the forces acting at each atom; thus the energies, as well as, the coordinates and velocities of the atoms are calculated at a desired temperature. When an atom is moved to a new position then the coordinates and the velocities are updated for this new position. Thus the MD method generates a trajectory at which the conformational variations are presented over a period of time. It could be also considered as a snapshot taken at specific intervals. The trajectory files are very useful because they contain information on the structure variations, energies, volume, pressure and temperature. The trajectory files can usually be animated so that one can observe how a molecular system behaved during a specific period of time (54, 81).

MD simulations can be performed at a variety of experimental conditions in order to mimic to some extent natural phenomena where a molecular system is exposed at a specific pressure or temperature. Some of the most widely used thermodynamic ensembles are the following:

NVE: constant number of particles  $N$ , constant volume  $V$  and constant energy  $E$ .

NPT: constant number of particles  $N$ , constant pressure  $P$  and constant temperature  $T$ .

NVT: constant number of particles  $N$ , constant volume  $V$  and constant temperature  $T$ .

The NVE ensemble is also known as the microcanonical ensemble and it may be obtained by solving the Newtons equation of motion without any pressure or temperature control. This ensemble is not appropriate when the system of interest is in the equilibration stage. The NPT (isothermal-isobaric) ensemble allows control of both the pressure and temperature. This method is useful for solvated molecular systems and when periodic boundary conditions (explained later on) are applied. The pressure is adjusted by changing the volume and the size of the system. The NVT ensemble (grand canonical ensemble) allows control of both the volume and the temperature. This method is usually useful when the simulations are performed in vacuum and without periodic boundary conditions (81).

Temperature is a very important variable during molecular dynamics simulations since it is directly related to the average kinetic energy of a system (96). It can be calculated as following:

$$\sum \frac{(p_i)^2}{2m_i} = \frac{k_B T}{2(3N - N_c)} \quad \text{Eq 2.21}$$

In the equation  $p_i$  is the total momentum of an atom  $i$  with a mass  $m_i$ ,  $T$  is the thermodynamic temperature.  $N_c$  is the number of constraints in the system and  $N$  the number of particles in a system each with three degrees of freedom.  $k_B$  is the Boltzman constant. The thermodynamic temperature can be controlled as stated earlier by the kinetic energy of the system. In order to maintain the temperature during a simulation the velocities of the atoms need to be adjusted. The atomic velocity is calculated by the Maxwell-Boltzman distribution. The probability that a system will have a configuration with energy  $E$  is proportional to  $\exp(-E/k_B T)$  (96).

Several methods exist to control the temperature during molecular dynamics simulations like the Berendsen, Nosé-Hoover and Andersen.

In Berendsen's method of temperature-bath coupling the velocities of the atoms are multiplied by a factor lamda  $\lambda$  which can be characterised as following:

$$\lambda = \left[ 1 + \frac{\Delta t}{\tau} (T - T_0) \right]^{1/2} \quad \text{Eq 2.22}$$

Where  $\Delta t$  is the timestep size,  $\tau$  is a characteristic relaxation time (picoseconds).  $T_0$  is denoted as the target temperature and  $T$  the instantaneous temperature (81).

In the Nosé-Hoover method an additional degree of freedom is applied in the molecular system which is a fictitious mass  $Q$ . The Newton equations of motion are solved for both real and fictitious system as following:

$$H^* = \sum \frac{(p_i)^2}{2m_i} + \phi(q) + \left( \frac{Q}{2} \right) \zeta^2 + gkT \ln S \quad \text{Eq 2.23}$$

Where  $H^*$  is the Hamiltonian function of potential energy as a function of coordinates and momenta. Real coordinates and momenta are denoted as  $q$  and  $p$  respectively. The corresponding fictitious coordinates and momenta are  $S$  and  $\zeta$ . The interaction potential is  $\phi$  (54, 81).

Another important variable that can be controlled in molecular dynamics simulations is the pressure. Unlike the temperature, the velocities of the atoms are not affected but rather the volume of the simulation system is modified by scaling the coordinates of the particles by a factor  $\varphi$  which is similar to Eq 2.22 (54).

$$\varphi = \sqrt[3]{1 - k \frac{\Delta t}{\tau} (P_{desired} - P_{actual})} \quad \text{Eq 2.24}$$

Where  $\Delta t$  is the timestep size,  $\tau$  is a characteristic relaxation time (picoseconds) and  $k$  is the compressibility of the system. This approach to constant pressure simulations suggested by Berendsen and co-workers allows the volume to fluctuate by changing uniformly not the shape but rather the dimensions of the system (54).

### 2.5.1 Periodic boundary conditions

When doing calculations on biological molecules it is becoming more frequent to do them in the presence of a solvent like water. This however brings further complications due to two main problems. The first being the increased CPU time due to the large number of atoms. The second problem is that the water molecules surrounding the biomolecule tend to drift away from it and get ‘lost’ during the calculation. These two problems can be solved using the Periodic Boundary Conditions. According to this method a molecule of interest solvated by water can be placed in a box of a specific size and then surround that box with infinite images of itself in all directions (Fig 2.9). The solute in the box of interest only interacts with its nearest neighbour images. When a molecule leaves a box, its image enters from an adjoining copy hence the total amount of particles is conserved. Each image cell is identical at the atomic level with the parent cell and as each atom undergoes changes at the same time its image will in every copy (54, 63).

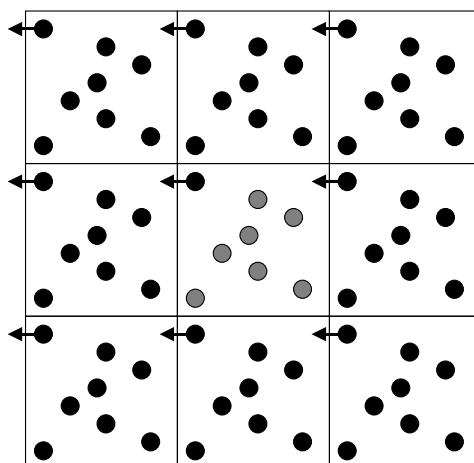


**Figure 2.9 Periodic boundary conditions.** Parent box with molecules shown in grey is surrounded by its images in two dimensions. As one molecule leaves the box (black circle with arrow) its image enters from the other side.

The geometry of the periodic box used may affect the total number of pairwise interactions. The cubic or rectangular boxes are the simplest and most commonly used for



periodic boundary conditions. However there are cells with different shapes that might be more appropriate for a given simulation. Some of these shapes are the hexagonal prism, the truncated octahedron and the rhombic dodecahedron. The software programs used to energy optimise the system are also capable of solvating the molecule of interest including the surface and the cavities of the molecule filling up the whole space of the periodic box (63).

### 2.5.2 The cut-offs of non-bonded energy terms

The most time consuming part of the molecular modelling simulations is the calculation of the non-bonded interactions. In order to save computer time, it is usual to neglect non-bonded interactions that occur between atoms separated by more than a given distance (say 10-20 Å). So when a ‘cut-off’ is applied the interactions between all pairs of atoms that are further apart from the cut-off value are set to zero. It should be noted that when periodic boundary conditions are used the value of the cut-off should be less than half the length of the box so that the molecule does not see its image (63).

It is very common that when large systems are simulated, group-based cut-offs are used. In group-based cut-offs the molecules are divided into groups which are composed of a relatively small amount of atoms. For example solvent molecules like water are often regarded as a single group. In the case of larger molecules for example like in Figure 2.10 the molecule is divided in small groups (81).

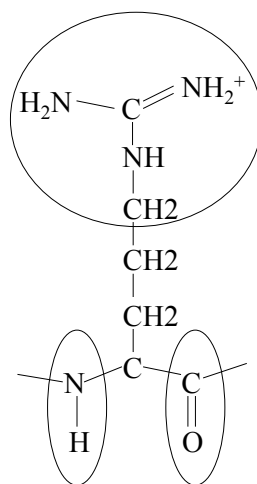


**Figure 2.10 Separation of an amino acid residue of a protein into charge groups.**

It would be ideal if the charge-groups have a net charge of zero; however it is not always possible to arrange atoms in neutral groups and some of them will be charged. Usually charge groups have a size of 1-3 Å. Some of them can be larger, in such a case the cut-off distance must be increased.

It has been considered that the use of a non-bonded cut-off does not affect the accuracy of the calculation of the van der Waals interactions, since they tend to zero very quickly as the distance between the two atoms increases, however for calculation of the electrostatic interactions, the use of a cut-off cannot be easily justified and may lead to errors due to the long range interactions (60). One way to solve this problem is to use a bigger simulation box, however sometimes this is impossible and impractical either due to limitations on the amount of atoms that can be simulated by the software or increasing computer power is inadequate to deal with long-range forces. Mathematical functions such as the Particle Mesh Ewald (PME) and the cell multipole methods have been used to approximately correct for long-ranged electrostatic interactions.

The PME method is particularly useful for simulations involving highly charged systems like lipid bilayers, proteins and DNA. It is considered though to be a computationally expensive method. It divides the potential energy into the Ewald's direct and reciprocal sum and uses conventional Gaussian charge distributions. The direct term is evaluated using cut-offs whereas the reciprocal term is approximated using fast Fourier transform algorithm (FFT) where each atomic point charge is distributed among surrounding grid points. The more grid points are used the more accurately the potential of the charge is approximated at that location and the more time consuming is this procedure (63).

Cell multipole algorithm is another method which enables all  $N(N-1)$  pairwise non-bonded interactions to be approximated. In contrast to Ewald summation it scales linearly with  $N$  rather than  $N^2$ . In this method the simulation space is divided into uniform cubic cells. In each cell the multipole moments like charge, dipole and quadrupole are calculated by summing all the atoms inside the cell. The interactions between the atoms inside the cell and outside the cell or from another cell can be calculated using the multipole expansion. More specifically for interactions within one cell (i.e. within few Å) the atomic pairwise interaction method is used, however for interactions that are more than one cell distance away then the Taylor's series of multipole expansion are used (81).

## 3 Materials

---

### 3.1 Chemicals

Agarose	Karl Roth, Karlsruhe
Calcium chloride	Fluka, Taufkirchen
Cisplatin (Platinex <sup>®</sup> )	Bristol-Myers Squibb, Munich
DMSO (Dimethylsulfoxide)	Fluka, Taufkirchen
DTT (Dithiothreitol)	Sigma-Aldrich, Taufkirchen
EDTA (Ethylendiamintetraacetate)	Sigma-Aldrich, Taufkirchen
Ethanol 100%	Mallinckroft Baker, Deventer -Holland
Ethidium bromide	Roche, Mannheim
HEPES (Hydroxyethylpiperazinethansulfonic acid)	Sigma-Aldrich, Taufkirchen
Magnesium chloride	Merck, Darmstadt
Magnesium sulfate	Merck, Darmstadt
PMSF (Phenylmethyl-sulfonyl fluoride)	Sigma-Aldrich, Taufkirchen
Potassium phosphate	Merck, Darmstadt
Potassium chloride	Fluka, Taufkirchen
SDS (Sodiumdodecylsulfate)	BioRad, München
Sodium chloride	Merck, Darmstadt
Sodium phosphate	Merck, Darmstadt
Tris	Karl Roth, Karlsruhe

### 3.2 Proteins, enzymes and plasmids

Albumin (human serum albumin)	Sigma-Aldrich, Taufkirchen
Trypsine	Roche, Mannheim
pcDNA3.1	Eucaryotic expression vector Invitrogen, Karlsruhe

### 3.3 Cell culture media, sera and culture plates

DMEM	Gibco, Karlsruhe
Gold fetal calf serum	PAA, Marburg
L-Glutamin	Merck, Darmstadt
100x Non-essential amino acids	Gibco, Karlsruhe
MEM	Gibco, Karlsruhe
Penicillin G	Hoechst, Frankfurt
Streptomycine	Sigma-Aldrich, Taufkirchen
RPMI1640	Gibco, Karlsruhe
Cell culture plates 25 and 75 cm Ø	Biochrom, Berlin
96 microtiter well plates	Peter Oehmen, Essen
White opaque 96 microtiter well plates	Nunc, Karlsruhe

### 3.4 Molecular weight standard

1 kb DNA ladder	Promega, Mannheim
-----------------	-------------------

### 3.5 Kits

Apo-One Homogeneous Caspase 3/7 Assay	Promega, Mannheim
Cell Titer 96 AQueous One Solution	Promega, Mannheim
Cell Proliferation Assay	

### 3.6 Laboratory instruments

96 Microtiter well spectrophotometer	MRXII, Dynex Technologies
96 Microtiter well fluorescence spectrophotometer	FL600, Biotek Instruments
Gamma counter	1480 Wizard™, Wallack
Eppendorf Centrifuge 5417R	Eppendorf, Hamburg
Electrophoresis power supply Phero-stab.200	Peter Oehmen, Essen

### 3.7 Buffers and solutions

Hypotonic Buffer	10 mM HEPES, pH 7.5 1.5 mM MgCl <sub>2</sub> 5 mM NaCl 0.2 mM PMSF 0.5 mM DTT
50 mM NaCl Buffer	50 mM NaCl in 20 mM HEPES pH 7.9 at 4°C 1.5 mM MgCl <sub>2</sub> 0.2 mM EDTA 0.2 mM PMSF 0.5 mM DTT
0.4 M NaCl Buffer	0.4 M NaCl in 20 mM HEPES pH 7.9 at 4°C 1.5 mM MgCl <sub>2</sub> 0.2 mM EDTA 0.2 mM PMSF 0.5 mM DTT
0.8 M NaCl Buffer	0.8 M NaCl in 20 mM HEPES pH 7.9 at 4°C 1.5 mM MgCl <sub>2</sub> 0.2 mM EDTA 0.2 mM PMSF 0.5 mM DTT
TAE	40 mM Tris-Acetate 1 mM EDTA

PBS	4 mM MgSO <sub>4</sub> 7 mM CaCl <sub>2</sub> 1.4 mM KH <sub>2</sub> PO <sub>4</sub> 137 mM NaCl 2.7 mM KCl 6.5 mM Na <sub>2</sub> HPO <sub>4</sub>
-----	--

### 3.8 Cell lines

BLM	Established human melanoma cell line, frequently metastatic (113).
CCD-919Sk	Established human skin fibroblast cell line (ATCC) (2).
HeLa	Established human cervical cancer epithelial cell line (ATCC) (2).
Hek-12	Established human embryo kidney epithelial cell line transformed with adenovirus 12 DNA (118).
MC3T3-E1	Established mouse fibroblast cell line (ATCC) (2).
MOR/P	Established human lung cancer cell line (53).
MOR/CPR	Human lung cancer cell line cisplatin resistant subline (53).
MV3	Established human melanoma cell line, frequently metastatic (112).
SK-ES-1	Established human osteosarcoma epithelial cell line (ATCC) (2).
SK-Mel-28	Established human melanoma cell line (ATCC) (2).
U-2OS	Established human osteosarcoma epithelial cell line (ATCC) (2).

## 4. Methods

---

### 4.1 Computational methods

Molecular mechanics and dynamics simulations were performed using the Discover 3 module of Accelrys where as molecular docking simulations were performed using the Affinity module.

#### 4.1.1 Molecular structures

##### (a) Formation of Au<sub>13</sub> nanowires-Nanotechnology

The crystal structures of dodecameric A-DNA and B-DNA (PDB:1BNA) molecules were obtained from the “Protein Data Bank” (PDB)(5) . Hydrogen atoms were added to each structure. Two copies of each crystal structure were joined by phosphodiester bonds to form a 24 A-DNA or B-DNA molecules, respectively.

##### (b) Anticancer properties of Au<sub>55</sub>-Medicine

The crystal structures of decameric and dodecameric B-DNA molecules were obtained from the PDB. The molecules investigated can be found in the PDB under the following names, 1BNA, 1DN9, 1D65, 167D and 1D28, Hydrogen atoms were added to each structure prior energy minimisation.

The crystal structure of monomeric albumin protein (PDB:1AO6) was obtained from the PDB. The missing hydrogens were added at a pH value of 7 prior application of the PCFF forcefield (71, 109) and subsequent minimisation.

### 4.1.2 Molecular mechanics simulations

The molecular mechanics simulations were performed using the Steepest Descents and subsequent Conjugate Gradient algorithms for large molecules like DNA and albumin protein whereas for small molecules like gold clusters Au<sub>13</sub> and Au<sub>55</sub> the Newton-Raphson algorithm was used. The main forcefield used in this study is the PCFF.

The PCFF forcefield is a second generation forcefield which is appropriate for simulations performed on nucleic acids, carbohydrates and lipids, and includes Lennard-Jones parameters for many metals including Au. It has also been parameterised for calculations performed for zeolites. The analytical form of the potential energy expression used in PCFF is shown below (71, 109).

$$E_{pot} = \sum_b [K_2(b-b_0)^2 + K_3(b-b_0)^3 + K_4(b-b_0)^4] \quad \text{bond stretching (1)}$$

$$+ \sum_\theta [H_2(\theta-\theta_0)^2 + H_3(\theta-\theta_0)^3 + H_3(\theta-\theta_0)^4] \quad \text{angle bending (2)}$$

$$+ \sum_\phi [V_1 [1 - \cos(\phi - \phi_1^0)] + V_2 [1 - \cos(2\phi - \phi_2^0)] + V_3 [1 - \cos(3\phi - \phi_3^0)]] \quad \text{torsions (3)}$$

$$+ \sum_\chi K_\chi \chi^2 \quad \text{out_of_plane (4)}$$

$$+ \sum_b \sum_{b'} F_{bb'}(b-b_0)(b'-b'_0) \quad \text{bond stretching-bond stretching (5)}$$

$$+ \sum_\theta \sum_{\theta'} F_{\theta\theta'}(\theta-\theta_0)(\theta'-\theta'_0) \quad \text{angle bending\_angle bending (6)}$$

$$+ \sum_b \sum_\theta F_{b\theta}(b-b_0)(\theta-\theta_0) \quad \text{bond stretching\_angle bending (7)}$$

$$+ \sum_b \sum_\phi (b-b_0)[V_1 \cos \phi + V_2 \cos 2\phi + V_3 \cos 3\phi] \quad \text{bond stretching\_torsions (8)}$$

$$+ \sum_{b'} \sum_\phi (b'-b'_0)[V_1 \cos \phi + V_2 \cos 2\phi + V_3 \cos 3\phi] \quad \text{bond stretching\_torsions (9)}$$

$$+ \sum_\theta \sum_\phi (\theta-\theta_0)[V_1 \cos \phi + V_2 \cos 2\phi + V_3 \cos 3\phi] \quad \text{angle bending\_torsions (10)}$$

$$+ \sum_\phi \sum_\theta \sum_{\theta'} K_{\phi\theta\theta'} \cos \phi (\theta-\theta_0)(\theta'-\theta'_0) \quad \text{angle bending\_torsions\_angle bending (11)}$$



$$+ \sum_{i>j} \frac{q_i q_j}{\epsilon r_{ij}} \quad \text{coulomb (12)}$$

$$+ \sum_{i>j} \left[ \frac{A_{ij}}{r_{ij}^9} - \frac{B_{ij}}{r_{ij}^6} \right] \quad \text{van der Waals (13)}$$

The first four terms calculate the bonding interactions between two atoms. Terms 5-11 calculate the cross terms. Terms 12 and 13 calculate the non-bonding interactions such as the Coulombic interaction between the atomic charges and van der Waals forces, respectively.

#### 4.1.3 Molecular dynamics simulation of Au<sub>13</sub> clusters with A-DNA molecules

Minimisation of DNA structures is a molecular mechanics simulation occurring at a temperature of 0 °K. Molecular dynamics simulations represent a more realistic system resulting at a specific temperature. The behaviour of molecules in vacuo or in the presence of solvents, and specific interactions with various ligands can be then studied in great detail. An energy-minimised system with four DNA molecules, each comprising four Au<sub>13</sub> clusters, was used for the molecular dynamics simulation. The entire system was placed in a cubic box with periodic boundary conditions. Periodic boundary conditions imitate a bulk system. They enable a dynamic simulation to be performed using a relatively small number of particles. A cubic box with the A-form DNA-Au<sub>13</sub> system can be duplicated in all directions to give a periodic system. The dimensions of the simulation box were 60 × 75 × 60 Å. The simulation was performed at constant number of particles (N), constant pressure (P) of 10<sup>5</sup> Pa and constant temperature (T) of 300 °K. The cut-offs applied for the intermolecular van der Waals and electrostatic interactions were each 12.5 Å. The molecular dynamics simulation was performed for 500 picoseconds, and trajectories were saved every 200 fs for subsequent analysis.

Molecular dynamics simulations were also performed on a single DNA structure with four Au<sub>13</sub> clusters. The trajectory with the lowest potential energy was used for further analysis. The difference in potential energy ( $\Delta E^P$ ) between the potential energy of the single DNA structure with Au<sub>13</sub> clusters ( $E^P_1$ ) and the potential energy of the four DNA structures with Au<sub>13</sub> clusters ( $E^P_4$ ) was calculated as following:  $\Delta E^P = 4 \times (E^P_1) - E^P_4$

Of the two types of gold clusters used in this study, only the Au<sub>13</sub> cluster was used to investigate its interactions with the major grooves on the A-DNA molecule because, as explained previously, this structure is consistent with experimental observations. Four Au<sub>13</sub> clusters were positioned along the phosphate backbone of a single DNA molecule, corresponding to every second or third phosphate residue; however, in the case of B-DNA, both Au<sub>13</sub> and Au<sub>55</sub> were studied separately to assess any respective interactions with the major grooves of the B-DNA. Three Au<sub>55</sub> clusters were arranged along the phosphate backbone of B-DNA, and four Au<sub>13</sub> clusters were arranged in the major grooves throughout the helix of the B-DNA molecule.

#### 4.1.4 Molecular dynamics simulations of zeolite beta with various amino acids

The zeolite beta (BEA) structure was constructed having the Miller plane 010. Its surface was hydroxylated. The amino acids lysine, phenylalanine and glutamic acid protonated according to pH=6 (Figure 4.1).

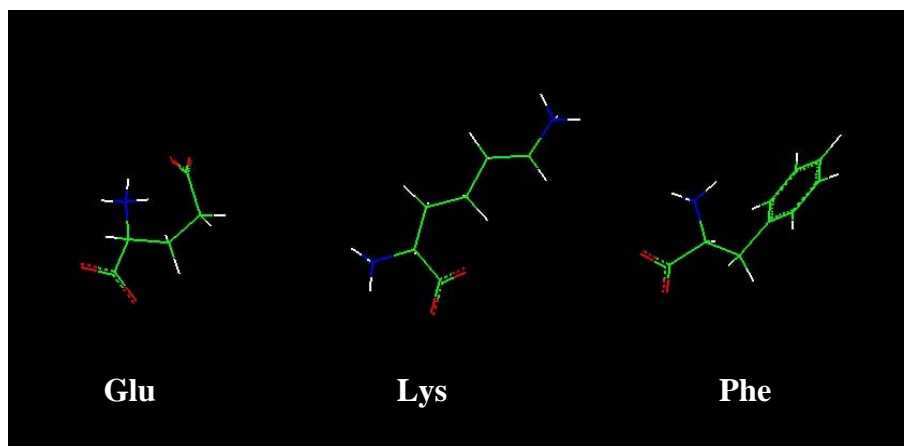


**Figure 4.1 Molecular models of the amino acids glutamic acid, lysine and phenylalanine.** In green colour are indicated the C atoms, in red the O atoms, in blue the N atoms and in white the H atoms. Bonds indicated in dotted lines represent the partial double bonds.

Zeolite and amino acid structures were minimised separately using the PCFF forcefield. For MD simulations the zeolite with a single amino acid being located at different positions was placed in a box and then solvated with water molecules. As shown in Figure 4.2, each amino acid was placed at the surface of different sides of the 3D zeolite structure, at the bulk phase as well as inside one of the pores.

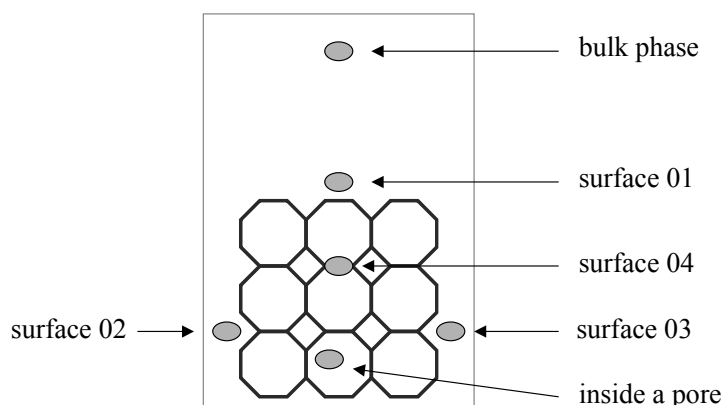


**Figure 4.2 Schematic representation at one dimension of the different positions of an amino acid being placed around the zeolite structure.** For each MD simulation one amino acid depicted in grey colour, was placed inside the simulation box at different locations at the surface of the zeolite, at the bulk phase or inside one of the zeolite's pore.

The dimensions of the simulation boxes varied for each case. MD simulations were performed using the PCFF forcefield at 300 °K using the NVT ensemble. The cut-off values for the non-bonded intermolecular interactions was chosen to be 12.5 Å. The simulations were performed up to 200 ps with the resulting structures being collected into a trajectory file every 200 fs. In total 18 MD simulations were performed and the average total energies of each zeolite-amino acid system were compared after the simulations were finished. Since all the structures which are collected in the trajectory files can not be presented as an animation in the thesis, for this reason adsorption of amino acids onto the zeolite surface are presented as graphs. In the graphs the distances between the center of the mass of each amino acid, of the amino group, of the carboxyl group and the zeolite structure are separately measured. Since the zeolite structure contains many pores and cavities a plane is constructed on its surface as indicated on Figure 4.3.

**Side view of plane                      Front view of the plane**

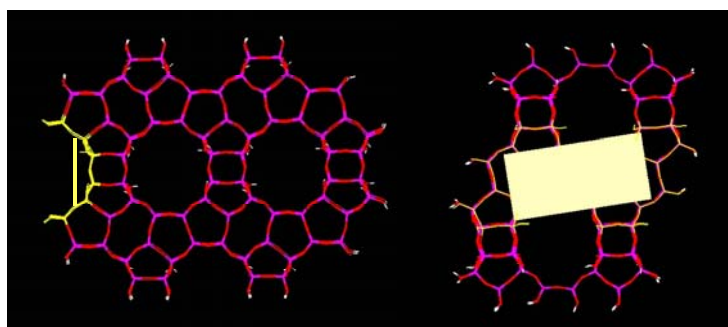


**Figure 4.3 Construction of a plane on the zeolite surface.** Atoms located on the surface of the zeolite are presented in yellow and are used by the program to construct a plane.

#### 4.1.5 Molecular docking simulations

The docking method used for the simulations of DNA or albumin molecules with Au<sub>55</sub> is the fixed docking method which uses a Monte-Carlo type procedure to automatically dock a guest molecule to a host. The program evaluates the calculated energies and checks whether a docked structure is acceptable. One of the advantages of this method is that it allows during docking, both guest and ligand structure to be energetically minimised while the rest of the structure remains rigid. In addition after docking Affinity uses molecular mechanics for further refinement of the docked guest-ligand structure.

As a binding site for the docking simulations of DNA molecules, the nitrogen, oxygen and phosphorus atoms were considered. During the docking procedure these atoms are allowed to move while the rest of the atoms in the DNA molecules like the positions of the carbon and the hydrogen atoms remained rigid.

In the case of albumin docking we separated the monomeric protein into three domains as stated by the literature (12). Each docking simulation considered one only domain each time as a binding site while the rest were kept rigid. In addition for each simulation a cysteine residue was chosen as a starting docking point.

A flow chart of the docking procedure is given in Figure 4.4. The starting structures (ligand and receptor) used for the docking simulations should always be previously energetically optimised in order to minimise any steric hindrance. The program also minimises the structures and saves them as the starting structures, however it is faster if the molecules of interest are previously energy minimised. The docking method is based on the Monte Carlo simulation procedure which causes random changes in the structure of the molecules rather than applying a force like MD simulations. These structural changes are caused by applying translation, rotation and torsional changes. After these three basic movements the program evaluates the potential energies of the randomly moved structures. If the energies are within a user-specified energy tolerance parameter of the previous then the docked structure is accepted. The docked structure is minimised to avoid any bad contacts between the ligand and the receptor. The minimised docked structure is further evaluated based on energy criterion and similarity to previous docked structures. The energy criteria that can be used are the *energy range* or *Metropolis*. If the user chooses the Metropolis then the docked structure whose energy is lower than that of the last accepted

structure, or whose Boltzman factor is greater than a random number between zero and one, are accepted. If the user chooses the energy range as a criterion then the docked structures whose energy is within a user-specified energy range of the lowest energy obtained so far is accepted. Usually the energy range is used to obtain more diverse structures where as Metropolis is used only when the investigator wants to obtain few only structures with low energies.

The algorithm also checks for structure similarity by calculating the root mean square (RMS) distances between a docked structure and all the structures found so far. The RMS distances are calculated only for the ligand atoms. It should be noted that RMS distance is different from RMS deviation since on the first one no superimposition is done by translating and rotating the ligand.

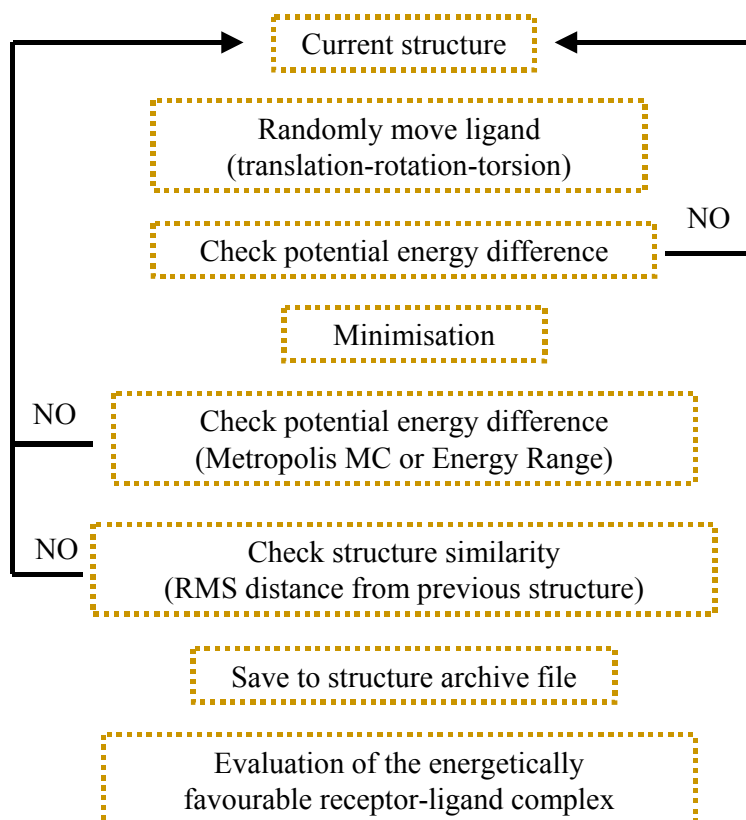


**Figure 4.4 Representation of the docking procedure in the form of a flowchart.**

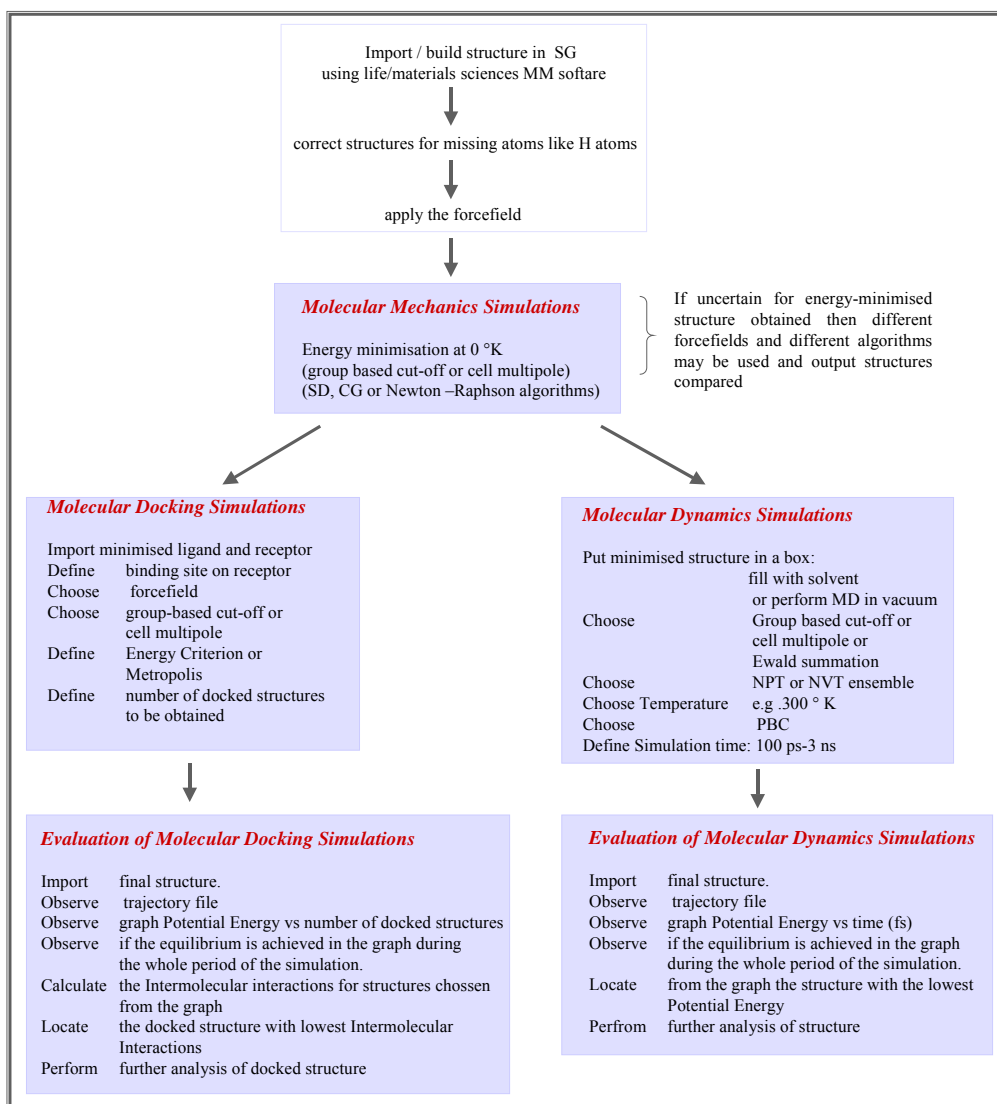
Even though the docking algorithm minimises the docked structures it has been found that the minimisation performed is not enough, so docked structures are further refined by energy optimisation. For the treatment of the long-range electrostatic forces the *cell multipole* method was used. Energy minimisation was performed using the *Steepest*

*descents* and the *Conjugate Gradient Polak-Ribiere* method. The atom types and partial charges were assigned according to the PCFF forcefield.

After energy optimisation all the docked structures are evaluated based on the intermolecular interactions which is the sum of the Coulomb and van der Waals interactions. The docked structures which obtain the lowest intermolecular interaction is the most favourable docked structure.

### 4.1.5 Molecular modelling flowchart

Below is a flowchart describing the main steps followed for the molecular modelling procedures used so far in this study. It is provided in order for the reader to understand the sequence of steps that occurs from building structures until the final structures are obtained after molecular mechanics, docking or dynamics simulations.



## 4.2 Experimental methods

### 4.2.1 Synthesis of gold cluster Au<sub>55</sub>

Au<sub>55</sub> clusters were prepared by Mrs Giebel at the Institute for Inorganic Chemistry as described in the literature (97). The cluster is made of fifty-five gold atoms surrounded by twelve water soluble monosulfonated triphenylphosphane ligand molecules (Figure 4.5).

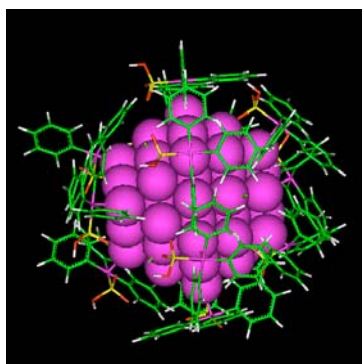


**Figure 4.5 Schematic representation of gold cluster Au<sub>55</sub>.** The cluster is made of fifty-five gold atoms indicated in purple and is surrounded by twelve water soluble monosulfonated triphenylphosphane ligand molecules indicated in green with the sulfur atoms being shown in yellow.

### 4.2.2 Cell culturing and maintenance

Most of the cell lines used in this study are human cultured cell lines. HeLa and Hek cell lines were maintained in DMEM medium with 10% fetal calf serum (PAA Laboratories), 2 mM L-glutamine essential amino acids (Gibco), and antibiotics. MOR/P and MOR/CPR were kindly provided by Dr Müller (Institute for Clinic and Policlinic, University of Duisburg-Essen Medical School). Both cell lines were grown in RPMI medium with 10% FCS, 2 mM L-glutamine and antibiotics, however medium for MOR/CPR was also supplemented with 1 µg/ml cisplatin (Platinex<sup>®</sup>, Bristol-Myers Squibb). The cell lines U-2 OS and MC3T3-E1 were a generous gift from Prof. Bingman (Institute for Physiology, University of Duisburg-Essen Medical School), U-2OS was maintained in DMEM medium with 10% FCS, 2 mM L-glutamine and antibiotics where as MC3T3-E1 in MEM 10% FCS, 2 mM L-glutamine essential amino acids and antibiotics. SK-ES-1 and CCD-919K were obtained from the American Cell Culture Collection. SK-ES-1 was grown on Quantum media, where as CCD-919Sk was maintained in MEM with 10% FCS, 2 mM L-glutamine



essential amino acids and antibiotics. The metastatic melanoma cell lines BLM and MV3 were kindly provided by Dr Opalka ( Institute for Clinic and Policlinic, University of Duisburg-Essen Medical School). Both cell lines were grown in DMEM medium with 10% FCS, essential amino acids 2 mM L-glutamine and antibiotics.

SK-Mel-28 were a generous gift from Prof. Goos, (Institute for Dermatology, University of Duisburg-Essen Medical School). SK-Mel-28 was grown in MEM medium with 10% FCS, 2 mM L-glutamine, essential amino acids and antibiotics. Cells were incubated at 37 °C in air containing 5% CO<sub>2</sub> and the culture medium was changed after three days.

#### **4.2.3 *In vitro* cytotoxicity assays- MTT**

*In vitro* cytotoxicity was investigated by the MTT assay (Cell Titer 96 AQueous One Solution Cell Proliferation AssayPromega) a colourimetric method according to which a tetrazolium-based compound is reduced in formazan by living cells. The amount of formazan produced is directly proportional to the number of living cells in the culture. Each cell line was incubated for 48 hours at 37 °C with 5 % CO<sub>2</sub> before the addition of drugs in 96 well microtiter plates in the appropriate media. Fresh medium containing various concentrations of cisplatin (Platinex<sup>®</sup>, Bristol-Myers Squibb) or Au<sub>55</sub> was added to each well and the microtiter plates were incubated further for 72 or 24 hours. After incubation with each drug, 35 µl of the tetrazolium-based compound was given to each well. The plates were incubated for three hours at 37 °C with 5% CO<sub>2</sub>. The microtiter plates were measured with a spectrophotometer at 490 nm.

In order to investigate the effect of albumin or higher concentration of fetal FCS on the activity of Au<sub>55</sub>, the same assay was performed as described above however, the gold cluster was incubated in fresh media for about twenty hours with 30 µg/ml albumin or in medium which contained 20 % of FCS before it is given in the cells. The microtiter plates were incubated further for 24 hours and the MTT assay was performed as described above.

#### **4.2.4 Apoptosis / Necrosis assays**

The induction of apoptosis in cancer cells by anticancer drugs is an important aim for the treatment of malignant tumors. Caspase activation has been considered as one of the major

steps in the genesis of apoptosis. The measurement of the activities of the caspases -3 and -7 were performed with Apo-One Homogeneous Caspase 3/7 Assay provided by Promega. This fluorometric assay uses a profluorescent substrate which contains a peptide DEVD conjugated with rhodamine 110. In the presence of caspase 3/7 activity the peptide is cleaved and the amount of the fluorescent product generated is directly proportional to the amount of caspase -3 and -7 present in the sample. Each cell line was incubated for 24 hours at opaque white microtiter plates before the addition of the drugs. Cells were incubated with various concentrations of Au<sub>55</sub> for 2 hours. After incubation the medium was removed and the cells were incubated in drug-free media for 22 hours. Various cell lines were also incubated with Au<sub>55</sub> or cisplatin for 24 hours. After incubation the media were removed and the cells were suspended in PBS. Aliquots of 100 µl of the profluorescent substrate were added into the microtiter wells. The plates were shaken gently and were incubated for 3 hours at 37 °C with 5% CO<sub>2</sub>. After incubation the plates were read in a fluorescent reader.

#### **4.2.5 Agarose gel electrophoresis**

Plasmid DNA ( 0.1 µg/µl ) was incubated in eppendorf tubes in a final volume of 20 µl in PBS with 0.00008% H<sub>2</sub>O<sub>2</sub> and with or without various concentrations of Au<sub>55</sub> for 24 hours at room temperature. After incubation each aliquot was loaded in a 0.8% agarose gel ( with ethidium bromide). The gel was run in 1% TAE buffer at 75 Volt . After electrophoresis the gel was visualised with UV light and a photograph was taken with a camera.

#### **4.2.6 Cellular fractionation**

Gold clusters were initially prepared as described in section 4.2.1. The clusters were gamma-irradiated (Atomic Reactor in Kernforschungsstoff Jülich).

BLM cells were grown at 37 °C in 25 ml culture flasks until cells were sub-confluent in 10 ml of DMEM supplemented with serum and antibiotics as described above. Cells were exposed to 0.1 µM, 0.5 µM and 1.0 µM radioactive gold clusters for 3, 6 and 24 hours, with the exception that BLM cells were incubated with 1 mM Au<sub>55</sub> up to 6 hours since after 24 hours the cells do not survive. Each culture has been performed in triplicate. After incubation cells were washed twice with cold PBS, trypsinised and re-suspended in 3 ml of

PBS. Cells were collected in eppendorf tubes and centrifuged at  $1,000 \times g$  for 5 min. Cells were re-suspended once more in 1 ml PBS and were centrifuged at  $2,500 \times g$  for 2 min. Cell pellets were re-suspended in 50  $\mu$ l hypotonic buffer solution. The pellets were frozen for 30 sec in dry ice-ethanol and then thawed for another 30 sec at 37 °C water bath. This freeze-thawing procedure was performed 3 times for each pellet in order to disrupt the cell membrane. To each sample 1.25  $\mu$ l of 0.1 M NaCl was added and incubated for 10 min on ice. Cells were centrifuged for 1 min at  $10,000 \times g$ . The supernatants which contain all the cytoplasmic and cell membrane components were kept aside for analysis. The pellets which consist of the cell nuclei were further washed twice with 100  $\mu$ l of 50 mM NaCl buffer. Pellets were re-suspended in 100  $\mu$ l of 0.4 M NaCl buffer. The pellets were shaken gently for 30 min at 4 °C to extract the nuclear proteins. The samples were centrifuged for 5 min at  $10,000 \times g$ . After centrifugation the supernatant which contained the nuclear extract was kept aside for analysis. The pellets which contained chromosomes and remaining proteins including histones were further analysed. Each pellet was washed twice with 100  $\mu$ l of 0.4 M NaCl buffer and then re-suspended in 100  $\mu$ l of 0.8 M NaCl buffer. Pellets were shaken gently for 30 min at 4 °C to extract the nuclear proteins and then centrifuged at  $10,000 \times g$  for 5 min. After centrifugation, both pellets which were composed of genomic DNA, and supernatants which contained nuclear proteins, were kept aside for further analysis.

During the extraction procedure a large variety of samples were collected including those obtained prior to cell extraction like medium changes, PBS washes, as well as trypsinisation. During all these steps samples were collected and radioactivity was measured with a gamma counter. Each measurement has been corrected for the half life of radioactive  $^{198}\text{Au}$ .

## 5. Results

---

### 5.1 Interactions between Au clusters and DNAs: formation of nanowires

#### 5.1.1 Characterisation of naked A- and B-DNA structures after minimisation.

DNA structures of the A- and B- forms have different geometries in terms of their major and minor grooves (Figure 5.1). The A-DNA used for these simulations is 6.0 nm long. The major groove is deeper and broader than that of the B-DNA. Its dimensions are 1.33 nm deep and 0.74 nm long. The minor groove is very shallow. It has a depth of about 0.2 nm but a length of 1.5 nm. The groove geometry of this form of DNA is appropriate for the accommodation of Au<sub>13</sub> clusters. Each Au<sub>13</sub> cluster is about 0.314 nm long. In addition, the phosphates along the major grooves are orientated towards the groove and can hold the Au<sub>13</sub> clusters more tightly. The B-DNA is 7.74 nm long. Its groove geometry is significantly different from that of the A-DNA. It is composed of distinct major and minor grooves. The major groove is much higher but less deep than that of the A-form. It has a depth of 0.9 nm and a length of 1.43 nm. Such dimensions can accommodate a Au<sub>55</sub> cluster, i.e. a diameter of 0.862 nm. The minor groove of the B-form is shallower than the major groove. Its dimensions are 0.75-0.85 nm long and 0.67 nm deep. The authors that provided the crystal structures of the A-form and B-form of DNA have not mentioned any length or depth values of the major or minor grooves. However it has been found that the depth values of our minimised structures are in agreement with the depth values of A- form and B-form DNA structures reported in other literature (30).

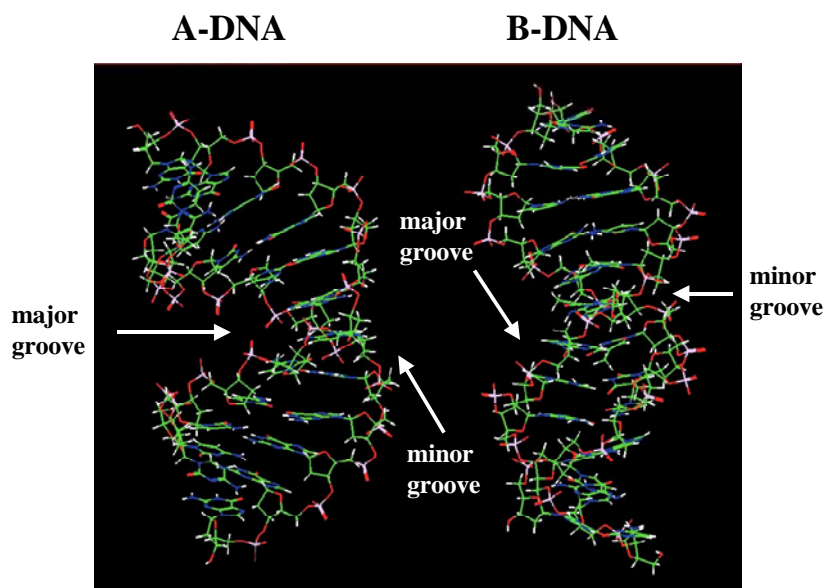


**Figure 5.1 Model structures of energy-minimised A-, and B-DNA molecules.** Each structure is characterised as double stranded with alternating subunits of phosphates and deoxyriboses stabilised by base-pair stacking and hydrogen-bond formation between the nitrogenous bases. The asymmetry of the DNA structures generates spaces which are denoted as major and minor grooves. The helical grooves are dependent on the interactions between DNA and solvent leading to the generation of different forms of DNA like the A- and B- form. The A-DNA is characterised as the dehydrated form of DNA where as B-DNA is the canonical form of DNA found in every living organism.

#### *Characterisation of A- and B- DNA with gold clusters*

DNA molecules, due to their helicity and groove geometry are composed of cavities that the gold clusters could accommodate themselves. Based on molecular mechanics simulations of DNA molecules with and without the gold clusters the stabilisation energies (i.e. difference in Potential Energy) have been calculated in order to understand which DNA groove each gold cluster would energetically prefer. The stabilisation energies were calculated based on the following formula.

$$\Delta E^{stab} = (E_{DNA}^P + E_{Au}^P) - (E_{DNA+Au}^P)$$

where  $E_{DNA}^P$  and  $E_{Au}^P$  are the potential energies of a single energy-minimised DNA structure and gold cluster respectively,  $E_{DNA+Au}^P$  is the potential energy of the minimised DNA-Au cluster complex.

The stabilisation energies shown below on Table 5.1 clearly indicate that  $Au_{13}$  prefers to interact with the major groove of the A-DNA where as,  $Au_{55}$  prefers to interact with the major groove of B-DNA.

	Major groove		Minor groove	
	Au <sub>13</sub>	Au <sub>55</sub>	Au <sub>13</sub>	Au <sub>55</sub>
A-DNA	-28	+75	+65	+237
B-DNA	-22	-286	+118	+163

**Table 5.1 Stabilisation energies calculated by energy-minimisation of the two forms of DNA with and without the gold clusters.** The minor groove is not preferred by any of the gold clusters as indicated by the positive stabilisation energies. The major grooves of the B-DNA is clearly preferred by the Au<sub>55</sub> as indicated by the lower negative stabilisation energies comparing to Au<sub>13</sub>. In the case of A-DNA, its major grooves are energetically preferred by Au<sub>13</sub> cluster than Au<sub>55</sub> as indicated by the low negative stabilisation energy.

Since in the TEM pictures the width of the nanowires is consistent with the width of the Au<sub>13</sub> cluster which is about 0.7 nm and since under vacuum conditions the DNA is dehydrated, this thesis will be focused on results which are based on the interactions of Au<sub>13</sub> with A-DNA. Based on the stabilisation energies which have indicated that the major grooves rather than the minor grooves are energetically preferred, molecular mechanics simulations were employed for investigating the interactions of A-DNA with many Au<sub>13</sub> clusters being decorated on its major grooves.

The A-form of DNA with Au<sub>13</sub> clusters is shown in Figure 5.2. The DNA structure is energy-minimised using the PCFF forcefield. Initially the Au<sub>13</sub> clusters were placed randomly around the phosphate backbone. In the resulting structure the actual distance between each Au<sub>13</sub> cluster is about 1.46 nm whereas the projection of each gold cluster from the other is about 0.5-0.6 nm. This value is in agreement with the distances between the Au<sub>13</sub> nanowires obtained by the TEM measurements at Prof. Schmid's laboratory.

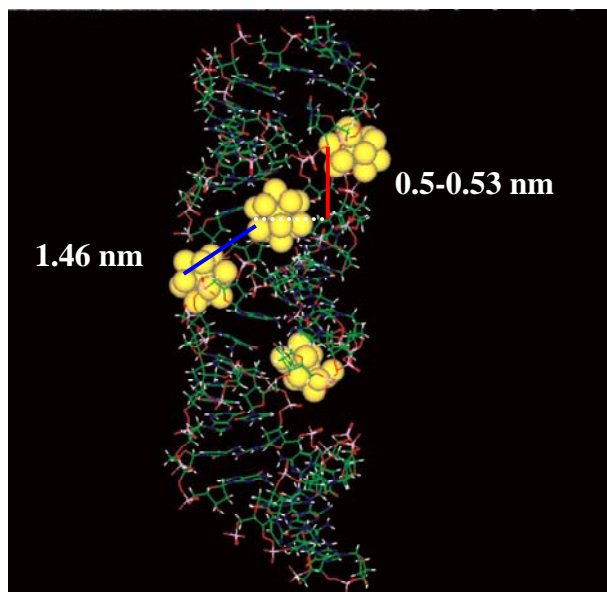


**Figure 5.2 Energy minimised structure of A-DNA with Au<sub>13</sub> clusters located along the phosphate backbone of the DNA major grooves.** Each Au<sub>13</sub> cluster is about 1.46 nm away from each other, however the projection distance of each cluster is measured to be between 0.50 and 0.53 nm.

### 5.1.2 Formation of Au<sub>13</sub> nanowires

Figure 5.3 shows different views of an A-form DNA-Au<sub>13</sub> system investigated by MD simulation under periodic boundary conditions. More specifically, two cubic boxes with only two DNA structures are visible (Figure 5.3a). The other two structures on each box are obscured. Two clusters on a single DNA molecule are spaced about 1.46 nm apart, and each corresponding Au<sub>13</sub> cluster on the adjacent DNA molecule is about 2.1 nm apart. If the whole system is rotated as shown in Figure 5.3b, a projection which shows a wire-like structure is obtained. The formation of four Au<sub>13</sub> wires is clearly observed; The majority of the Au<sub>13</sub> clusters are separated from one another by 0.47-0.68 nm; however there are two gold clusters that are about 0.8 Å apart and another two that have almost aggregated. The projection (Figure 5.3b) gives the illusion that the distance between each Au<sub>13</sub> cluster on a single wire is much smaller than 2.1 nm.

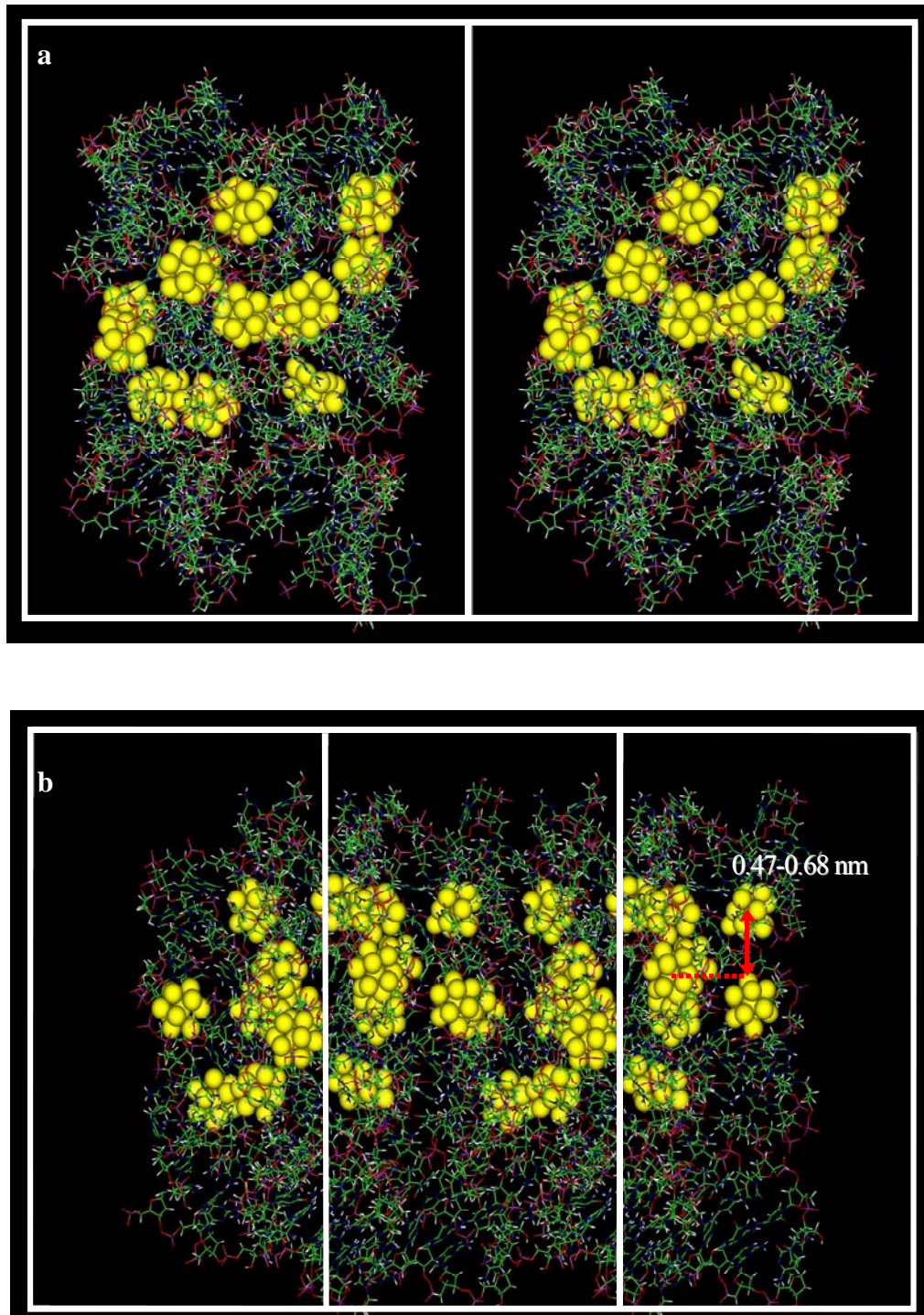


**Figure 5.3** Different orientations of A-DNA structures decorated each with Au<sub>13</sub> clusters generated by the molecular dynamics simulation; (a) side view of the parent cell and of the exact image created by PBC. From each box only 2 A-DNA molecules each being decorated with four Au<sub>13</sub> clusters are shown whereas the other two are hidden behind; (b) 90° projection (rotation) of the whole system where the additional DNA molecules which were previously hidden can be clearly observed. The gold clusters Au<sub>13</sub> form almost four arrays which could be characterised as nanowires. The projection distance of each nanowire is about 0.47 to 0.68 nm apart. The image cell was only used in order to make the nanowires appear longer.



Finally, it has been calculated the difference in Potential energy  $\Delta E^{stab}$  between a single structure of A-DNA with gold clusters  $E_1^P$  (molecular dynamics simulation structures not shown) and the system consisting of 4 A-DNA-Au<sub>13</sub> structures  $E_4^P$ .

$$\Delta E^{stab} = 4 \times (E_1^P) - E_4^P$$

$$\Delta E^{stab} = 4 \times (-5,796) - (-20,350)$$

$$\Delta E^{stab} = -2,834 \text{ kcal mol}^{-1} \text{ A}^{-1}$$

This indicates that the cubic conformational arrangement of the DNA structures with Au<sub>13</sub> clusters is energetically much more favourable than a single DNA structure with Au<sub>13</sub> clusters.

## 5.2 Anticancer properties of gold cluster Au<sub>55</sub>.

### 5.2.1 *In vitro* cytotoxicity assays

Different cancer and healthy human cell lines were employed for investigating the cytotoxic effects for Au<sub>55</sub>. Of the eleven cell lines being examined the metastatic melanomas MV3 and BLM showed significant sensitivity to Au<sub>55</sub>. BLM cells exposed to different concentrations of Au<sub>55</sub> for 24 and 72 hours resulted in a dose-dependent reduction in cell viability (Figure 5.4). BLM cells appear very sensitive to the Au<sub>55</sub> cluster after 24 h incubation period. A longer incubation period of 72 hours with Au<sub>55</sub> cluster can significantly decrease further the viability of the BLM cells. In order to obtain similar curves for both Figures 5.4a and 5.4b, BLM cells were incubated with lower concentrations of Au<sub>55</sub> for the 72 h period. After 72 h incubation with Au<sub>55</sub> 100% death of the cells at the Au<sub>55</sub> concentrations of 0.4  $\mu\text{M}$  where as for cisplatin almost 50% of the cells are still viable (Figures 5.4b and 5.4c). Due to the low solubility of cisplatin the cytotoxicity assay could not be carried out until 100% of the cell population is dead. The effective concentration to reduce the cell number by 50 % is approximately 180-fold higher for Au<sub>55</sub> than for cisplatin for the BLM cells and over 200-fold for the MV3 cell line (Table 5.2).

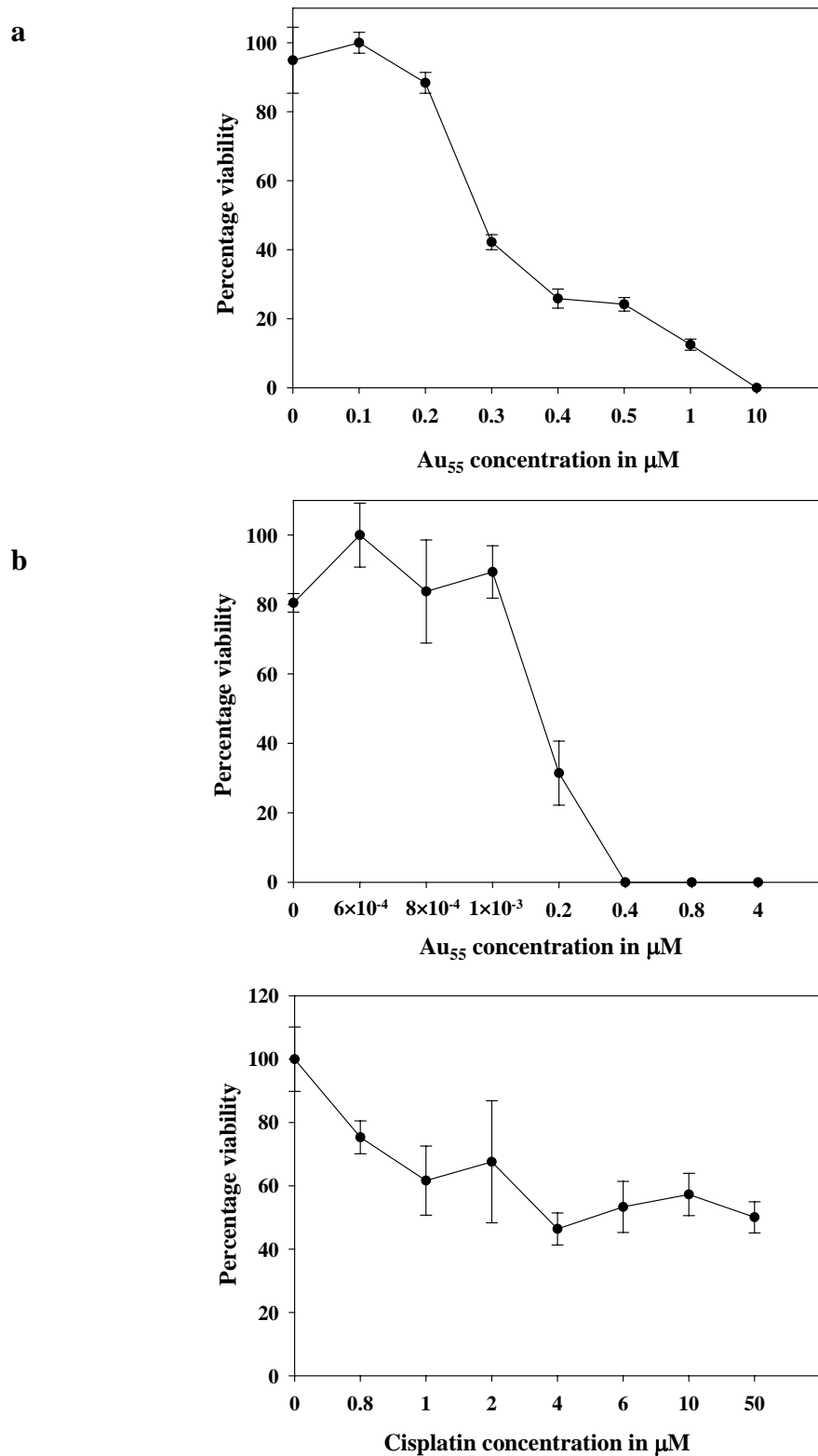


**Figure 5.4** *In vitro* cytotoxicity assay of metastatic melanoma cells BLM, exposed to Au<sub>55</sub> or cisplatin for various periods of time; (a) & (b) 24 and 72 hour incubation respectively of BLM cells with Au<sub>55</sub> clusters prior to MTT assay; (c) 72 hour incubation of BLM cells with cisplatin prior to MTT assay. The values reported in these graphs are the average of three independent experiments each performed in triplicate.

Apart from the melanoma cell lines which exhibited a high sensitivity towards Au<sub>55</sub> there were in the same assay two more cell lines the Hek-12 and the U-2OS which have also indicated a significant reduction in cell numbers comparing to cisplatin. As shown on Table 5.2 the Au<sub>55</sub> effectivity is almost 32-fold higher than cisplatin for the Hek-12 cell line, where as for U-2 OS almost 18-fold higher. Interestingly the osteosarcoma cell line SK-ES-1 showed slightly greater sensitivity to cisplatin than Au<sub>55</sub>. The rest of the cancer cell lines were also susceptible to Au<sub>55</sub> however not so significant as in the cell lines discussed above.

In the very same assay Au<sub>55</sub> showed higher toxicity than cisplatin for the healthy cell line MC3T3-E1. Au<sub>55</sub> is almost 1.6-fold and 2.6-fold more effective to osteosarcoma cell lines SK-ES-1 and U-2OS respectively than to the healthy bone cell line MC3T3-E1. The same comparison for the melanoma cells and their respective fibroblasts CCD-919Sk (healthy cells) indicates a 2- and 2.6-fold more toxicity, however in the case of SK-Mel-28 is obvious that this melanoma is less susceptible than the healthy cells CCD-919Sk to Au<sub>55</sub>. Generally it can be observed for almost all cell lines, Au<sub>55</sub> is more toxic and more effective than cisplatin.

Cell Line		IC <sub>50</sub> Cisplatin 72 h	IC <sub>50</sub> Au <sub>55</sub> 24 h
MC3T3-E1	Bone cells	26.10 ± 1.27 µM	1.65 ± 0.14 µM
U-2OS	Osteosarcoma	11.17 ± 2.02 µM	0.64 ± 0.04 µM
SK-ES-1	Osteosarcoma	0.79 ± 0.17 µM	1.03 ± 0.18 µM
MOR/P	Lung cancer cells Cisplatin sensitive	3.30 ± 0.30 µM	2.10 ± 0.10 µM
MOR/CPR	Lung cancer cells Cisplatin resistant	7.10 ± 1.2 µM	2.50 ± 0.10 µM
CCD-919Sk	Fibroblast cells	0.45 ± 0.10 µM	0.62 ± 0.07 µM
BLM	Metastatic Melanoma	54.70 ± 7.60 µM	0.30 ± 0.10 µM
MV3	Metastatic Melanoma	>50 µM	0.24 ± 0.02 µM
SK-Mel-28	Melanoma	15.60 ± 2.26 µM	1.12 ± 0.16 µM
HeLa	Cervical cancer cells	7.93 ± 0.95 µM	2.29 ± 0.10 µM
Hek-12	Kidney cancer cells transformed with adenovirus	20.13 ± 6.0 µM	0.63 ± 0.02 µM

**Table 5.2 Inhibitory concentrations (IC<sub>50</sub>) of cisplatin and Au<sub>55</sub> incubated with various human cancer and healthy cell lines for 72 and 24 hours respectively.** The IC<sub>50</sub> s were calculated from the graphs obtained from the *in vitro* cytotoxicity assays. The IC<sub>50</sub> values reported in this table are the average of three independent experiments each performed in triplicate.

As a control experiment the effect of the monosulfonated triphenylphosphane ligand was examined for possible cytotoxic effects upon the cell lines BLM, MC3T3-E1 and MOR/CPR. It can be observed in Figure 5.5 that the ligand alone does not affect the viability of the cancer cells BLM even at concentrations up to 500  $\mu\text{M}$  where as *in vitro* cytotoxicity assays demonstrate that the gold cluster exhibits its toxicity at concentrations ranging from 0.24-2.5  $\mu\text{M}$ . The same effect has also been observed for the cell lines MC3T3-E1 and MOR/CPR (results presented in Appendix Section 10.1)

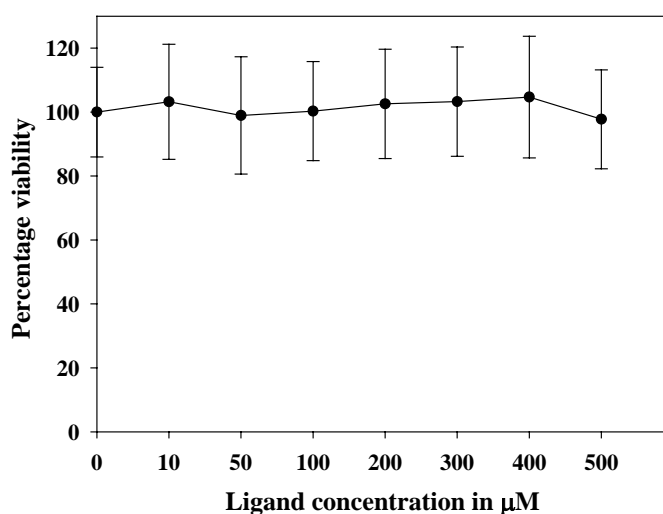


**Figure 5.5** *In vitro* cytotoxicity assay of metastatic melanoma cells BLM, exposed for 24 hours with various concentrations of the triphenylphosphane ligand. The values reported in this graph are the average of two independent experiments each performed in triplicate.

### 5.2.2 Apoptosis/ Necrosis assays

In order to determine whether the reduction in cell number was due to apoptosis or necrosis a flurometric assay was performed which measures the levels of induction of caspases 3 and 7 which are involved in the apoptosis cascade. The use of a fluorogenic substrate is used to detect the activity of caspases 3 and 7. Generally there is a variation on the response of the cells to  $\text{Au}_{55}$ . As indicated by Figure 5.6a there is maximum of a 2-fold induction of caspase induction in the osteosarcoma cell line U2-OS after 24 hours of incubation with  $\text{Au}_{55}$  and a maximum of almost 2.6-fold induction in the presence of cisplatin. In both cases the increase is dose-dependent and it can be followed that this increase of caspase induction is accompanied by a decrease in viability as shown by the respective MTT assays (Figure 5.6b).

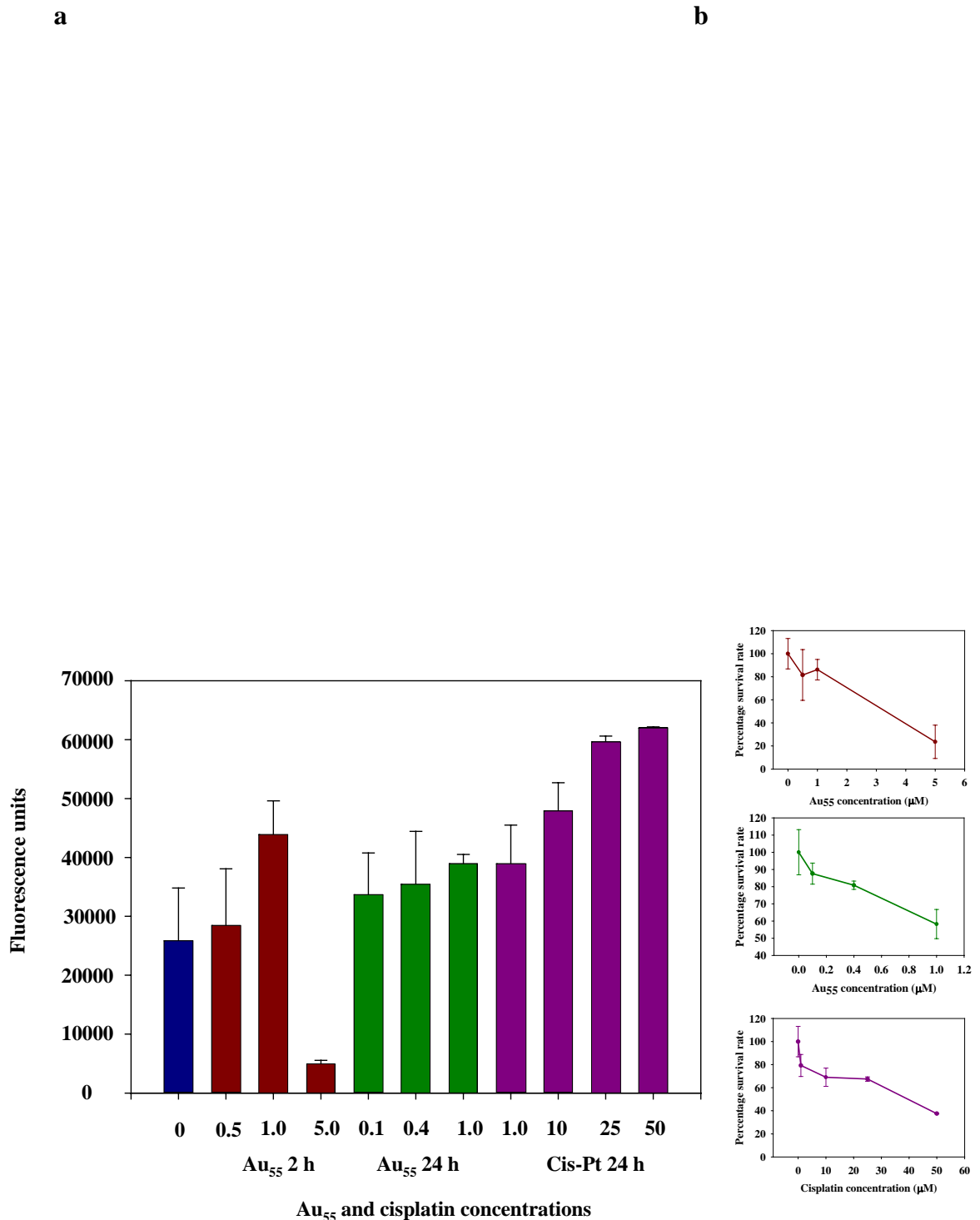


**Figure 5.6 Apoptosis assay performed for the osteosarcoma cell line U-2OS in the presence of cluster Au<sub>55</sub> and cisplatin** (a) Induction of caspases -3 and -7 after incubation of U-2OS cells with various concentrations of, Au<sub>55</sub> for 2 h (red bars) 24 h (green bars) and for 24h incubation with various concentrations of cisplatin (purple bars); In the blue bar is depicted the induction of caspases -3 and -7 in the control; (b) Simultaneously to caspase 3/7 assay, MTT assay was performed for the cell line U-2OS with exactly same concentrations and incubation periods as described above for Au<sub>55</sub> cluster and cisplatin.

The values reported in these graphs are the average of two independent experiments each performed in triplicate.

The melanoma cell line BLM exhibited a different response to Au<sub>55</sub> and cisplatin than U-2OS. It can be clearly observed from Figure 5.7a that for almost every concentration there has been no difference between the basal expression and caspase induction due to Au<sub>55</sub> or cisplatin. Similar effect has been observed for the cell lines MC3T3-E1 and SK-Mel-28 (results provided in Appendix Section 10.2). In addition a decrease in caspase induction is accompanied by a decrease in cell viability as indicated by the respective in vitro cytotoxicity assay as shown in Figure 5.7b.

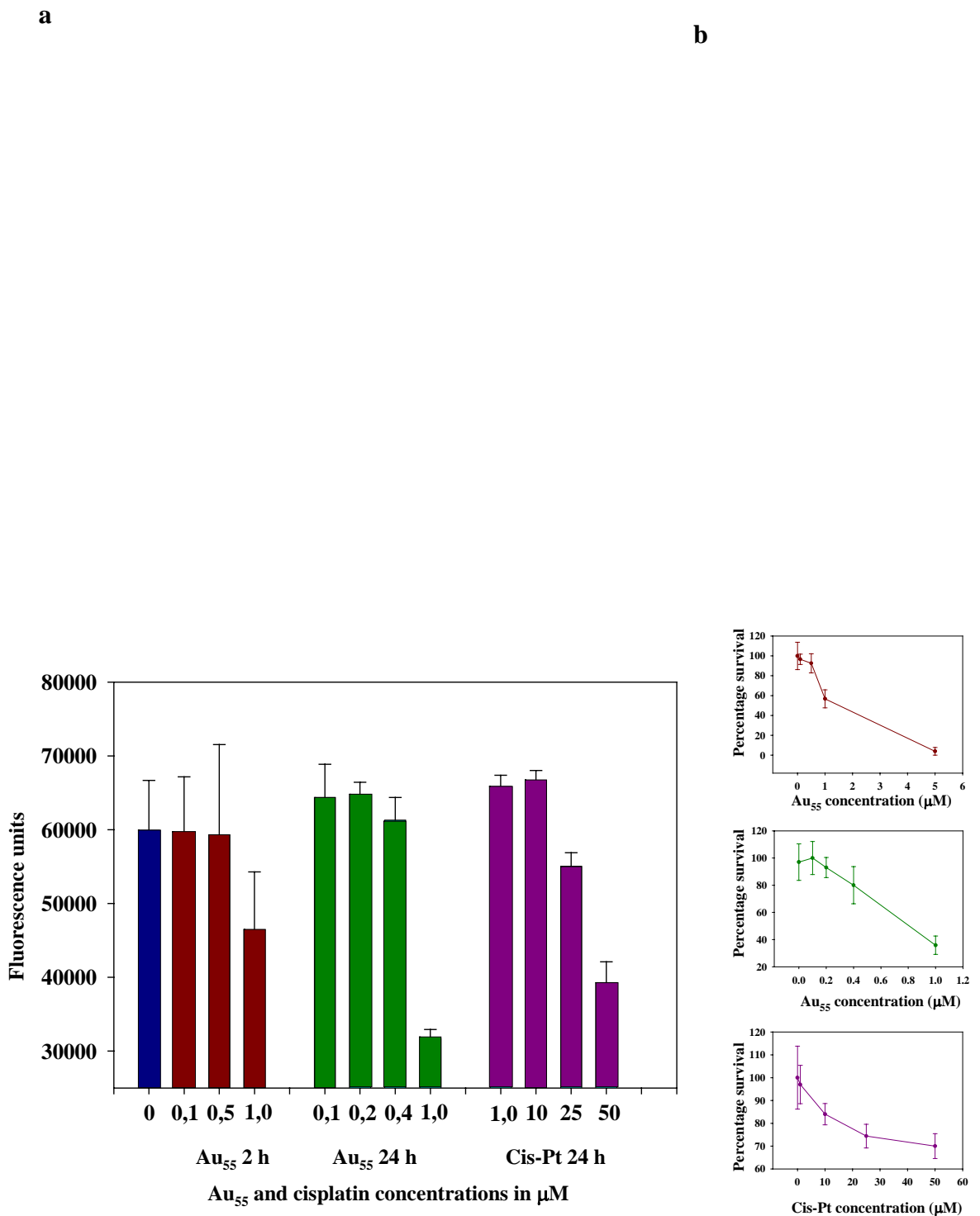


**Figure 5.7 Apoptosis assay performed for the melanoma cell line BLM in the presence of cluster Au<sub>55</sub> and cisplatin** (a) Induction of caspases -3 and -7 after incubation of BLM cells with various concentrations of, Au<sub>55</sub> for 2 h (red bars) 24 h (green bars) and for 24h incubation with various concentrations of cisplatin (purple bars); In the blue bar is depicted the induction of caspases -3 and -7 in the control; (b) Simultaneously to caspase 3/7 assay, MTT assay was performed for the cell line BLM with exactly same concentrations and incubation periods as described above for Au<sub>55</sub> cluster and cisplatin. The values reported in these graphs are the average of two independent experiments each performed in triplicate.

### 5.2.3 *Interaction of Au<sub>55</sub> with plasmid DNA analysed by agarose gel electrophoresis*

The interaction of the gold cluster with plasmid DNA was analysed with agarose gel electrophoresis. Such an approach would indicate any changes occurring in the different forms of DNA plasmid. There are three forms of plasmid DNA which can be easily distinguished by their rate of migration in an agarose gel; the supercoiled form (s), the nicked open (oc), characterised as circular DNA with one strand being nicked, and the linear form (l) which is nicked at both strands resulting in a long DNA molecule. Plasmid DNA was exposed to increasing concentrations of Au<sub>55</sub> at room temperature overnight. It can be observed at Figure 5.8a that the Au<sub>55</sub> does not affect the plasmid DNA which seems to migrate at the same rate as the control (untreated plasmid). Only after 300 µM there are small changes seen in the visibility of the plasmid indicating that the Au<sub>55</sub> inhibits slightly ethidium bromide intercalation leading therefore to reduced visibility under UV light. When H<sub>2</sub>O<sub>2</sub> is provided together with Au<sub>55</sub> then it can be clearly observed in the agarose gel that with increasing Au<sub>55</sub> concentration there is an increased conversion of supercoiled plasmid DNA to open-circular indicating the direct damage on DNA structure leading to the introduction of a cut in one strand of the DNA (Figure 5.8b). In addition the presence of linear plasmid which is located between the 'oc' and the 's' forms can also be observed however rather faintly, indicating that a small amount of DNA can be so drastically damaged at both strands or the opposite strand of the oc DNA form be recognised and further converted into the linear form.



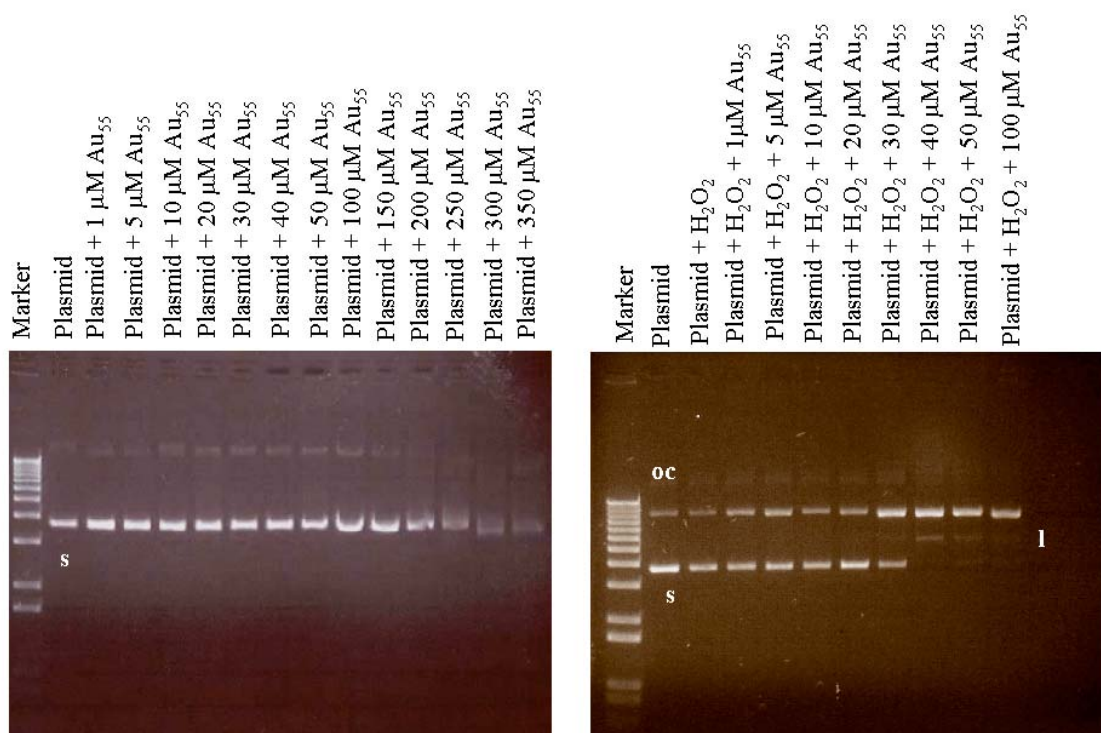


**Figure 5.8** Agarose gel electrophoresis of DNA plasmid with increasing concentrations of Au<sub>55</sub> (a) incubated in PBS at room temperature for 24 hours with increasing concentrations of Au<sub>55</sub>; (b) in PBS incubated at room temperature for 24 hours in the presence of 0.0008 % H<sub>2</sub>O<sub>2</sub> and various concentrations of Au<sub>55</sub>. Supercoiled plasmid is denoted as 's'; nicked, open circular plasmid as 'oc' and linear plasmid as 'l'.

#### 5.2.4 Cellular fractionation

To further understand whether the cytotoxic effect of the gold cluster is related to the cellular uptake and intracellular distribution in cancer cells, the gold cluster was irradiated and introduced at various concentrations and for different incubation times in the melanoma cell line BLM. After incubation the cells were fractionated and each fraction and washing step was measured for gamma emission. It is observed from Figure 5.9a that the accumulation of radioactive Au<sub>55</sub> in the nucleus is dose-and time dependent. The gold

cluster is bound to the nuclear DNA. It appears from radioactive measurements of the washing steps of the DNA pellet (results presented in Appendix Section 10.3) that the gold cluster is quite strongly bound to the DNA with very small amount being washed out. A relatively large amount of Au<sub>55</sub> was also found in the cytoplasmic fraction been as shown in Figure 5.9b. In this case also the accumulation is generally dose and time dependent with the exception of the 24 hour incubation which shows the opposite. We should note that in this experiment the fractionation of the cytoplasmic sample was not further progressed, therefore the distribution of Au<sub>55</sub> in various organelles like mitochondria and cell membrane is not explored. Nevertheless in the case of the nucleic sample, every washing step was measured for radioactivity, including the multiple fractionations which were responsible for the removal of various nuclear proteins as well as histones at which a only small fraction of Au<sub>55</sub> was found (results presented in Appendix Section 10.3).

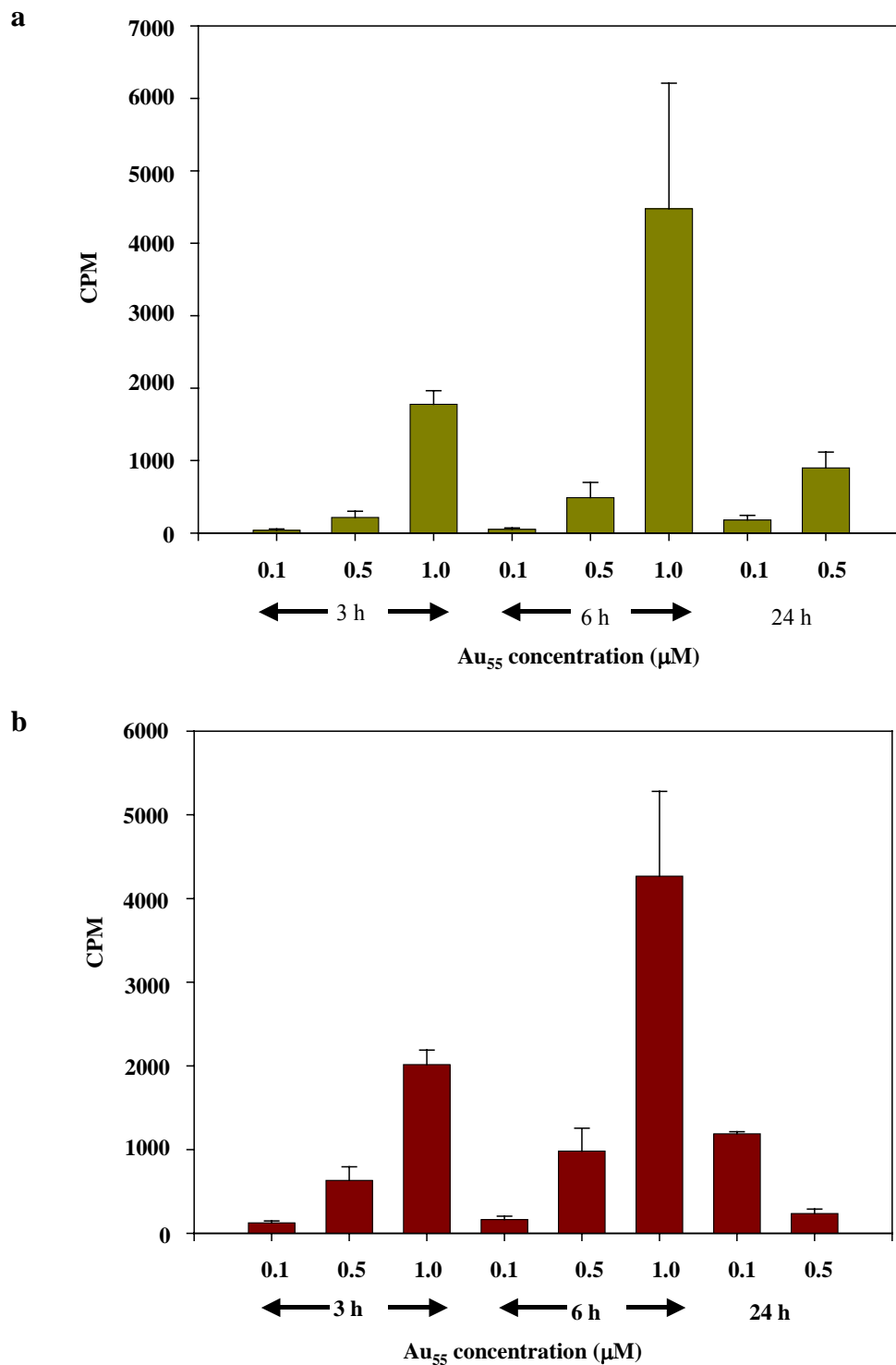


**Figure 5.9 Cellular fractionation of BLM cells being exposed to various concentrations of radioactive  $^{198}\text{Au}_{55}$  for different periods of time; BLM cells previously treated with  $^{198}\text{Au}_{55}$  are fractionated with buffers containing different concentrations of NaCl. (a) Nuclear pellet is composed of DNA and perhaps of a small fraction of histones, (b) Cytoplasmic extract is composed of cytoplasmic components as well as cell membrane. The values reported in these graphs are the average of a single experiment performed in triplicate.**

### 5.2.5 *Molecular docking simulations of the interactions between different DNA structures with Au<sub>55</sub>*

Since the cellular fractionation experiments confirm the presence of Au<sub>55</sub> in the nucleus bound to genomic DNA and agarose gel electrophoresis indicates damage of DNA we have investigated further the interactions of Au<sub>55</sub> cluster with DNA structures.

Molecular docking simulations were performed in various DNA sequences obtained from the Protein Data Bank in order to have a wider range of nucleobase arrangements. The sequences chosen do not differ greatly from each other. A simple reason for this is that nucleic acid structures that adopt the B-DNA conformation are highly dependent on nucleotide sequence as well as on the amount of nucleotides present. Given this reason it was not possible to obtain many B-DNA structures with greater sequence variability.

Molecular docking simulations gave a maximum of fifty docked structures. In these docked structures it has been observed that Au<sub>55</sub> could interact at various sites along the helix. Sometimes though docked structures were obtained that were very similar to others indicating a drawback in this docking method that it can not distinguish sometimes between similar structures. However this method can distinguish energetically favoured positions that could be up to one nucleobase apart. On Figures 5.10 and 5.11 is given a series of four structures obtained by the docking simulation of 1BNA structure with Au<sub>55</sub>. It can be clearly seen that the major groove of the DNA is preferred over the minor groove since in the case of the first the cluster can fit geometrically in the DNA molecule. The dimensions of the minor groove are narrow and less deep compared to the major groove thus giving no opportunity for the gold cluster to come in close contact with the nucleobases. Clearly specific sequences are energetically favourable over others for example adenine(A) – thymine (T) rich sites are preferred over guanine (G) cytosine (C) sites. In the best docked structure it can be observed that the gold cluster is in a very close proximity with various N and O atoms either in the nucleobases or at the phosphate backbone.

In Table 5.3 are given all the DNA structures explored in molecular docking simulations named according to PDB code and their nucleotide sequences. The exact sequence at which the gold cluster was docked for which it exhibited the lowest intermolecular interactions is also given. Clearly A and T bases are preferred by the gold cluster in all

DNA molecules. It should be noted that the intermolecular interactions of docked structures of different DNA molecules can not be directly compared. Intermolecular interactions are used only as a measure to distinguish different docked structures in individual docking experiments.

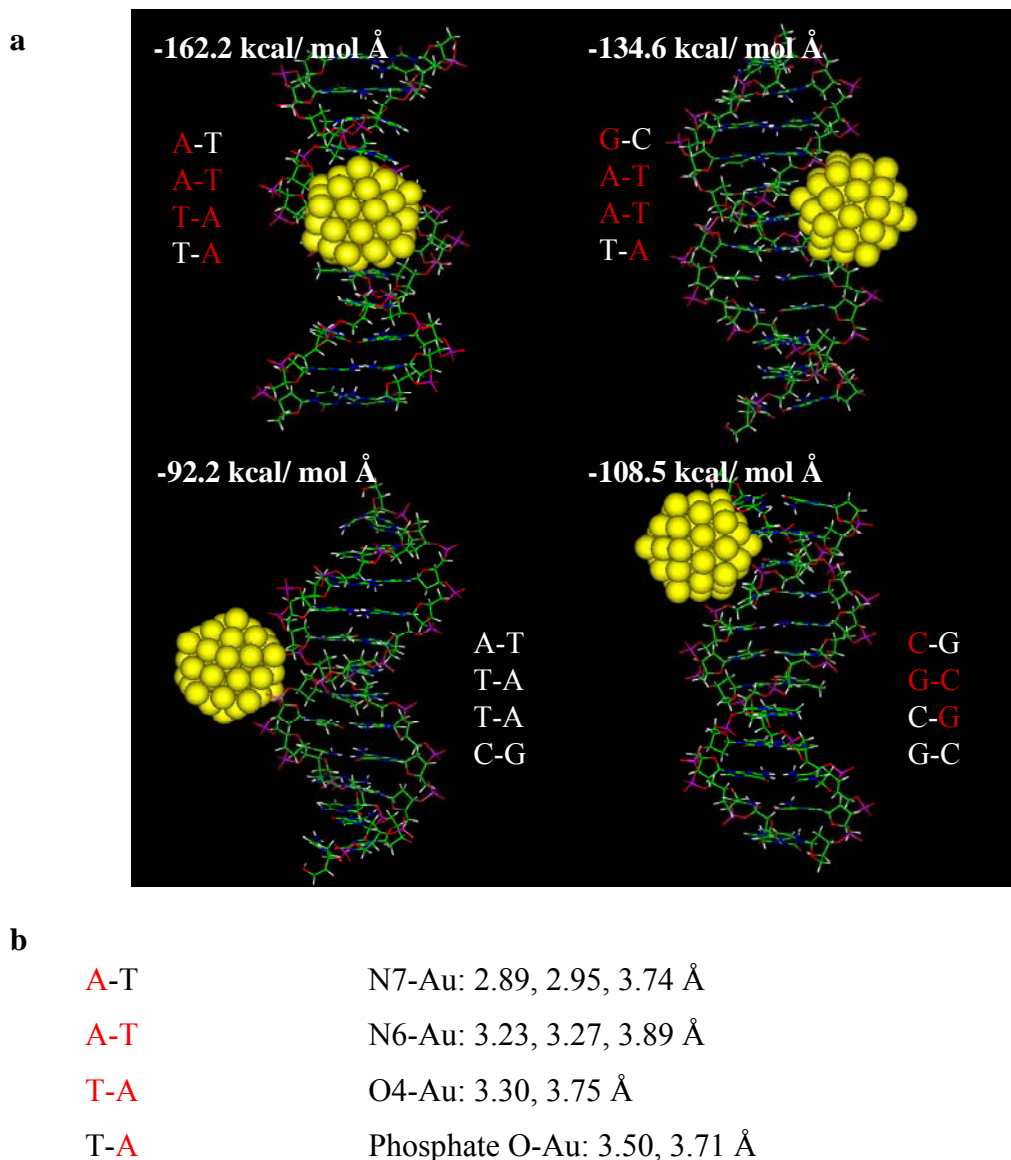


**Figure 5.10 Different structures obtained by the docking of 1BNA molecule with Au<sub>55</sub> and their respective intermolecular interactions.** Exact binding sites – sequence specificities are shown in red letters whereas in white colour are indicated the nucleobases located further away from the gold atoms. (b) DNA sequence at which the Au<sub>55</sub> cluster binding has the lowest intermolecular interactions; the closest distances between specific nucleobase atoms and Au atoms are displayed in Å.

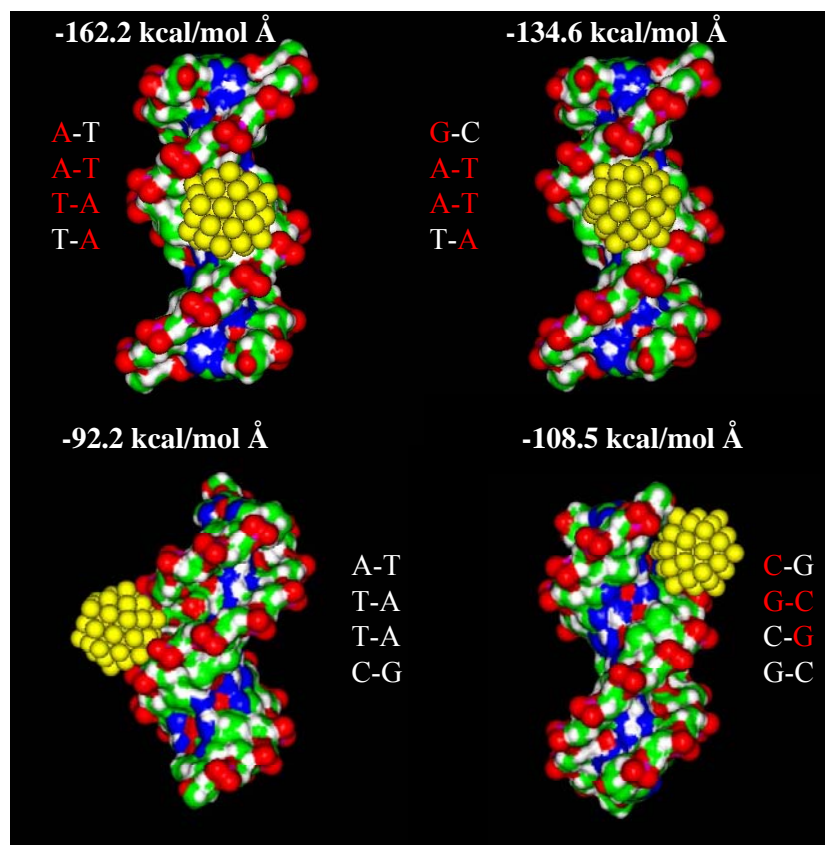


**Figure 5.11** Conolly surface representations of the docked structures of 1BNA molecule with their respective intermolecular interactions. Exact binding sites – sequence specificities are given in red letters whereas in white colour are indicated the nucleobases located further away from the gold atoms.

DNA Form	DNA sequence	Binding seq	Intermol. Int.
1BNA B-DNA	CGCGAATTCGCG	AATT	-162.2 Kcal/molÅ
1DN9 B-DNA	CGCATATATGCG	TATG	-160.3 Kcal/molÅ
1D65 B-DNA	CGCAAATTTGCG	AATT	-178.9 Kcal/molÅ
167D B-DNA	CCATTAATGG	CATT	-136.7 Kcal/molÅ
1D28 B-DNA	CGTGAATTCACG	AATT	-145.2 Kcal/molÅ

**Table 5.3** Summary of the molecular docking simulations. Various structures of DNA classified according to their PDB names. The nucleotide sequences of each DNA structure are given. The exact sequences at which the most energetically favourable binding occurred is indicated together with the lowest intermolecular interactions.

### 5.2.6 Interactions between albumin and Au<sub>55</sub>

The presence of gold clusters in the cytoplasm of BLM cells led to further investigation of the interactions of Au<sub>55</sub> with proteins. As a model protein albumin was used. The effect of albumin and FCS concentration was compared to the standard assay where normal FCS concentration of 10 % of FCS was used to explore the cytotoxicity of Au<sub>55</sub> towards BLM cells. It can be observed from the Figure 5.12 that in the presence of 20 % serum the cells seem to be less susceptible to Au<sub>55</sub> than in the presence of 10% serum leading to an almost 6.5-fold increase in the tolerance of the gold cluster. The presence of albumin resulted in an 2.0-fold increase in the IC<sub>50</sub> of Au<sub>55</sub>. It should be noted that in all cases the viability of the cells decreases at high concentrations of Au<sub>55</sub> like 10  $\mu$ M. Nevertheless in the case of additional FCS and albumin they still remain less susceptible to Au<sub>55</sub> unlike the control (cells incubated in the presence of Au<sub>55</sub> with 10% FCS) (result given in Appendix Section 10.1).

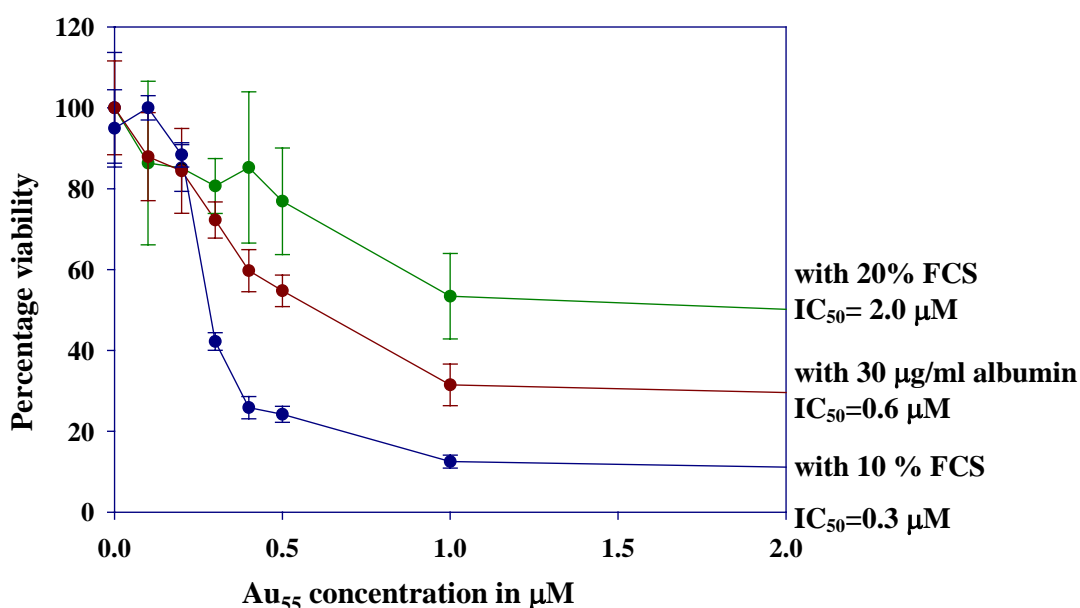


**Figure 5.12 Drug sensitivity profile of BLM towards various concentrations of Au<sub>55</sub> in the presence of additional FCS and albumin protein;** MTT assay being performed in normal medium with 10% FCS is assigned in blue colour and gave an IC<sub>50</sub> = 0.30  $\mu$ M; in the presence of 20% FCS the assay is indicated in green and gave an IC<sub>50</sub> = 2.0  $\mu$ M and in the presence of 30  $\mu$ g/ml albumin the assay is presented in red and gave an IC<sub>50</sub> = 0.6  $\mu$ M. The values reported in these graphs are the average of two independent experiments each performed in triplicate.

Using molecular docking simulations, the potential binding sites of Au<sub>55</sub> at the albumin protein was investigated. The rationale on choosing a starting binding site was different to that in DNA docking simulations. In this case the binding site for the docking simulations was chosen each time to be one of the three domains of the protein. It should be noted though, that the surface of the protein is large, and therefore multiple binding sites were explored as starting binding sites. It has been documented that specific cysteine residues play an important role on metal binding therefore for each docking simulation a protein domain was chosen as the general searching site but the gold cluster was placed manually at each cysteine residue. Molecular docking resulted in about 15 to 20 different structures each time. In all cases the Au<sub>55</sub> did not remain stable at the starting site but moved towards different directions along the surface of the binding site. Some docked structures appeared to be similar with the gold cluster being moved only slightly indicating that the method does not always perform optimally, however a variation in docking positions was generally achieved by the docking program.

Selected docked structures generated by various docking simulations are displayed in Figure 5.13. The first three structures were among the most energetically favourable exhibiting the lowest intermolecular interactions. The fourth docked structure has only been used as an example to indicate a binding site which was rather less energetically favourable as shown by the high intermolecular interactions. Interestingly the most favourable positions were those which contained cysteine residues nevertheless there were of course other cysteines which were less important for the interaction between Au<sub>55</sub> and albumin. The program generated docked structures on which cysteine residues were not involved, however these exhibited intermolecular interactions which were up to 20 Kcal/mol Å higher from the structures a, b and c and will be not be discussed in this study.



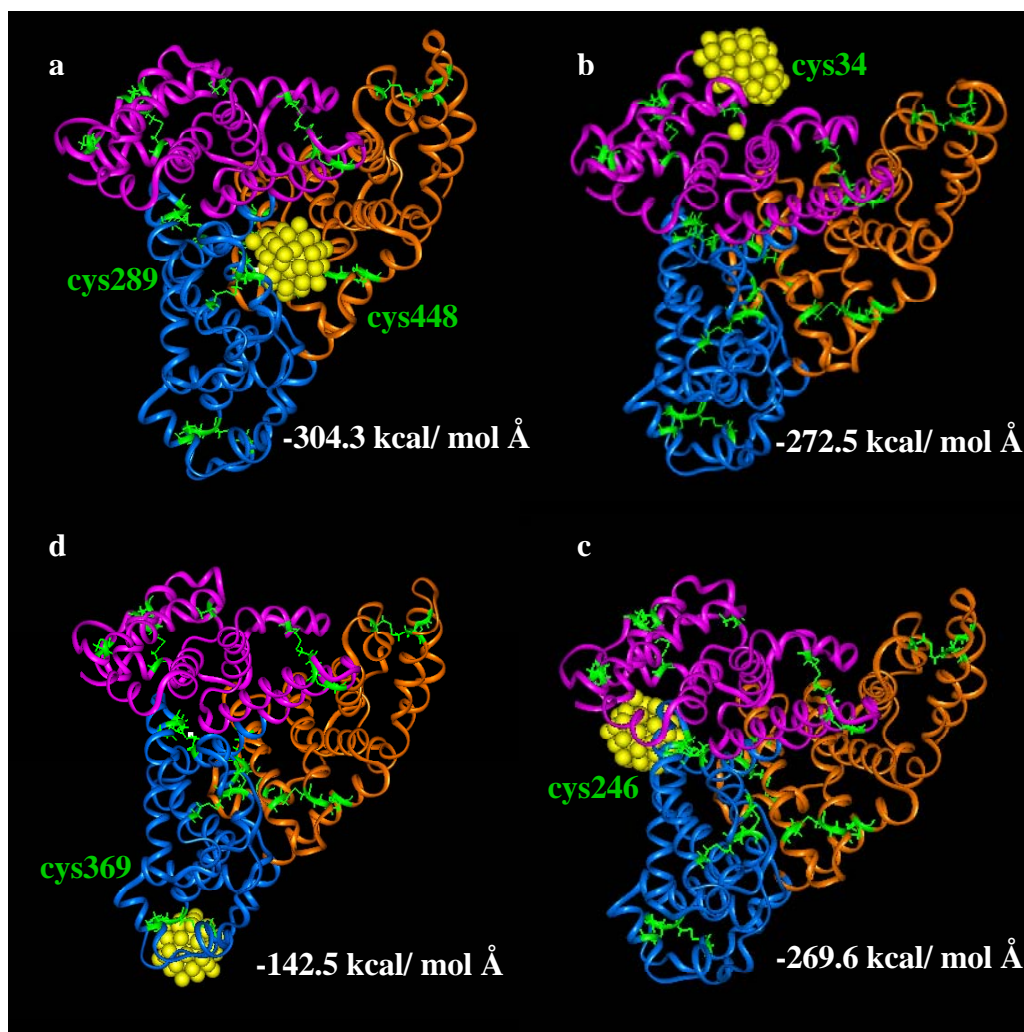


**Figure 5.13** Structures obtained from the docking simulations of albumin and  $Au_{55}$  with respective intermolecular interactions given in Kcal/mol Å. Protein domains are coloured with pink, blue and orange whereas in green are depicted cysteine residues and disulfide bonds. Cysteine residues involved at the docking site are also written in green colour.

A closer version of Figure 5.13 is displayed in Figure 5.14 where it can be clearly seen the  $Au_{55}$  been relatively well buried inside the albumin surface for the best docked structure (Figure 5.14a). It is obvious that the more the cluster is exposed the higher the intermolecular interactions become (Figure 5.14b, c & d).

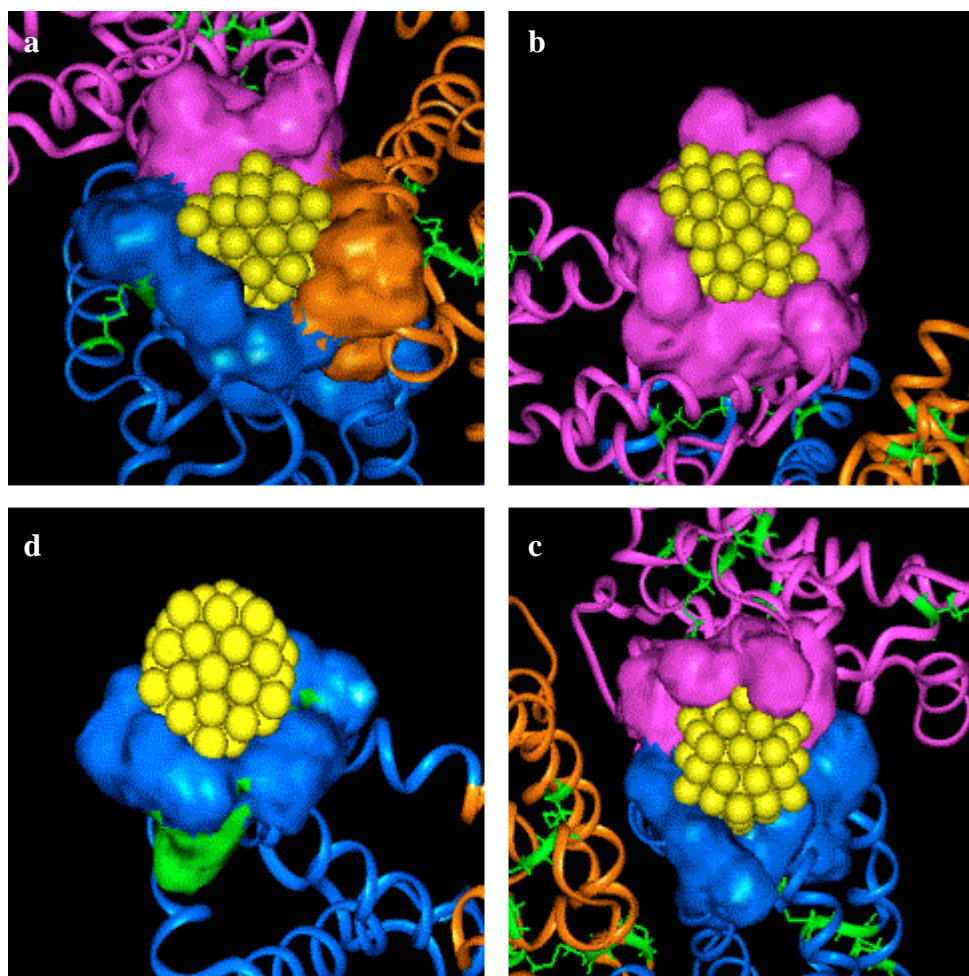


**Figure 5.14** Enlarged images of the binding sites of Au<sub>55</sub> in docked structures visualised as CPK models. Protein domains are coloured with pink, blue and orange whereas in green are depicted cysteine residues and disulfide bonds. Cysteine residues involved at the docking site are also given in green colour. Docked structures are presented in the same order as in the previous figure.

### 5.3 Interactions between zeolite beta and various amino acids

The interactions of the amino acids, glutamic acid, lysine and phenylalanine with zeolite beta were investigated by molecular dynamics simulations. The simulations were performed in the presence of water molecules. The amino acids were placed on four different positions on the zeolite surface, inside a zeolite pore and away from the surface in the bulk water. Each simulation which was run for 200 ps, resulted in 1000 structures. During the first 30-60 ps the Total energy (TotE) which is the sum of the potential and the kinetic energy of one whole (zeolite-amino acid) system was observed to be fluctuating with the TotE increasing. After this fluctuation period an equilibrium was observed where TotE, was fluctuating around a constant value.

The evaluation of MD simulations was performed on structures obtained during the period of 80 ps to 200 ps. This equilibrium interval corresponds to 600 structures for each simulation. Average TotE values from 600 structures of each (zeolite-amino acid) system is listed on Table 5.4 It can be clearly seen that for each amino acid specific surface locations are preferred. It should be noted that there is no structural difference between the surface02 and surface 03 since they are mirror images of each other. Nevertheless the simulation was performed as a control. It has been found that there is no significant difference for preference over surfaces 02 and 03 for all three amino acids. It can be clearly seen that for all amino acids surface01 and surface04 are not preferred since the average TotE are higher than in the case for surface02 and surface03. All three amino acids also do not prefer to be inside the zeolite pore as well as in the bulk water. Therefore the most favorable interactions occur when the amino acids are associating with specific surface sides of the zeolite.

	surface01	surface02	surface03	surface04	bulk	pore
<b>GLU</b>	6029.92 ± 58.94	4946.98 ± 50.24	4937.49 ± 51.25	6314.69 ± 49.91	5704.88 ± 55.74	5715.85 ± 51.55
<b>LYS</b>	5702.21 ± 53.17	4939.72 ± 45.19	4928.31 ± 48.93	6132.33 ± 52.71	5687.68 ± 55.01	5700.56 ± 58.75
<b>PHE</b>	5725.22 ± 50.28	4938.43 ± 48.79	4947.36 ± 50.64	5915.23 ± 56.55	5722.60 ± 54.00	5707.26 ± 56.02

**Table 5.4 Average Total Energies (TotE) in kcal of the structures obtained from the MD simulations.** MD simulations of zeolite beta were performed with the amino acids, glutamic acid (GLU), Lysine (LYS) and Phenylalanine (PHE). Each simulation was run for 200 ps resulting each in 1000 structures. TotEs and their standard deviations were calculated from the structures obtained from the interval 80 ps until 200 ps i.e. when the simulation was in equilibrium. This corresponds to 600 structures from the 1000 obtained totally. Equilibrium is considered the stage where during the simulation the TotE is constantly fluctuating. In each simulation each amino acid was placed manually at four different positions around the zeolite beta surface. These locations correspond to surfaces 01, 02, 03 and 04. In addition MD simulations were performed with each amino acid being placed inside a pore of zeolite beta. MD simulations were also performed with each amino acid being located in bulk water, away from the zeolite surface.

Stabilisation energies have been calculated in order to understand which amino acid prefers energetically to interact more with the zeolite. The stabilisation energy  $E_{aa}$  has been calculated with the following formula:

$$E_{aa} = Ave\_TotE_{surface} - Ave\_TotE_{bulk}$$

$$E_{GLU} = 4937.49 - 5704.88 = -767.39 \text{ kcal},$$

$$E_{LYS} = 4928.31 - 5687.68 = -759.37 \text{ kcal},$$

$$E_{PHE} = 4938.43 - 5722.60 = -784.17 \text{ kcal}$$

This indicates that Phe prefers energetically to interact more with the zeolite more than Lys or Glu.

On Figure 5.15 is given a snapshot of structures obtained from three different times during the MD simulation of Glu with zeolite at its surface03. Each structure is presented with the front and side view. The water molecules are omitted so that the positions of the Glu can be clearly observed. At 80 and 120 ps Glu remains relatively close to the surface of the zeolite. At 160 ps the amino acid is located further away from the surface.

This can be further supported by Figure 5.16 which indicates the distances between the centre of the mass of the Glu structure and the surface of the zeolite. Since the zeolite surface is composed of many cavities and pores, a plane was constructed on its surface. This plane, rather than a specific point on the zeolite structure, was used, to calculate the distances of the 600 structures from it. It can be observed that almost up to 140 ps the amino acid is relatively close to the surface, however as the simulation proceeds the distance of Glu MD structures from the zeolite surface become greater.



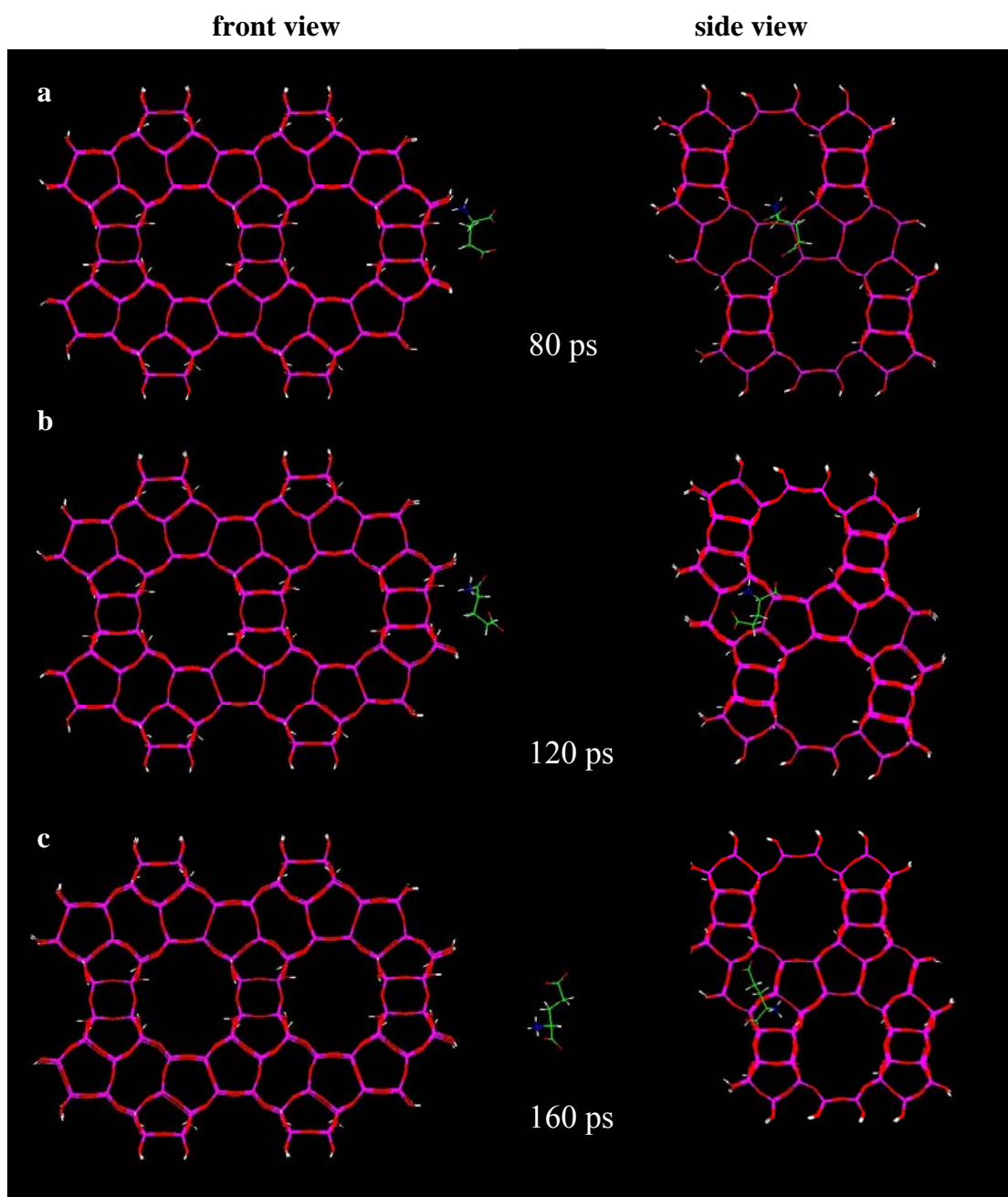


**Figure 5.15: MD simulation of glutamic acid with zeolite beta.** Structures are collected from a trajectory file which is generated during the simulation period of 200 ps. (a) structure is collected at the 80th ps, (b) structure is collected at the 120th ps, (c) structure is collected at the 160th ps. Structures are presented at both front and side views. Water molecules are omitted from the structures for reasons of clarity. Zeolite Al and O atoms are shown in pink and red colour respectively. In glutamic acid the C atoms are given in green where as the N are presented in blue. O atoms are in red and H atoms are in white colour.

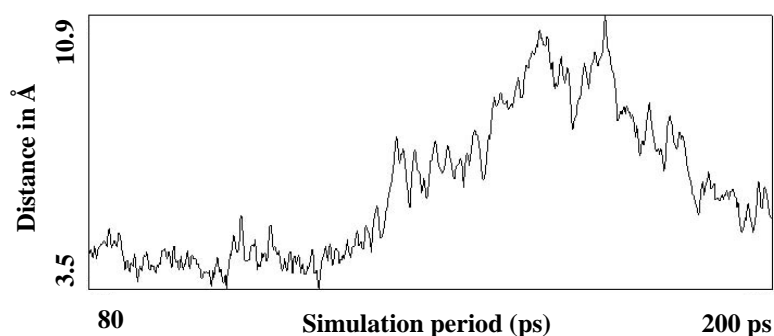


**Figure 5.16 Distances between the centre of the mass of the glutamic acid and the surface of the zeolite.** The distances presented for all the structures collected in the trajectory file during the MD simulation between the period of 80 and 200 ps. The distances are measured in Å and have been calculated between the centre of the mass of Glu and the plane generated on the surface of zeolite.

It has been observed that almost until the first half of the simulation the amino group of Glu interacts with the oxygen atoms of the zeolite where as the carboxyl group forms hydrogen bonds with the water molecules. Towards the end of the simulation the interactions between the amino group and the zeolite become less obvious. This can be easily seen if one observes an animation of the trajectory file however for the purpose of this thesis this can be demonstrated on Figures 5.17 and 5.18 where the amino and the carboxyl groups are used to measure their distances from the surface (plane) of the zeolite. It should be noted that these graphs do not indicate the amount of hydrogen bonds but rather the distances to the surface. The amino group, it appears to be relatively close to the surface early during the equilibrium stage, however later on its distance increases as the amino acid moves away from the surface. In the case of the carboxyl group, its distance to the surface appears to be close at some times during early equilibrium stage, however the hydrogen bonding formation has been only observed with the water molecules.

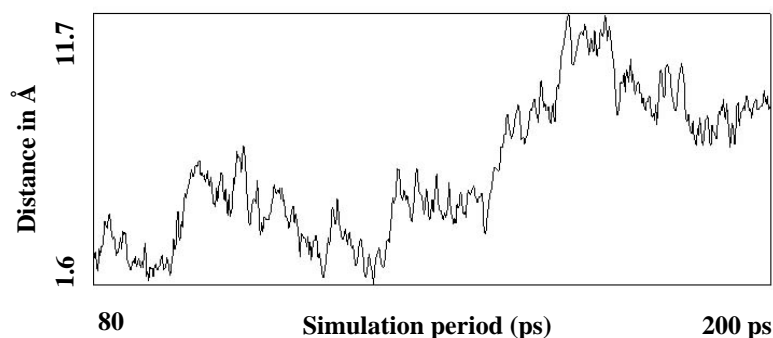


**Figure 5.17 Distances between the amino group of the glutamic acid and the surface of the zeolite.** The distances presented are for all the structures collected in the trajectory file during the MD simulation between the period of 80 and 200 ps. The distances are measured in Å and have been calculated between the N atom of the amino group of Glu and the plane generated on the surface of zeolite.

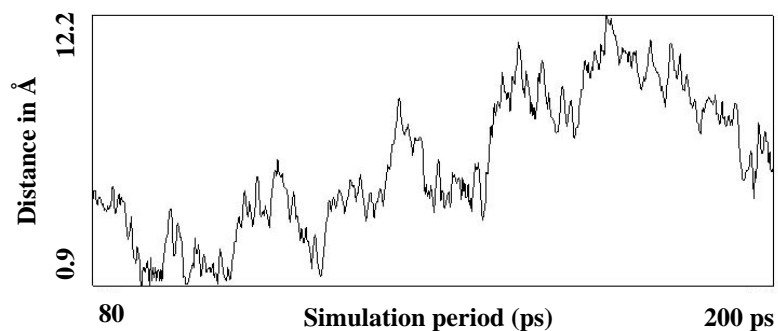


**Figure 5.18 Distances between the carboxyl group of the glutamic acid and the surface of the zeolite.** The distances presented are for all the structures collected in the trajectory file during the MD simulation between the period of 80 and 200 ps. The distances are measured in Å and have been calculated between the C atom of the carboxyl group of Glu and the plane generated on the surface of zeolite.

Lysine behaves almost the same way as Glu. It remains close to the surface during early equilibrium stage (Figure 5.19a and 5.19b). As the simulation proceeds it moves further away from the surface however not closer to the bulk water molecules like Glu but rather away from its initial location point (Figure 5.19c). Figure 5.20 clearly indicates the distances between the center of the mass of Lys and the surface (plane) of the zeolite become greater as the simulation proceeds.



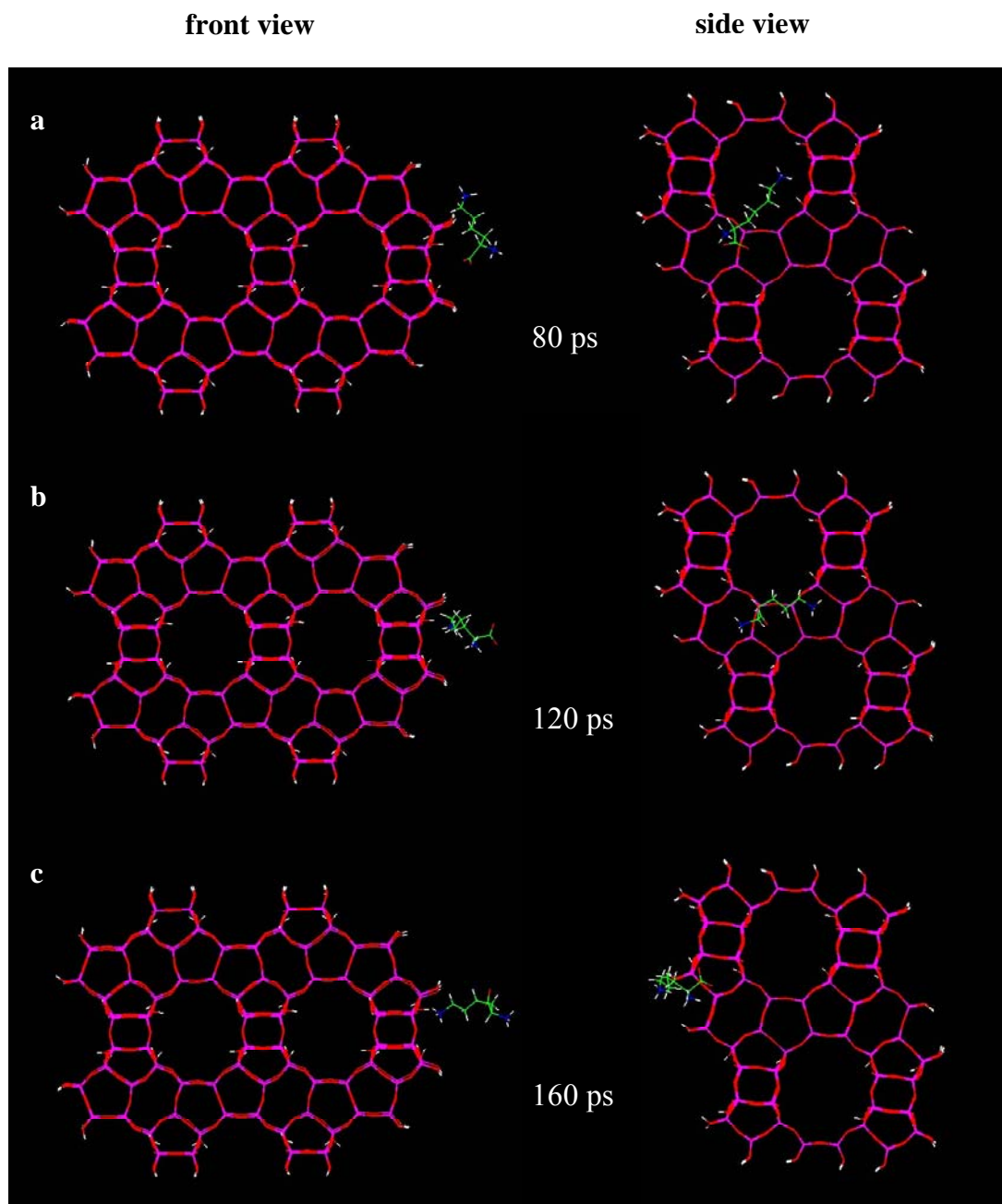


**Figure 5.19: MD simulation of lysine with zeolite beta.** Structures are collected from a trajectory file which is generated during the simulation period of 200 ps. (a) structure is collected at the 80th ps, (b) structure is collected at the 120th ps, (c) structure is collected at the 160th ps. Structures are presented at both front and side views. Water molecules are omitted from the structures for reasons of clarity. Zeolite Al and O atoms are shown in pink and red colour respectively. On lysine the C atoms are given in green where as the N are presented in blue. O atoms are in red and H atoms are in white colour.

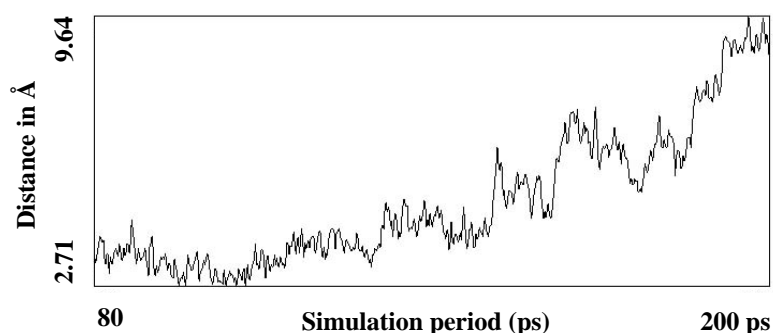


**Figure 5.20 Distances between the centre of the mass of the lysine and the surface of the zeolite beta.** The distances presented are for all the structures collected in the trajectory file during the MD simulation between the period of 80 and 200 ps. The distances are measured in Å and have been calculated between the centre of the mass of Lys and the plane generated on the surface of zeolite.

During the equilibrium stage has been also observed the prevalence of hydrogen bonds between the amino groups of Lys and oxygen atoms of the zeolite. On Figure 5.21 can be clearly observed the small distances between the amino group of the Lys and the surface of the zeolite. While the simulation proceeds the amino acid moves further away from its initial location thus the distances increase. The carboxyl group like in the case of Glu was interacting with the water molecules. It can be clearly shown on Figure 5.22, that, during most of the simulation the carboxyl groups stay away from the surface of the zeolite.

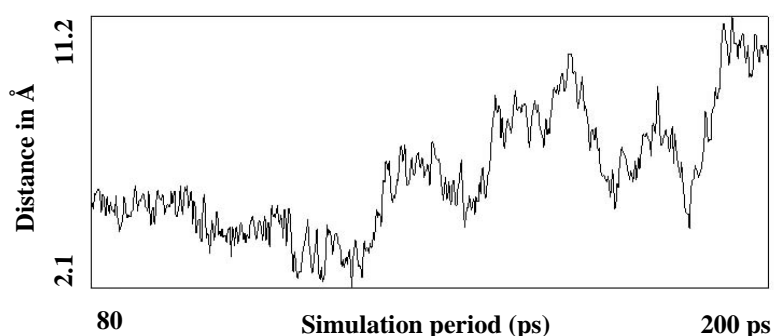


**Figure 5.21 Distances between the amino group of the lysine and the surface of the zeolite.** The distances presented are for all the structures collected in the trajectory file during the MD simulation between the period of 80 and 200 ps. The distances are measured in Å and have been calculated between the N atom of the amino group of Lys and the plane generated on the surface of zeolite.

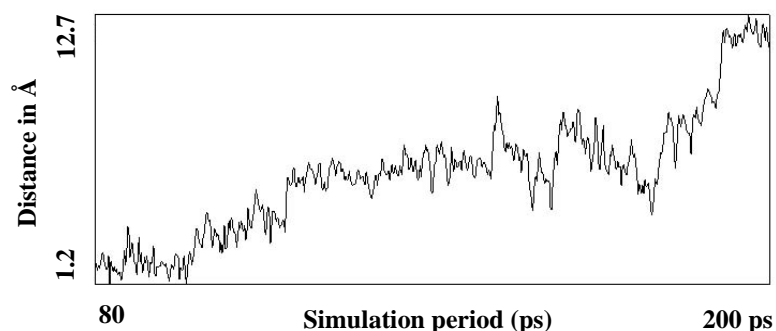


**Figure 5.22 Distances between the carboxyl group of the lysine and the surface of the zeolite.** The distances presented are for all the structures collected in the trajectory file during the MD simulation between the period of 80 and 200 ps. The distances are measured in Å and have been calculated between the C atom of the carboxyl group of Lys and the plane generated on the surface of zeolite.

Phenylalanine has been found based on its stabilisation energy to be the amino acid exhibiting the most favorable interaction with zeolite beta. It can be clearly indicated from Figure 5.23 that as the simulation proceeds Phe remains very close to its initial location inside the cavity, unlike to Glu and Lys which at 160 they are located away from their initial positions. The same effect can be demonstrated with Figure 5.24, where it can be observed that during the equilibrium period, the distance between the centre of the mass of Phe and the zeolite surface remains stable.

During the animation of the trajectory file it has been observed that the amino group of Phe is frequently involved in hydrogen bond formation with the oxygens of the zeolite. This could be also demonstrated on Figure 5.25, where it can be clearly seen that the distances between the amino group and the zeolite surface is very stable. On the other hand the carboxyl groups have been often observed to involved in hydrogen bond formation with the water molecules. As indicated by Figure 5.26 the distances between the zeolite surface and the carboxyl group fluctuate stronger.

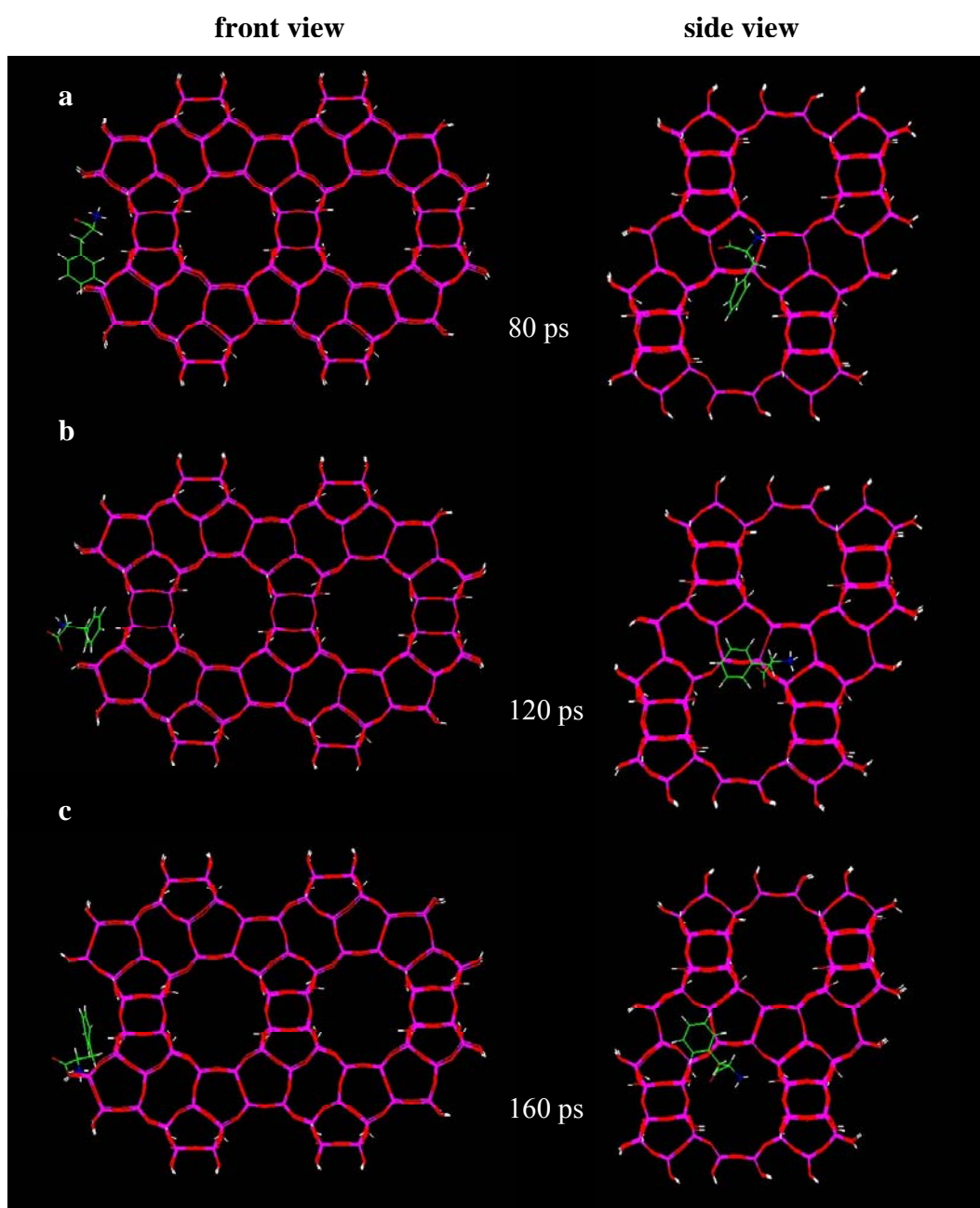


**Figure 5.23: MD simulation of phenylalanine with zeolite beta.** Structures are collected from a trajectory file which is generated during the simulation period of 200 ps. (a) structure is collected at the 80th ps, (b) structure is collected at the 120th ps, (c) structure is collected at the 160th ps. Structures are presented at both front and side views. Water molecules are omitted from the structures for reasons of clarity. Zeolite Al and O atoms are shown in pink and red colour respectively. On phenylalanine the C atoms are given in green where as the N are presented in blue. O atoms are in red and H atoms are in white colour.

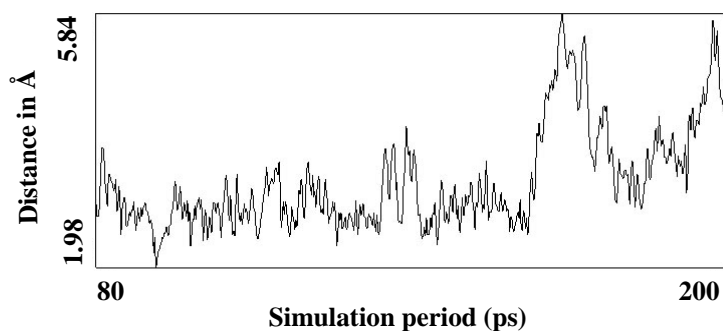


**Figure 5.24 Distances between the centre of the mass of the phenylalanine and the surface of the zeolite beta.** The distances presented are for all the structures collected in the trajectory file during the MD simulation between the period of 80 and 200 ps. The distances are measured in Å and have been calculated between the centre of the mass of Phe and the plane generated on the surface of zeolite.

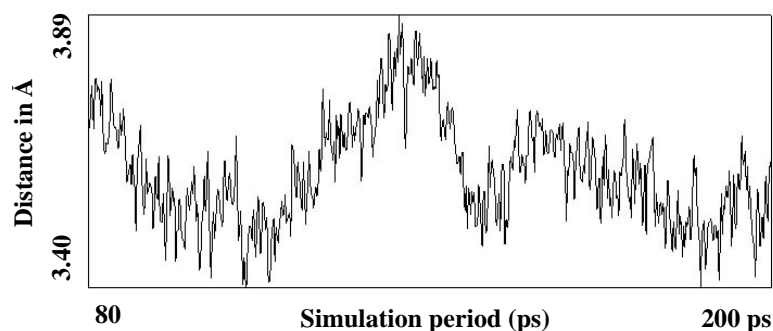


**Figure 5.25 Distances between the amino group of the phenylalanine and the surface of the zeolite.** The distances presented are for all the structures collected in the trajectory file during the MD simulation between the period of 80 and 200 ps. The distances are measured in Å and have been calculated between the N atom of the amino group of Phe and the plane generated on the surface of zeolite.

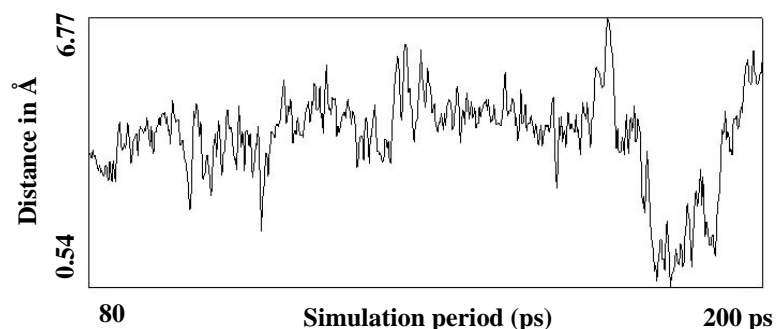


**Figure 5.26 Distances between the carboxyl group of the phenylalanine and the surface of the zeolite.** The distances are presented for all the structures collected in the trajectory file during the MD simulation between the period of 80 and 200 ps. The distances are measured in Å and have been calculated between the C atom of the carboxyl group of Phe and the plane generated on the surface of zeolite

## 6. Discussion

---

### 6.1 Interactions between Au clusters and DNA: Formation of nanowires.

Two different forms of DNA the A- and the B- form were investigated in this study for their interaction with gold clusters  $Au_{13}$  and  $Au_{55}$ . The molecular mechanics simulations and the characterisation of the groove geometry of each form of DNA have indicated that the PCFF forcefield is appropriate for further computer simulations.

Gold wires observed by TEM are structures which could be influenced by the preparation protocol, in which the DNA is firstly air-dried and then further dehydrated under vacuum. Given these conditions, the transition from the B- to the A-form is likely to occur. At high relative humidity, the N atoms of the purine bases as well as the sugar and phosphate O atoms are hydrated. The minor groove of B-DNA appears to have a “spine” of hydration on which the water molecules form highly ordered layers; however, the majority of the water molecules in the major grooves seem to be disordered (35). During progressive dehydration, the spine of hydration on the minor grooves of the B-DNA is disrupted, the integrity of the B-DNA structure is destroyed, and the transition into the A-form occurs. Many theoretical and experimental studies have shown the importance of solvents, and counterions on the stability of A-DNA and B-DNA structures (15, 23, 39).

Molecular simulations of A-DNA structures in different ethanolic solutions have demonstrated the importance of hydration and ion association in the major grooves for conformational stability. In pure ethanol, the A-DNA is dehydrated and its native helical structure has been observed to distort. In 80 % ethanol, A-DNA remains in its canonical (usual) form, which is stabilised by ion association, hydration and ion-mediated interhelical bonding across the major groove (15). Under vacuum conditions typical for TEM, the majority of the water molecules bound to the A-DNA are removed, thereby distorting the structure unless it is somehow stabilised by molecules other than water, specifically those capable of bridging opposing phosphates. In this case,  $Au_{13}$  clusters can replace the water bridges along the major grooves given their appropriate dimensions. It is believed that the presence of the  $Au_{13}$  clusters along the major grooves of the A-DNA are responsible for the integrity of the structure, however the influence of this substitution on the prolonged stability of the structure in vacuo cannot be ascertained. Subsequent TEM

micrographs suggest that the wire structures are less apparent over time, which is probably due to structural instability of DNA in vacuum. Nevertheless the formation of aggregates could also be due to gold atoms being removed by Au<sub>55</sub>. Interestingly our molecular mechanics simulations and calculation of stabilisation energies suggest that the Au<sub>13</sub> cluster would energetically prefer to interact with the major groove of the A-DNA whereas the Au<sub>55</sub> cluster prefers the major groove of the B-form of DNA. This suggests that the phosphate backbone on both forms of DNA is stabilised by the presence of the gold clusters.

During the transition of B-DNA into A-DNA, where a continuous alteration of the major and minor groove geometry takes place, a transition from Au<sub>55</sub> into Au<sub>13</sub> is also possible. It is known that the Au<sub>55</sub> cluster can fit in the major groove of the B-DNA; however, it is too large to fit in the major groove of A-DNA, where a Au<sub>13</sub> cluster can easily fit. The exact mechanism by which Au<sub>55</sub> clusters can be transformed into Au<sub>13</sub> is not understood; however, it is possible that the DNA acts as template for such a transformation. Gradual dehydration can induce the transition from B-DNA to A-DNA and therefore cause dramatic changes in the groove geometry. As the major groove of the B-DNA becomes shorter, it is possible to force Au<sub>55</sub> to become reduced into a Au<sub>13</sub> cluster which can fit easily in the major groove of the A-DNA.

The molecular modelling results are in good agreement with TEM observations. Firstly the formation of nanowires seems to be dependent on the equidistant decoration of Au<sub>13</sub> clusters along the phosphate backbone of A-DNA (Figure 5.2) The formation of gold wires is shown clearly in Figures 5.3a and 5.3b. Since the TEM micrographs show only the top projection of the wires, the gold wire effect could be caused by the location of the Au<sub>13</sub> clusters around the phosphate backbone of many DNA molecules. Molecular dynamic calculation of  $\Delta E^P$  has shown that the configuration of four A-DNA molecules with Au<sub>13</sub> clusters is energetically more stable than a single A-DNA molecule with Au<sub>13</sub> clusters. As shown in Figure 5.3a and 5.3b an apparently continuous gold wire is formed, when the whole system is rotated. From the molecular dynamics calculation, we have found that each wire does not appear to be equidistant from each other, but varies between 0.47 nm Å and 0.8 nm. It is possible that Au<sub>13</sub> clusters move during molecular dynamics simulations because of a high kinetic energy, but also it is possible for short-range electrostatic forces to cause such an effect, especially when a Au<sub>13</sub> cluster is not interacting optimally with an

adjacent DNA molecule. Even though the phosphates in the major grooves of A-DNA are an important part of the interaction with the Au<sub>13</sub>, it is possible for the minor groove to further stabilise the whole system and keep the Au<sub>13</sub> in place, possibly via an amino group or an oxygen of a nucleobase on an adjacent DNA molecule. According to the TEM micrographs, the gold wires appear to have different lengths. If the models are representative of the TEM observations, the length of the wires will depend on the amount of DNA available as a template. This however can not be confirmed from the present TEM images, since the DNA is not visible.

## **6.2 Anticancer properties of gold cluster Au<sub>55</sub>**

There is a variety of metal-based drugs that are known to interact with important biomolecules like DNA such as platinum complexes, exhibiting in some cases better or worse cytotoxicities than cisplatin an antineoplastic drug that has been used for a long time in chemotherapy either alone or in combination with other antitumor drugs or radiotherapy (14). Unfortunately cisplatin has a relatively narrow range of applicability in cancer treatment as well as exhibiting severe toxicity like nephrotoxicity and neurotoxicity. Apart from the toxic side effects, platinum resistance is also often developed in many cancer patients. These drawbacks have been the impetus for the development of improved antineoplastic medicaments which are not only founded on platinum but are also based on other metals like gold, and ruthenium (122).

Gold-based compounds have exhibited a significant activity in a variety of cancer cell lines. Many gold compounds have been synthesised and screened with promising antitumor properties. Some of them unfortunately exhibited cardiovascular toxicity and have not been investigated further by clinical trials (100). Nevertheless the effort for generating optimal antineoplastic gold-based drugs continues, however, their mechanism of action and the ultimate intracellular target is still disputed.

Gold clusters have been shown to interact with different forms of DNA leading to their degradation upon conversion of A-DNA into B-DNA (68). This observation leads to the incentive for gold cluster Au<sub>55</sub> to be investigated for its possible anticancer activity since its ability to interact with DNA has been shown experimentally by TEM and theoretically by molecular mechanics simulations (68).



In vitro cytotoxic screening represents a widespread method for the rapid selection of anticancer drug candidates. Based on the very same assay the National Cancer Institute (USA) uses a panel of 60 human cancer cell lines for screening the anticancer potential of various compounds. We have investigated the killing properties of gold cluster Au<sub>55</sub> by using a relatively small panel of tumor and normal cell lines. The gold cluster showed favourable activity towards all the cell lines at shorter periods of time and at lower concentrations than cisplatin. The IC<sub>50</sub> values ranged between 0.24 to 2.5 μM and are in good agreement with the literature where gold (I) and gold (III)-based compounds have been shown to exhibit IC<sub>50</sub> values that range between 0.05-100 μM in the presence of various ligands (110). It is clear that the killing effect of the gold cluster is not due to the ligand but rather of the gold core itself as has been shown by the Figure 5.5. Nevertheless chemical composition of the ligand is very important for the whole integrity and solubility of the gold cluster. There is a relatively large amount of gold (I) and gold(III) compounds evaluated for their antitumor activity. Many gold (I)-based compounds that were liganded with phosphorus-bound phenyl groups or thiol-based groups have exhibited the highest activity than other ligands (110). It is possible that the good solubility of the gold cluster in the media is a reason for the faster cytotoxicity than cisplatin which is poorly soluble. Currently much of the research is directed towards the generation of phosphine-supported gold-based compounds with biologically active groups so that drug properties like solubility and acidity can be controlled (105).

Au<sub>55</sub> has been able to produce a significant killing effect on the metastatic melanoma cell lines BLM and MV3 and overcome at a large extent resistance to cisplatin. These are very promising results since it has been considered that there is virtually no effective treatment for patients with advanced melanoma. Apparently biochemotherapy which is composed of a sequential administration of cisplatin followed by interleukin-2 (IL-2) and interferon-α (INF-α) has indicated a relatively good response rate, however the clinical significance and the precise mechanism of its effects need to be clarified (94). The mechanism by which melanoma cell lines develop cellular resistance to various chemotherapy agents including cisplatin has not been elucidated yet. Nevertheless some of the molecular factors that have been considered to attribute to chemoresistance are the Multidrug-resistance associated protein (MRP) (7), enhanced repair of DNA damage (28, 31, 85), increased levels of sulfur-containing molecules (77), as well as the oncogenes *N-Ras*, *Bcl-2* and *p53* (48, 99,

102). *p53* is one of the most commonly mutated genes in human cancers. The *p53* protein is involved in cellular response when there is DNA damage induced by anticancer drugs by initiating chemotherapy-induced apoptosis. In addition *p53* induces the activation of various caspases which are considered as one of the key steps in the genesis of apoptosis. In a recent study has been demonstrated that in wild-type *p53* apoptosis was induced however in mutant *p53* it was not, indicating that resistance to chemotherapy may be related to the status of *p53* (65). It is not known whether MV3 and BLM have a defect on *p53*. It has been suggested that aggressive chemoresistant tumors usually have mutations on gene *p53* however this does not occur often in melanomas. Nevertheless it has been demonstrated that metastatic melanomas often lose Apaf-1 a mediator that acts with caspase-9 and cytochrome c that induce *p53*-dependent apoptosis (104). It is not clear yet if the gold cluster would have an effect at Apaf-1 or *p53* proteins directly or at some stage during the pathway they mediate in since BLM cells are resistant to cisplatin but not Au<sub>55</sub>. According to the caspase 3/7 assay we have found in the presence of either Au<sub>55</sub> or cisplatin the same levels of caspases are observed as in the untreated cells. This could indicate that the BLM cells might be dying by necrosis. In the case of cisplatin-mediated necrosis could be possible since melanoma cells are resistant to cisplatin, however in the case of Au<sub>55</sub> perhaps the induction of apoptosis could have been expected since the melanoma cells are significantly sensitive to the gold clusters. Nevertheless it could be possible that apoptosis is indeed induced but by a pathway that is independent by either *p53* protein or caspases. A study performed in renal cells has shown that cisplatin induced 50% of a *p53* mediated apoptosis by activating normally caspase-3 through the previous activation of caspases-8 and -9 as well as independently of caspases -9 or -8 or mitochondrial dysfunction. The remaining 50% of apoptosis was mediated by an additional mechanism independent of *p53* and caspases-3, -8 and -9 (27).

Apart from melanoma, osteosarcoma is also a relatively common malignant tumor. Chemotherapy is considered as the first choice including the use of many anticancer drugs either metal-based such as cisplatin or non-metal. Many antitumor agents have been used in combination in order to increase the efficacy and reduce the development of drug resistance. In the case of the osteosarcoma cell line U-2OS it could be concluded that the cells are relatively resistant to cisplatin and quite sensitive in the presence of Au<sub>55</sub>. There is a smaller induction of caspases -3 and -7 in the presence of Au<sub>55</sub> than cisplatin. The induction of apoptosis by cisplatin in U-2OS cells has been verified in a previous study

(86). In this study it was also found that resistance to apoptosis is associated with reduced susceptibility to apoptosis with not only *p53* but also *bcl-2* gene expression as well as Bcl-2 – independent factors like Bcl-x playing an important role. Another study performed in osteosarcoma cell line HOS has indicated the activation of caspases -8, -3 and -6 by cisplatin (98). Since there are so many signalling pathways that can induce apoptotic death, that the contribution of molecular factors other caspases cannot be ruled out. In addition it could be possible of both modes of cell death apoptosis and necrosis occurring in the same population of cells are present. The induction of necrosis can not be ruled since some preliminary results obtained by Annexin V-FITC and propidium iodide staining revealed the presence of necrotic cells either under the influence of cisplatin or Au<sub>55</sub> (results not presented).

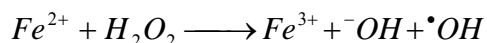
Nevertheless the characterisation of the mode of cell death induced by anticancer drugs is rather complicated and great care is required when interpreting results. The induction of apoptosis by Au<sub>55</sub> should be treated only as a preliminary result since it needs to be verified more systematically and by other methods. More specifically, using the combination of Annexin V-FITC/propidium iodide staining followed by flow cytometry it is possible to recognise an early event of apoptosis i.e. the exposure of phosphatidylserine residues at the surface of plasma membrane (111). Tunnel assay is another method for the detection of apoptosis, however it recognises DNA fragmentation by detecting the 3'-OH single stranded ends of DNA (119). Finally the expression of apoptosis-related genes could also be investigated.

The ultimate target and the main mechanism of action for gold-based compounds is still not known. There are rather contradicting views, whether gold-based drugs interact with biomolecules such as DNA. Some studies have shown that particular gold (III) compounds can bind rapidly and tightly to DNA (11), damage DNA through the formation of interstrand crosslinks and single strand breaks (116) while others have shown that gold drugs have a low binding affinity for the DNA double helix (72, 78).

Regarding the distribution of gold compounds in cells, one study has shown that triphenylphosphine gold(I) compounds can be rapidly incorporated into cells, distributed in the cytoplasm and in the nuclear fraction and induce single stranded breaks in DNA (46, 52, 110). The results presented in this thesis are in a good agreement with the above study. Nevertheless it is not clear yet whether the incorporation of Au<sub>55</sub> into the DNA is responsible for the cytotoxic effects observed on the various cell lines investigated in this

study. Regarding the incorporation of gold clusters inside the cells remains to be elucidated. According to the literature drugs can enter cells by different mechanisms. The antineoplastic drug cisplatin has been found to enter cells by passive diffusion (49). Nevertheless some reports also have indicated the involvement of an active transport mechanisms mediated by a copper transport protein (57). Mutations in this protein have indicated resistance of the cells into cisplatin. Interestingly a recent study has indicated that the status of cisplatin is very important for which mechanism will mediate the transport. It was supported that passive diffusion occurred when cisplatin was in its neutral dichloroform whereas active transport was mediated when cisplatin was hydrolysed (87). Gold clusters are relatively small consisting of about 2.5 nm with the ligand and of hydrophilic nature. The whole compound would be charged and it is not certain whether a passive diffusion across the membrane could occur. Nevertheless the involvement of an energy dependent method such as by active transport in the presence of membrane protein channels like in the case for cisplatin can not be ruled out and the cluster's size is small enough to fit through most of the pores. Recently has been reported that protein-gold-cluster complexes with diameter of 25 nm have been transferred across nuclear pores in normal fibroblasts. Interestingly enough an increase in the transport was correlated with a decrease in *p53* levels (40).

It has been found based on cellular fractionation experiments, the distribution of radioactive Au<sub>55</sub> in the nucleus, as well as in the cytoplasm. A large fraction of Au<sub>55</sub> cluster was tightly bound to the genomic DNA rather than in the nuclear protein fractions. Agarose gel electrophoresis indicated that Au<sub>55</sub> can cause single stranded breaks in plasmid DNA as shown by Figure 5.7b. These DNA breaks are only induced in the presence of H<sub>2</sub>O<sub>2</sub>. Such an effect has also been observed after the incubation of bleomycin or copper complexes with DNA. In this case a Fenton reaction has been suggested to occur which generates hydroxy radicals that can damage and cleave DNA (9, 93).



Whether the hydroxyl radicals are the only reactive oxygen species is still disputed (9). It is still possible that the Fenton reaction also occurs in the presence of gold.

In this study a large fraction of the gold cluster was found in the cytoplasmic fraction which included cytoplasmic proteins, organelles as well as plasma membrane components. It is possible that gold clusters could mediate their cytotoxic effect in the mitochondria. A

recent study performed in rat liver cells has indicated the interaction of a gold-based compound auranofin which is widely utilised in the treatment of rheumatoid arthritis with mitochondrial thioredoxin reductase at the seleno-group of the protein's active site. In addition auranofin was able to induce a transition in the permeability status of mitochondria, which was characterised by swelling and loss of the membrane potential (92). Another study has also indicated inhibition of viability as well as of oxidative phosphorylation and ATP production in rat hepatocytes by triethylphosphine gold(I) chloride (75). Interestingly there is no documentation so far on the interaction of metal-based compounds with mitochondrial DNA.

It is not certain yet whether the cytotoxicity of Au<sub>55</sub> is due to its direct interaction with DNA inhibiting DNA- protein interaction, damaging DNA in the presence of oxygen free radicals produced by respiration or due to the direct interaction of Au<sub>55</sub> with cytoplasmic components. In order to gain more insight into the interactions of this new potential anticancer drug we investigated the interactions with DNA structures of different sequences using molecular docking simulations. Computer simulations involving methods such as molecular docking can provide very useful information not only in the design of novel drugs based on potential energies, chemical properties, and geometrical fitting but also in understanding how an existing drug or any type of ligand would interact with a biomolecule such as DNA (25, 69, 106).

Molecular docking simulations were performed in a variety of DNA structures since we wanted to investigate any sequence specificity of Au<sub>55</sub> in a variety of different sequences. This method could be considered rather elegant since the most energetically favourable binding site can be found without direct contribution by the molecular modeller. We have found that the major groove is preferred by the Au<sub>55</sub> cluster to the minor groove. As has been mentioned earlier the major groove has a different geometry to the minor groove and it has such dimensions that the gold cluster could be easily accommodated. This method calculated the intermolecular interactions based on the sum of the van der Waals and electrostatic interactions. The electrostatic interactions in this case are not taken into account since the forcefield PCFF gives the Au atoms a partial charge of zero. This means that no electrostatic effects are taken into account during the docking simulations but only steric effects. Therefore we could say that the best binding site is where the gold cluster fits best which means at sites which are not too big neither too small but have dimensions that

fit the clusters own dimensions. It is clear therefore based on groove dimensions the preference of the gold cluster for the major groove rather than the minor groove (Figures 5.10a and 5.11a).

Molecular docking simulations also indicated for all structures the preference of AT rich sequences. More specifically AATT sequences are the mostly preferred and TATG is more favourable than alternating ATAT sequences (Table 5.3). If the electrostatic effects were taken indeed into account this sequence preference would be understood since in the first and second arrangement the gold cluster would come into contact with more N or O groups than in the case of ATAT. Nevertheless DNA structure is so delicate and even though around the helix each major groove appears to be the same, however, in reality each nucleobase is stacked in such a way in order to avoid steric effects. The most simple way of explaining small changes in groove dimensions is by looking at the distances of directly opposite phosphates at the major grooves. For example such distances have been measured for the structure 1BNA (see Appendix) to range between 18.01 and 19.32 Å. At the smallest distance of 18.01 the location of Au<sub>55</sub> in the structure with the lowest intermolecular interaction was observed. In the other two docked structures which exhibited higher intermolecular interactions the cluster was located between phosphates which were 18.19 and 19.32 Å respectively apart. Obviously the gold cluster prefers sites that it would considered 'comfortably' big enough.

Studies performed so far with gold-based compounds have shown that the probable binding sites for Au are O6 of guanine, N1/N7 of adenine, N3 of cytosine and N3 of thymine (6, 50). One more study has shown that gold (III) complexes can bind strongly and rapidly to calf-thymus DNA with preferential binding at GC sequences (11). These studies only partly contradict our findings which based on molecular docking simulations have shown that mainly the interaction probably takes place with the gold atoms that are in close proximity with the atoms, N7 of adenine, O4 of thymine, and with phosphate oxygens (Figure 5.9b). Nevertheless these results need to be verified experimentally. It should also be noted that only few DNA structures have been investigated in this study. Polynucleotide structures composed of 10-12 base-pairs long can adopt different conformations which are very dependent on the sequence, for example GC rich segments adopt A-DNA conformation whereas AT containing sequences adopt the B-DNA conformation (30). In order to investigate every sequence possibility many structures are

required to be built and evaluated first by molecular dynamics simulations in the presence of different solvents and ion concentrations in order to adopt the correct conformation. Nevertheless there are thousands of possible nucleotide arrangements that can occur. To investigate them all firstly, by molecular dynamics and subsequently, by molecular docking simulations would be practically impossible.

It is also worth mentioning that the binding site could be influenced by the presence of not too many phosphate groups. Towards the prime ends of DNA structures the gold clusters are not so heavily surrounded by phosphate groups therefore one needs to be careful in the interpretation of docking results regarding DNA sequence specificities.

It is rather interesting the specificity that Au<sub>55</sub> cluster exhibits for the AATT sequence. It is possible that this could be one of the reasons why this drug has been able to overcome significantly cisplatin resistance. Cisplatin is known to form intrastrand (GpG) and interstrand (ApG) cross-links (36, 42). Therefore cisplatin interacts at nucleobase sequences which are different to that of Au<sub>55</sub>. In addition AT pairs are easier to deform than GC pairs due to presence of one less hydrogen bond. Therefore Au<sub>55</sub> attacks DNA at a site which is structurally weaker than the cisplatin-binding site. Whether Au<sub>55</sub> is capable of forming inter or intrastrand cross links or its main mechanism of action is to block a large part of the major groove remains to be investigated. It would not be surprising if the mechanism is to just block the major groove since that would inhibit the formation of hydrogen bonds between proteins and DNA which could subsequently lead to an inhibition of the specific and non-specific binding of many major-groove associating proteins (96).

Apart from direct DNA- gold cluster interactions it is possible that the Au<sub>55</sub> interacts with proteins which are important either intracellularly or extracellularly. It has been observed from the cellular fractionation experiments that a relatively high amount of radioactive gold cluster is also present at the cytoplasmic fraction. The effect of Au<sub>55</sub> on albumin has been investigated experimentally as well as theoretically for two main reasons; firstly albumin is the most abundant protein in the human organism and it is known to interfere with many anticancer drugs and is known to play an important role for their distribution throughout the human body. Therefore it can interfere with their biological activity and clinical effectiveness (43). Secondly it is used as a model protein for investigating the interactions of Au<sub>55</sub> with sulfur-containing sites since it consists of 17 disulfide bridges and of one free thiol group (18). Clearly the higher IC<sub>50</sub> value obtained by an increase in serum

concentration (Figure 5.11) indicates that the gold cluster can become captured by components of FCS. Fetal calf serum is composed by a large protein content including albumin, as well as cholesterol, free fatty acids etc. Specifically albumin seems to attract a relatively large amount of Au<sub>55</sub>. Literature indicates that generally gold(I) and (III), platinum(II) and (IV) complexes interact primarily with the free sulfhydryl group of Cys34 residue (12, 38) where as ruthenium(III) and rhodium(II) interact with histidine residues (38). The molecular docking simulations presented in this study were conducted in a way that exploits every cysteine residue and its surrounding area as a possible binding site. As indicated by Figures 5.12 and 5.13, the cysteine residues are preferred over other binding sites. In addition the most favourable binding site was at two disulfide bonds located between the three domains of albumin. At this site the most of gold cluster surface is engulfed by the protein surface. The next most favourable binding site was at the Cys34 residue which is in agreement with the literature. Again the gold cluster is less exposed to the surface. Similarly to DNA binding sites the gold cluster interacts with sites that are ‘comfortably’ big enough. It is indicated in the literature that interaction of gold(I) compounds to other cysteine residues is possible through the oxidation of the ligand by the disulfide bond in the presence of water molecules. Therefore if there is a chemical reaction occurring between albumin and gold cluster it does not necessarily mean that it will only happen at the site where there is a free thiol. In addition the albumin crevice-opening as well as the exposure of the cysteine are one of the most determining steps for the interaction of gold compounds with this protein (38).

### **6.3 Interactions between amino acids and zeolite beta**

Zeolites are gaining an increasing importance in industrial applications with important applications in catalysis as well as in biotechnology for the purification of proteins and amino acids. Molecular simulations in conjunction with experiments can play a very important role in increasing our understanding on the atomic details involved during molecular adsorption into surfaces. There is a large amount of literature in MD simulations which focuses on the behavior of small molecules like, gases and hydrocarbons in zeolites (44). Nevertheless biomolecules like amino acids and their interactions with zeolitic materials have not been investigated computationally so far. In this study the interactions of three amino acids, Phe, Glu and Lys with zeolite beta have been investigated using MD



simulations. In order to symplify the system, simulations have been performed with the zeolite beta (BEA) free of any aluminum content.

In the MD simulations each amino acid was placed in different sides of the zeolite structure since it is not known which one is the most biologically significant location. Our simulations have shown that specific surfaces were preferred from others. In the surfaces preferred the amino acids could come at greater extent in contact with the oxygen atoms on the surface of the zeolite. The other surfaces are characterised by large openings and therefore the amino acids were mostly located outside a pore rather on a surface. The interiors of the pores of the zeolites were also not preferred since there were very few water molecules with which the amino acids could interact with. In this case we should note that the absence of aluminum atoms could perhaps influence this result. It has been demonstrated that aluminium atoms are usually randomly distributed in zeolite ZSM-5 and are mostly located in the interior rather than the surface or on pore openings (32, 73). In the case of placing the amino acids in bulk water also resulted in high energies indicating that it is not a favorable interaction. The most favorable interactions occurred when the amino acids were interacting with the surfaces 02 and 03 of the zeolite beta.

Especially in the case of the amino acid Phe, the interaction was the most favorable, based on stabilisation energies and hydrogen bond formation being observed between the amino group and the oxygen atoms at the zeolite surface. This is in agreement with experimental results reported by Ernst and his coworkers (83). Based on separate pHs they were capable to distinguish between the adsorption of Phe, Lys and Glu on zeolite Beta. Phe showed the highest adsorption at pH 6 followed by lower adsorption of Lys and then by minimal adsorption of Glu. The simulations performed in this study have not been able to distinguish between Glu and Lys. It has been clearly demonstrated by the MD simulations that Glu does not interact with the zeolite surface at the same extent as Phe. Perhaps the extra carboxyl group present in Glu influences it to interact more with water molecules which surround it. Based on the values obtained from the stabilisation energies we can not distinguish Lys from Glu. Nevertheless the simulations have shown that this amino acid does not leave the surface of the zeolite like Glu does. Nevertheless it does not remain stable on a zeolite cavity like Phe either. It could be characterised though as if it tries to 'walk' along the zeolite surface.

Finally it can be concluded that MD simulations have succesfully demonstrated the preference of Phe for zeolite beta comparing to Lys and Glu. Electrostatic interactions

between the amino groups and the zeolite oxygen atoms seem to play an important role. MD simulation based on energies can not distinguish the preference of Lys for the zeolite over Glu. Nevertheless at the molecular level differences between the adsorption characteristics of these two amino acids have been observed.

## 7. Summary

---

In this study the interactions of biomacromolecules with different inorganic nanostructured materials were investigated using experimental and theoretical approaches. A deeper understanding on the fundamental steps involved for such interactions is very important for the fields of nanotechnology, medicine and biotechnology. In nanotechnology biomolecules like DNA have often been considered as templates for the scaffolding of nanoparticles. TEM observations of DNA molecules with Au<sub>55</sub> cluster indicated the formation of equidistant gold nanowires. Interestingly the nanowires were composed of such dimensions that indicated that the Au<sub>55</sub> cluster initially used was reduced to the size of a cluster with 13 gold atoms. In order to understand the formation of gold nanowires, various molecular modelling techniques were employed. Based on molecular mechanics simulations, it was found that Au<sub>55</sub> cluster energetically prefers to interact with the major groove of B-DNA whereas Au<sub>13</sub> prefers to associate with the major grooves of A-DNA. It is not clear how the reduction of Au<sub>55</sub> to Au<sub>13</sub> occurs however it is assumed that it is influenced by the dramatic alterations occurring in the groove geometry during B-DNA to A-DNA transition. The formation of gold nanowires is determined by the equidistant decoration of Au<sub>13</sub> clusters around the major grooves of A-DNA. Molecular dynamics simulations indicated that the aggregation of such DNA-gold complexes leads to the formation of nanowires which are separated from each other almost 0.5 nm.

The ability of Au<sub>55</sub> to interact with the major grooves of B-DNA led to further investigations on the potential of this gold cluster as an anticancer drug. Gold-based compounds have not been studied as extensively as other metal-based drugs like platinum derivatives which have been employed as chemotherapeutic agents for many years in medical oncology. A variety of human cancer and healthy cell lines have been employed for investigating sensitivity towards Au<sub>55</sub> and cisplatin. *In vitro* cytotoxicity assays performed by a colourimetric-based method (MTT) have indicated that generally Au<sub>55</sub> is more toxic and efficient than cisplatin. Especially the cisplatin resistant metastatic melanoma cell lines exhibited the highest sensitivity towards Au<sub>55</sub>. Apoptotic or necrotic death influenced by Au<sub>55</sub> was investigated by performing a fluorometric assay which measures the induction of the apoptotic proteins caspases -3 and -7. The effect of Au<sub>55</sub> was different among the five cell lines investigated. In the case of the osteosarcoma cell

line U-2OS induction of caspases -3 and -7 in the presence either of Au<sub>55</sub> or cisplatin was observed indicating apoptosis being triggered. In the other four different cell lines the induction of caspases either in the presence of Au<sub>55</sub> or cisplatin was similar to the controls. This indicates that these cells could be dying either by necrosis, or apoptosis is induced through a caspase-independent pathway. Further information on the cellular localisation and possible target has been investigated by measuring the distribution of radioactive gold cluster in various cellular fractions of the BLM cell line. It has been found that slightly higher amount of Au<sub>55</sub> was located in the chromosomal DNA rather than in the cytoplasmic fraction. The Au<sub>55</sub> was strongly bound to the chromosomal DNA with a very small fraction of it being present in the nuclear proteins. This has indicated that DNA is one of the main cellular targets however it is not certain whether such an interaction is directly related to the cytotoxic effect of Au<sub>55</sub>. The gold cluster could possibly damage the chromosomal DNA in the presence of H<sub>2</sub>O<sub>2</sub> as indicated by the conversion of supercoiled plasmid DNA into open-circular form by agarose gel electrophoresis. Molecular docking simulations have shown the energetic preference of this agent for AATT sequences which is different to the GG and AG preference of cisplatin. Finally protein-gold cluster interactions could also play an important role on the cytotoxic effect of Au<sub>55</sub>. *In vitro* cytotoxicity assays in the presence of albumin have shown an increase in the IC<sub>50</sub> values indicating a sequestering effect of albumin protein. Molecular docking simulations suggest the interaction of Au<sub>55</sub> with specific cystein residues of human albumin.

Nanostructured inorganic materials have been considered very important in the field of biotechnology with major applications aiming towards the immobilisation or purification of biomolecules such as proteins and amino acids. In this study the interactions of three different amino acids with a zeolite structure have been investigated using molecular modelling. MD simulations have been performed in the presence of water molecules with Phe, Lys and Glu being placed around the structure of zeolite beta. The simulations have indicated that amino acids energetically prefer to interact with the surface of the zeolite-beta rather being placed inside the pores or in the bulk. MD simulations clearly indicate the preference of Phe to adsorb through the formation of hydrogen bonds with the O atoms of the zeolite structure. The amino acids Lys and Glu have indicated a lower preference as the formation of fewer hydrogen bonds with the zeolite surface has been exhibited. This is in agreement with experimental studies reported in the literature. Nevertheless MD simulations have not been able to distinguish any differences on the adsorption behavior of Glu and Lys.

## 8. Outlook

---

The exciting field of molecular modelling has been drawing significant attention from scientists from many different disciplines. The modelling of large biomolecules such as nucleic acids, proteins and lipids with applications either in the field of nanotechnology nanobiotechnology or medicine could be considered as a multidisciplinary enterprise. Biologists are capable of describing the cellular picture; Chemists provide atomic and molecular details; Physicists contribute further to our understanding of molecules by focusing at the electronic level; Mathematicians analyse and provide new algorithms for the investigation of biomolecules or biomaterials; Computer scientists and engineers provide important support for running molecular modelling calculations with complicated programs (96). This work could also be considered as a rather small link between the disciplines of biology and chemistry. The questions that have been addressed range from the formation of nanowires to the anticancer mechanism of action of a gold cluster. It is an interesting example indicating the interconnection of different disciplines. Experimental results (TEM) led to the investigation and further understanding by using molecular models how nanowire formation occurs and how it is influenced by gold-cluster-DNA interactions. Further computational work provided the basis for further experimental investigations which have led to the discovery of the tremendous potential of a nanocluster which previously was exploited for nanotechnology, now to be considered as an anti-tumor therapeutic. There are still a lot of aspects that require further investigation either by theoretical or experimental methods which can eventually contribute additional knowledge and hopefully lead to the successful development of nanomaterials with applications in the field of nanotechnology, nanobiotechnology and medicine.

In order to understand and realise the applications of the gold nanowire in the field of nanotechnology, it would be interesting to measure its conductivity. This could be performed in a similar manner to the work of Ben-Yoseph and colleagues where a piece of DNA molecule with single-stranded ends was glued between two electrodes by taking advantage of the strand-complementarity properties of DNA. This stretched piece of DNA was used further as a template for the growth of a silver nanowire (8). Based on the same thinking we could measure the electric properties of a single DNA nanowire. In this case

we would need to consider some additional steps i.e. we will need to decorate the DNA molecule with gold cluster and purify from the rest of the cluster solution prior to its location between the electrodes. Apart from DNA, proteins could be also used as interesting templates for the deposition of metal clusters. More specifically S-layer proteins could be considered as interesting candidates for the nano patterning of surfaces. S-layers are prokaryotic proteins capable of forming a precisely ordered monolayer composed of identical subunits. They are capable of forming a monolayer at the liquid-air as well as at the liquid-solid interface (103). This self-assembly ability could be exploited for the development of nanoparticle structures with well-defined geometries. Interestingly a preliminary study performed by molecular modelling has shown that the pore of the S-layer protein subunit of the archaeal microorganism *Methanosarcina mazei* (61) has such pore dimensions that can fit the Au<sub>55</sub> cluster (results not shown).

Another interesting biomolecule is the peptide DNA which does not exist in nature but is artificial. What makes this molecule interesting is its ability to provide the same sequence information like normal DNA with a backbone consisting of peptide linkages (N-glycine) rather than phosphodiester bonding. PNA exhibits the basic Watson-Crick hydrogen bonding scheme and due to its uncharged backbone its helical structure is considered more stable than that of a normal DNA helix. It is enzymatically resistant, comparing to DNA and very stable high temperatures (91). Perhaps it would be interesting to observe whether nanowires could still be formed in the presence of a PNA molecules. Due to the absence of the overall negative charge on PNA molecules they would have to be constructed with cysteine residues in their backbone in order to attract the gold clusters.

Many details on the mechanism of action of the antitumor activity of cluster Au<sub>55</sub> need to be discovered in order to have a better understanding on the potential of this drug as well as on its further optimisation if required (Figure 8.1). Significant processes like DNA unfolding by topoisomerase enzymes, DNA replication, transcription, and translation should be investigated whether they are inhibited in vitro as well as in vivo under the influence of Au<sub>55</sub> cluster. The interaction of Au<sub>55</sub> with mitochondrial-proteins-transporters as well as mitochondrial-DNA are other important aspects that require investigation. Possible interaction of the gold cluster with plasma membrane proteins like ion transporters could provide important information on how this drug enters the cells as well a possible resistance mechanism. Extracellular factors such as matrix metalloproteinases which are known to affect melanoma progression (55) should also be investigated and

regarded as potential targets. Such processes would definitely increase our understanding of the mechanism of action. *In vivo* studies conducted in mice would contribute a significant amount of information on the efficacy of this drug on tumors, response rate, distribution as well as possible side effects. At the same time structural studies performed by circular dichroism as well as x-ray crystallography and molecular dynamics simulations could provide a missing link on the events that take place during the molecular recognition of proteins or DNA with the gold cluster. Protein unfolding, blockage of active sites, sequence specificity, DNA damage, DNA bending or surprisingly increased or decreased stability at AT steps would be significant information at the molecular level that will definitely lead to a better understanding on the mechanism of action.

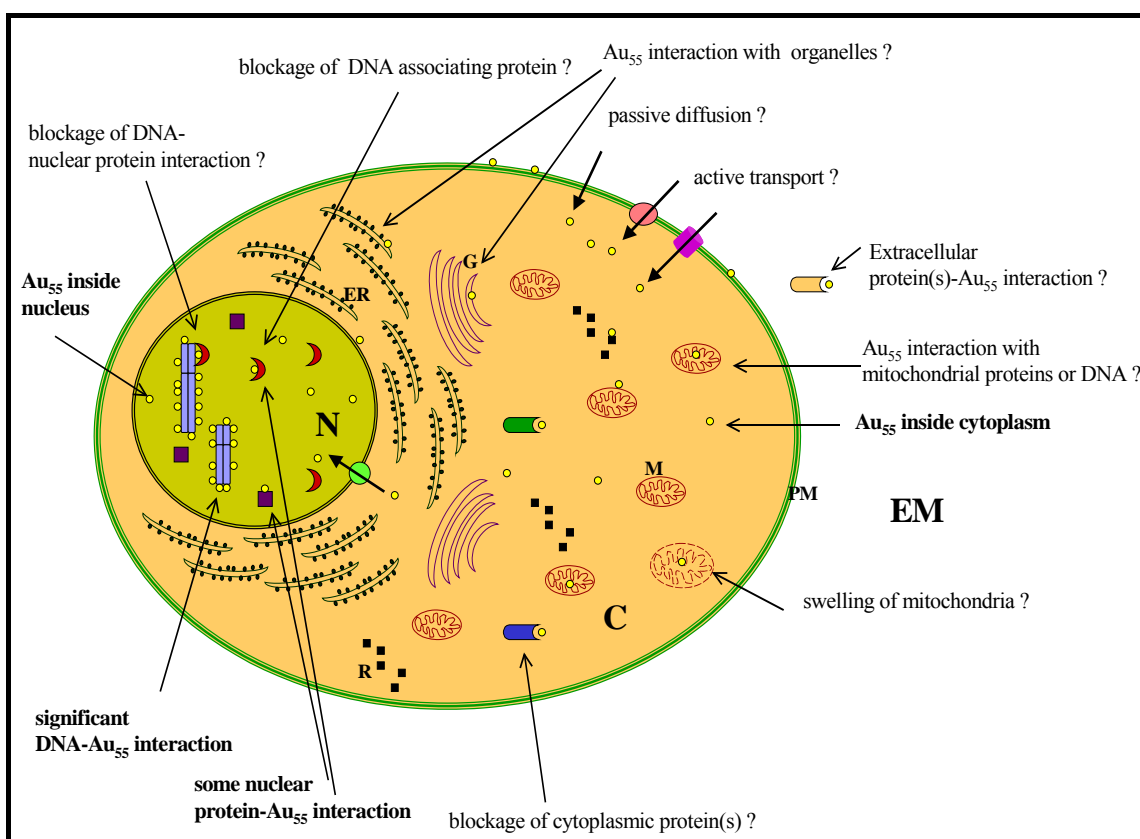


**Figure 8.1 Schematic representation of a mammalian cell.** Questions regarding the mechanism of action of Au<sub>55</sub> cluster being answered in this study are highlighted in bold characters and a lot of open questions for future investigations are written in standard characters. Where denoted N: nucleus, C: cytoplasm, EM: extracellular matrix, PM: plasma membrane, M: mitochondria, G: golgi apparatus, ER: endoplasmic reticulum, R: free ribosomes.

It is a particularly exciting time to be performing research. The marriage of various disciplines as well as the rapid development of molecular methods either in the field of molecular biology or molecular modelling allow the scientists to develop new ideas and most importantly produce new materials with important applications in nanotechnology, nanobiotechnology and medicine. Specifically molecular modelling is a very valuable tool for the designing and prediction of new nanomaterials with specific geometries and chemical properties. With the sequencing of the human genome it can be clearly understood the extreme significance of computational simulations. Once we know the sequence and therefore the structure and function of all of the genes in the human organism then rational drug design will play a central role in drug development. Especially molecular docking simulations will overcome the burden of synthesizing millions of compounds. Instead of performing screening of compounds *in vitro* the screening will be performed *in silico* by docking libraries of thousands of structures on a specific biomolecule of interest. The capability of molecular modelling has already been exploited by many pharmaceutical companies which have in mind the targeting of specific molecular factors that play an important role on disease. Targeting specific molecules and pathways would lead to the development of not only better but also safer medicaments and materials.

*This should not be simply considered as just a wish but rather as a duty.*



## 9. References

---

1. **Andersson, D., P. Hammarstrom & U. Carlsson.** 2001. Cofactor-induced refolding: refolding of molten globule carbonic anhydrase induced by Zn(II) and Co(II). *Biochemistry* **40**:2653-61.
2. **ATCC.** [www.lgcpromochem-atcc.com](http://www.lgcpromochem-atcc.com).
3. **Bashir, R.** 2001. DNA-mediated artificial nanobiostructures: state of the art and future directions. *Superlattices and Microstructures* **29**:1-16.
4. **Bellon, S. F., J. H. Coleman & S. J. Lippard.** 1991. DNA unwinding produced by site-specific intrastrand crosslinks of the antitumor drug *cis*-diamminedichloroplatinum (II). *Biochemistry* **30**:8026 -8035.
5. **Berman, H. M., J. Westbrook, Z. Feng, G. Gilliland, T. N. Bhat, H. Weissig, I. N. Shindyalov & P. E. Bourne.** 2000. The Protein Data Bank. *Nucleic Acids Research* **28**:235-242.
6. **Blank, C. E. & J. C. Dabrowiak.** 1984. Absorption and Circular Dichroism Studies of a Gold I DNA Complex. *Journal of Inorganic Biochemistry.* **21**:21-30.
7. **Borst, P., R. Evers, M. Kool & J. Wijnholds.** 2000. A family of drug transporters: the multidrug resistance-associated proteins. *Journal of the National Cancer Institute* **92**:1295-1302.
8. **Braun, E., Y. Eichen, U. Sivan & G. Ben-Yoseph.** 1998. DNA-templated assembly and electrode attachment of a conducting silver wire. *Nature* **391**:775-778.
9. **Breen, A. P. & J. A. Murphy.** 1995. Reactions of oxyl radicals with DNA. *Free Radical Biology & Medicine* **18**:1033-1077.
10. **Burda, J. V., J. Šponer, J. Leszczynski & P. Hobza.** 1997. Interaction of DNA base pairs with various metal cations ( $Mg^{2+}$ ,  $Ca^{2+}$ ,  $Sr^{2+}$ ,  $Ba^{2+}$ ,  $Cu^{+}$ ,  $Ag^{+}$ ,  $Au^{+}$ ,  $Zn^{2+}$ ,  $Cd^{2+}$ , and  $Hg^{2+}$ ): Nonempirical ab initio calculations on structures, energies, and nonadditivity of the interaction. *Journal of Physical Chemistry B* **101**:9670-9677.
11. **Calamai, P., S. Carotti, A. Guerri, L. Messori, E. Mini, P. Orioli & G. P. Speroni.** 1997. Biological properties of two gold (III) complexes:  $AuCl_3(Hpm)$  and  $AuCl_2(pm)$ . *Journal of Inorganic Biochemistry* **66**:103-9.
12. **Carter, D. C. & J. X. Ho.** 1994. Structure of serum albumin. *Advances in Protein Chemistry* **45**:153-203.

13. **Chabner, B. A.** 1993. Biological basis for cancer treatment. *Annals of Internal Medicine* **118**:633-637.
14. **Chabner, B. A., D. P. Ryan, L. Paz-Arez, R. Garcia-Carbonero & P. Calabresi.** 2001. Antineoplastic drugs, p. 1389-1460. In J. G. Hardman & L. L. Limbird (ed.), Goodman & Gilman's: The pharmacological basis of therapeutics, 10th ed. McGraw-Hill, New York.
15. **Cheatham, T. E., M. F. Crowley, T. Fox & P. A. Kollman.** 1997. A molecular level picture of the stabilization of A-DNA in mixed ethanol-water solutions. *Proceedings of the National Academy of Sciences of the United States of America* **94**:9626-9630.
16. **Chiku, H., M. Matsui, S. Murakami, Y. Kiyozumi, F. Mizukami & K. Sakaguchi.** 2002. Zeolites as new chromatographic carriers for proteins -easy recovery of proteins adsorbed on zeolites by polyethylene glycol. *Analytical Biochemistry* **318**:80-85.
17. **Chopra, S. S. & S. Kaufmann.** 1982. *cis*-Diamminedichloroplatinum-induced acute renal failure in the rat. *Kidney International* **21**:54-64.
18. **Christodoulou, J., P. J. Sadler & A. Tucker.** 1994. A new structural transition of serum albumin dependent on the state of Cys34. Detection by <sup>1</sup>H-NMR spectroscopy. *European Journal of Biochemistry* **225**:363-368.
19. **Chung, Y. C., D. H. Son & D. H. Ahn.** 2000. Nitrogen and organics removal from industrial wastewater using natural zeolite media. *Water Science & Technology* **42**:127-134.
20. **Clarke, M. J., Z. Fuchun & D. R. Frasca.** 1999. Non-platinum chemotherapeutic metallopharmaceuticals. *Chemical Reviews* **99**:2511-2533.
21. **Collins, J. A., C. A. Schandl, K. K. Young, J. Vesely & M. C. Willingham.** 1997. Major DNA fragmentation is a late event in apoptosis. *Journal of Histochemistry & Cytochemistry* **46**:923-934.
22. **Comba, P. & T. Hambley.** 2001. Molecular modelling of inorganic compounds. Wiley-VCH, Weinheim.
23. **Conner, B. N., T. Takano, S. Tanaka, K. Itakura & R. E. Dickerson.** 1982. The molecular structure of deoxy(iodo-CCGG), a fragment of right handed double helical A-DNA. *Nature* **295**:294-299.
24. **Corma, A.** 2003. State of the art and future challenges of zeolites as catalysts. *Journal of Catalysis* **216**:298-312.
25. **Craig, S. P. & A. E. Eakin.** 2000. Structure-based inhibitor design, p. 149, Vitamins and hormones - Advances in research and applications, vol. 58.

26. **Cramer, C. J.** 2002. *Essentials of Computational Chemistry: Theories and Models*. John Wiley & Sons, Chichester.
27. **Cummings, B. S. & R. G. Schnellman.** 2002. Cisplatin-induced renal cell apoptosis: Caspase 3-dependent and -independent pathways. *Journal of Pharmacology & Experimental Therapeutics* **302**:8-17.
28. **Dabholkar, M., J. Vionnet, F. Bostick-Bruton, J. J. Yu & E. Reed.** 1994. Messenger RNA levels of XPAC and ERCC1 in ovarian cancer tissue correlate with response to platinum-based chemotherapy. *Journal of Clinical Investigation* **94**:703-708.
29. **Darzynkiewicz, Z., G. Juan, X. Li, W. Gorczyca, T. Murakami & F. Traganos.** 1997. Cytometry in cell necrobiology: Analysis of apoptosis and accidental cell death (necrosis). *Cytometry* **27**:1-20.
30. **Daune, M.** 1999. *Molecular Biophysics: Structures in Motion*. Oxford University Press, Oxford.
31. **de Laat, W. J., N. G. Jaspers & J. H. Hoeijmakers.** 1999. Molecular mechanism of nucleotide excision repair. *Genes & Development* **13**:768-785.
32. **Dedecek, J., D. Kaucky & B. Wichterlova.** 2001. Al distribution in ZSM-5 zeolites: an experimental study. *Chemical Communications*:970-971.
33. **Dent, P. & G. Grant.** 2001. Pharmacologic interruption of the mitogen-activated extracellular-regulated kinase/mitogen-activated protein kinase signal transduction pathway: potential role in promoting cytotoxic drug action. *Clinical Cancer Research* **7**:775-783.
34. **Douglas, K., N. A. Clark & K. J. Rothschild.** 1986. Nanometer molecular lithography. *Journal of Applied Physics* **49**:676-678.
35. **Drew, H. R. & R. E. Dickerson.** 1981. Structure of B-DNA dodecamer III. Geometry of hydration. *Journal of Molecular Biology* **151**:535-556.
36. **Eastman, A.** 1986. Reevaluation of interaction of cis-dichloro(ethylenediamine)platinum(II) with DNA. *Biochemistry* **25**:3912 - 3915.
37. **Eguchi, E., S. Shimizu & Y. Tsujimoto.** 1997. Intracellular ATP levels determine cell death fate by apoptosis or necrosis. *Cancer Research* **57**:1835-1840.
38. **Esposito, B. P. & R. Najjar.** 2002. Interactions of antitumoral platinum-group metallodrugs with albumin. *Coordination Chemistry Reviews* **232**:137-149.
39. **Feig, M. & B. M. Pettitt.** 1999. Sodium and chlorine ions as part of the DNA solvation shell. *Biophysical Journal* **77**:1769-1781.

40. **Feldherr, C. M., D. Akin & R. Cohen.** 2001. Regulation of functional nuclear pore size in fibroblasts. *Journal of Cell Science* **114**:4621-4627.
41. **Ferreira, C. G., C. Tolis, S. W. Span, G. J. Peters, T. van Lopik, A. J. Kummer, H. M. Pinedo & G. Giaccone.** 2000. Drug-induced apoptosis in lung cancer cells is not mediated by the Fas/FasL (CD95/APO1) signaling pathway. *Clinical Cancer Research* **6**:203-212.
42. **Fichtiger-Schepman, A. M. J., J. L. van der Veer, J. H. J. den Hartog, P. H. M. Lohman & J. Reedijk.** 1985. Adducts of the antitumor drug *cis*-diamminedichloroplatinum(II) with DNA: formation, identification, and quantitation. *Biochemistry* **24**:707-713.
43. **Finkelstein, A. E., D. T. Walz, V. Batista, M. Mirzraji, F. Roisman & A. Mischer.** 1976. Auranofin. New oral compound for treatment of rheumatoid arthritis. *Annual Rheumatism Discussions* **35**:251-257.
44. **Fuchs, A. H. & A. K. Cheetham.** 2001. Adsorption of guest molecules in zeolitic materials: computational aspects. *Journal of Physical Chemistry B* **105**:7375-7383.
45. **Fuertes, M. A., J. Castilla, C. Alonso & J. M. Perez.** 2003. Cisplatin biochemical mechanism of action: From cytotoxicity to induction of cell death through interconnections between apoptotic and necrotic pathways. *Current Medicinal Chemistry* **10**:257-266.
46. **Garcia-Orad, A., P. Arizti, F. Sommer, L. Silvestro, P. Massiot, P. Chevallier, J. M. Gutierrez-Zorrilla, E. Colacio, M. Martinez De Pancorbo & H. Tapiero.** 1993. The (8-thiotheophyllinate) (triphenylphosphine) gold (I), (tTAUP): A new gold complex as an anticancer agent. *Biomedicine & Pharmacotherapy* **47**:363-370.
47. **Garzón, I. L., E. Artacho, M. R. Beltrán, A. García, J. Junquera, K. Michaelian, P. Ordejón, C. Rovira, D. Sánchez-Portal & J. M. Soler.** 2001. Hybrid DNA-gold nanostructured materials: an ab initio approach. *Nanotechnology* **12**:126-131.
48. **Gasco, M. & T. Crook.** 2003. p53 family members and chemoresistance in cancer: what we know and what we need to know. *Drug Resistance Updates* **6**:323-328.
49. **Ghezzi, A., M. Aceto, C. Cassino, E. Cabanno & D. Osella.** 2004. Uptake of antitumor platinum(II)-complexes by cancer cells, assayed by inductively coupled plasma mass spectrometry (ICP-MS). *Journal of Inorganic Biochemistry* **98**:73-78.
50. **Hadjiliadis, N., G. Pneumatikakis & R. Basosi.** 1981. Gold Complexes of Purine and Pyrimidine Nucleosides. *Journal of Inorganic Biochemistry* **14**:115-126.
51. **Hambley, T. W. & A. R. Jones.** 2001. Molecular mechanics modelling of Pt/nucleotide and Pt/DNA interactions. *Coordination Chemistry Reviews* **212**:35-59.

52. **Harker, C. S. W., E. R. T. Tiekink & M. W. Whitehouse.** 1991. Studies on the interaction of gold(I) phosphines with 2-thiouracil. Related studies with silver(I) phosphines. *Inorganica Chimica Acta* **181**:23-30.
53. **Heim, M. M., W. Eberhardt, S. Seeber & M. R. Müller.** 2000. Differential modulation of chemosensitivity to alkylating agents and platinum compounds by DNA repair modulators in human lung cancer cell lines. *Journal of Cancer Research & Clinical Oncology* **126**:198-204.
54. **Hinchliffe, A.** 2003. *Molecular Modelling for Beginners*. Wiley, Manchester.
55. **Hoffmann, U. B., J. R. Westphal, E. T. Waas, A. J. W. Zendman, I. M. H. A. Cornelissen, D. J. Ruiter & G. N. van Muijen.** 1999. Matric metalloproteinases in human melanoma cell lines and xenografts: increased expression of activated matrix metalloproteinase-2 (MMP-2) correlates with melanoma progression. *Journal of Cancer* **81**:774-782.
56. **Hudson, B. P. & J. K. Barton.** 1998. Solution structure of a metalointercalator bound site specifically to DNA. *Journal of the American Chemical Society* **120**:6877-6888.
57. **Ishida, S., J. Lee, D. J. Thiele & I. Herskowitz.** 2002. Uptake of the anticancer drug cisplatin mediated by the copper transporter Ctr1 in yeast and mammals. *Proceedings of the National Academy of Sciences of the United States of America* **99**:14298-14302.
58. **Jackson, L., I. Roberts & J. D. Morrow.** 2001. *Analgesic-antipyretic and antiinflammatory agents and drugs in the treatment of gout*, 10th ed. McGraw-Hill, New York.
59. **Jacobs, P. A. & R. A. van Santen (ed.).** 1989. *Zeolites: Facts, figures, future*, vol. 49. Elsevier, Amsterdam.
60. **Jensen, F.** 2001. *Introduction to Computational Chemistry*. John Wiley & Sons, Chichester.
61. **Jing, H., J. Takagi, J. Liu, S. Lindgren, R. Zhang, A. Joachimiak, J. Wang & T. Springer.** 2002. Archaeal surface layer proteins contain beta propeller, pkd, and beta helix domains and are related to metazoan cell surface proteins. *Structure* **10**:1453-1464.
62. **Kesraouiouki, S., C. R. Cheeseman & R. Perry.** 1994. Natural zeolite utilisation in pollution control- A review of applications to metal effluents. *Journal of Chemical Technology and Biotechnology* **59**:121-126.
63. **Leach, A. R.** 2001. *Molecular Modelling : Principles and Applications*, 2nd ed. Prentice Hall, Harlow.

64. **Lebrun, A. & R. Lavery.** 1999. Modeling DNA deformations induced by minor groove binding proteins. *Biopolymers* **49**:341-353.
65. **Li, G., L. Tang, X. Zhou, V. Tron & V. Ho.** 1998. Chemotherapy-induced apoptosis in melanoma cells is p53 dependent. *Melanoma Research* **8**:17-23.
66. **Lin, Y. S., I. Kumakiri, B. N. Nair & H. Alsyouri.** 2002. Microporous inorganic membranes. *Separation & Purification Methods* **31**:229-379.
67. **Lippert, B.** 2000. Multiplicity of metal ion binding patterns to nucleobases. *Coordination Chemistry Reviews* **200 - 202**:487 - 516.
68. **Liu, Y., S. Meyer-Zaika, S. Franzka, G. Schmid, M. Tsoli & H. Kuhn.** 2003. Gold cluster degradation by the transition of B-DNA into A-DNA and the formation of nanowires. *Angewandte Chemie* **42**:2853-2857.
69. **Lyne, P. D.** 2002. Structure-based virtual screening: an overview. *Drug Discovery Today* **7**:1047-1055.
70. **Machida, K.** 1999. Principles of Molecular Mechanics. Kodansha, John Wiley & Sons, Tokyo.
71. **Maple, J. R., M.-J. Hwang, T. P. Stockfish, U. Dinur, M. Waldman, C. S. Ewig & A. T. Hagler.** 1994. Derivation of Class II force fields. 1. Methodology and quantum force field for the alkyl functional group and alkane molecules. *Journal of Computational Chemistry* **15**:162-182.
72. **Marcon, G., S. Carotti, M. Coronello, L. Messori, E. Mini, P. Orioli, T. Mazzei, M. A. Cinellu & G. Minghetti.** 2002. Gold(III) complexes with bipyridyl ligands: Solution chemistry, cytotoxicity, and DNA binding properties. *Journal of Medicinal Chemistry* **45**:1672-1677.
73. **Marschmeyer, S. & H. Papp.** 1997. Surface analysis of a hydrothermally treated H-ZSM-5 zeolite. *Surface & Interface Analysis* **25**:660-666.
74. **Matsui, M., Y. Kiyozumi, T. Yamamoto, Y. Mizushina, F. Mizukami & K. Sakaguchi.** 2000. Selective adsorption of biopolymers on zeolites. *Chemical European Journal* **7**:1555-1560.
75. **Mc Keage, M. J., L. Maharaj & S. J. Berners-Price.** 2002. Mechanisms of cytotoxicity and antitumor activity of gold(I) phosphine complexes: the possible role of mitochondria. *Coordination Chemistry Reviews* **232**:127-135.
76. **McCrary, D. F. & P. J. Hobbs.** 2001. Additives to reduce ammonia and odor emissions from livestock wastes: A review. *Journal of Environmental Quality* **30**:345-355.

77. **Meijer, C., N. H. Mulder, G. A. Hospers, D. R. Uges & E. G. de Vries.** 1990. The role of glutathione in resistance to cisplatin in human small cell lung cancer cell line. *British Journal of Cancer* **62**.
78. **Messori, L., P. Orioli, C. Tempi & G. Marcon.** 2001. Interactions of selected gold(III) complexes with calf thymus DNA. *Biochemical & Biophysical Research Communications* **281**:352-360.
79. **Micheau, O., E. Solary, A. Hammann, F. Martin & M. T. Dimanche-Boitrel.** 1997. Sensitization of cancer cells treated with cytotoxic drugs to fas- mediated cytotoxicity. *Journal of the National Cancer Institute* **89**:783-789.
80. **Montemagno, C. & G. Bachand.** 1999. Constructing nanomechanical devices powered by biomolecular motors. *Nanotechnology* **10**:225-231.
81. **MSI, B.** 1995. Discover: User Guide Part I. Biosym MSI, San Diego.
82. **Mukhopadhyay, K., S. Phadtare, V. P. Vinod, A. Kumar, M. Rao, R. V. Chaudhari & M. Sastry.** 2003. Gold nanoparticles assembled on amine-functionalized Na-Y zeolite: A biocompatible surface for enzyme immobilization. *Langmuir* **19**:3858-3863.
83. **Munsch, S., M. Hartmann & S. Ernst.** 2001. Adsorption and separation of amino acids from aqueous solutions on zeolites. *Chemical Communications*.:1978-9.
84. **Nikoobakht, B., C. Burda, M. Braun, M. Hun & M. A. El-Sayed.** 2002. The quenching of CdSe quantum dots photoluminescence by gold nanoparticles in solution. *Photochemistry and Photobiology* **75**:591-597.
85. **Parker, R. J., A. Eastman, F. Bostick-Bruton & E. Reed.** 1991. Acquired cisplatin resistance in human ovarian cancer cells is associated with enhanced repair of cisplatin-DNA lesions and reduced drug accumulation. *Journal of Clinical Investigation* **87**:772-777.
86. **Perego, P., S. C. Righetti, R. Supino, D. Delia, C. Caserini, N. Carenini, B. Bedogne, E. Broome, S. Krajewski, J. C. Reed & F. Zunino.** 1997. Role of apoptosis and apoptosis-related proteins in the cisplatin-resistant phenotype of human tumor cell lines. *Apoptosis* **2**:540-548.
87. **Pereira-Maia, E. & A. Garnier-Suillerot.** 2003. Impaired hydrolysis of cisplatin derivatives to aquated species prevents energy-dependent uptake in GLC4 cells resistant to cisplatin. *Journal of Biological Inorganic Chemistry* **8**:626-634.
88. **Pileni, M. P.** 1998. Colloidal self-assemblies used as templates to control size, shape and self-organization of nanoparticles. *Supramolecular Science* **5**:321-329.

89. **Pindur, U. & G. Fischer.** 1996. DNA complexing minor groove-binding ligands: perspectives in antitumor and antimicrobial drug design. *Current Medicinal Chemistry* **3**:379-406.
90. **Šponer, J., M. Sabat, L. Gorb, J. Leszczynski, B. Lippert & P. Hobza.** 2000. The effect of metal binding to the N7 site of purine nucleotides on their structure, energy, and involvement in base pairing. *Journal of Physical Chemistry B* **104**:7535-7544.
91. **Ray, A. & B. Norden.** 2000. Peptide nucleic acid (PNA): its medical and biotechnical applications and promise for the future. *The FASEB Journal* **14**:1041-1060.
92. **Rigobello, M. P., G. Scutari, R. Boscolo & A. Bindoli.** 2002. Induction of mitochondrial permeability transition by auranofin, a gold(I)-phosphine derivative. *British Journal of Pharmacology* **136**:1162-1168.
93. **Saglam, N., A. Colak, K. Serbest, S. Dulger, S. Guner, S. Karabocek & A. O. Belduz.** 2002. Oxidative cleavage of DNA by homo- and heteronuclear Cu(II)-Mn(II) complexes of an oxime-type ligand. *BioMetals* **15**:357-365.
94. **Saida, T.** 2001. Recent advances in melanoma research. *Journal of Dermatological Science* **26**:1-13.
95. **Salvesen, G. S. & V. M. Dixit.** 1997. Caspases: intracellular signalling by proteolysis. *Cell* **91**:443-446.
96. **Schlick, T.** 2002. *Molecular Modeling and Simulation: An Interdisciplinary Guide*, vol. 21. Springer, New York.
97. **Schmid, G., N. Klein, L. Korste, U. Kreibig & D. Schönauer.** 1988. Large transition metal clusters VI. Ligand exchange reactions on Au<sub>55</sub>(PPh<sub>3</sub>)<sub>12</sub>Cl<sub>6</sub> - The formation of a water soluble Au<sub>55</sub> cluster. *Polyhedron* **7**:605-608.
98. **Seki, K., H. Yoshikawa, K. Shiiki, Y. Hamada, N. Akamatsu & K. Tasaka.** 2000. Cisplatin (CDDP) specifically induces apoptosis via sequential activation of caspase-8, -3 and -6 in osteosarcoma. *Cancer Chemotherapy & Pharmacology* **45**:199-206.
99. **Serrone, L. & P. Hersey.** 1999. The chemoresistance of human malignant melanoma: An update. *Melanoma Research* **9**:51-58.
100. **Shaw, C. F.** 1999. Gold-based therapeutic agents. *Chemical Reviews* **99**:2589-2600.
101. **Shimitzu, T. & A. Takada.** 1997. Preparation of Bi-based superconducting fiber by metal sorption of Na-alginate. *Polymer Gels & Networks* **5**:267-283.



102. **Siddik, Z. H.** 2003. Cisplatin: mode of cytotoxic action and molecular basis of resistance. *Oncogene* **22**:7265-7279.
103. **Sleytr, U. B., S. Margit, D. Pum & B. Schuster.** 2001. Characterisation and use of crystalline bacterial cell surface layers. *Progress in Surface Science* **68**:231-278.
104. **Soengas, M. S., P. Capodiecici, D. Polsky, J. Mora, M. Esteller, X. Opitz-Araya, R. McCombie, J. G. Herman, W. L. Gerald, Y. A. Lazebnik, C. Cordon-Cardo & S. W. Lowe.** 2001. Inactivation of the apoptosis effector Apaf-1 in malignant melanoma. *Nature* **409**:141-144.
105. **Song, Y. C., J. J. Vittal, N. Srinivasan, S. H. Chan & P. H. Leung.** 1999. Synthesis and anti-cancer activities of a pair of enantiomeric gold(I) complexes containing sulfanyl-substituted P-stereogenic phosphines. *Tetrahedron-Asymmetry* **10**:1433-1436.
106. **Sottriffer, C. A., W. Flader, R. H. Winger, B. M. Rode, K. R. Liedl & J. M. Varga.** 2000. Automated docking of ligands to antibodies: Methods and applications. *Methods-a Companion to Methods in Enzymology* **20**:280-291.
107. **Stein, G. S., R. Baserga, A. Giordano & D. T. Denhardt (ed.).** 1999. The molecular basis of cell cycle and growth control. Wiley & Sons, New York.
108. **Storhoff, J. J. & C. A. Mirkin.** 1999. Programmed materials synthesis with DNA. *Chemical Reviews* **99**:1849 - 1862.
109. **Sun, H., S. J. Mumby, J. R. Maple & A. T. Hagler.** 1994. An ab initio CFF93 all-atom force field for polycarbonates. *Journal of the American Chemical Society* **116**:2978-2987.
110. **Tiekink, E. R. T.** 2002. Gold derivatives for the treatment of cancer. *Critical Reviews in Oncology Hematology* **42**:225-248.
111. **van Engeland, M., L. J. W. Nieland, F. C. S. Ramaekers, B. Schutte & C. P. M. Reutelingsperger.** 1998. Annexin V-affinity assay: A review on an apoptosis detection system based on phosphatidylserine exposure. *Cytometry* **31**:1-9.
112. **van Muijen, G. N., K. F. Jansen, I. M. Cornelissen, D. F. Smeets, J. L. Beck & D. J. Ruiter.** 1991. Establishment and characterization of a human melanoma cell line (MV3) which is highly metastatic in nude mice. *International Journal of Cancer* **48**:85-91.
113. **van Muijen, G. N., C. L.M., C. F. Jansen, C. G. Figdor, J. P. Johnson, E. B. Brocker & D. J. Ruiter.** 1991. Antigen expression of metastasizing and non-metastasizing human melanoma cells xenografted into nude mice. *Clinical and Experimental Metastasis* **9**:259-272.

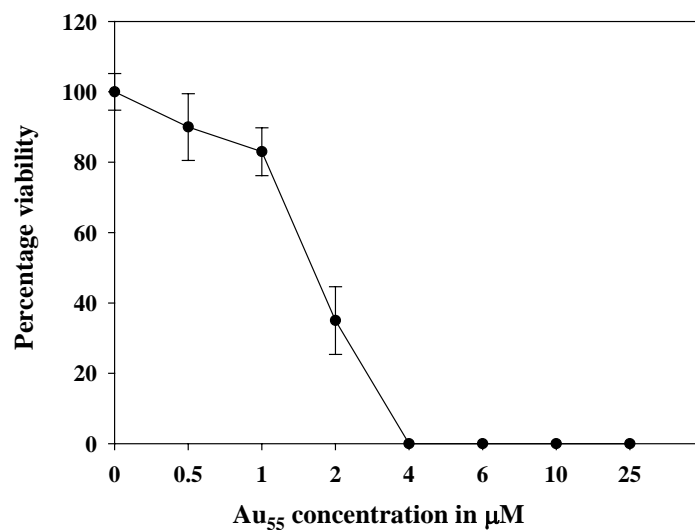
114. **Vaux, D. L. & A. Strasser.** 1996. The molecular biology of apoptosis. *Proceedings of the National Academy of Sciences of the United States of America* **93**:2239-2244.
115. **Wang, X., J. L. Martindale & N. J. Holbrook.** 2000. Requirement for ERK activation in cisplatin-induced apoptosis. *Journal of Biological Chemistry* **275**:39435-39443.
116. **Ward, B. & J. C. Dabrowiak.** 1987. DNA binding specificity of the gold(III) complex  $(C_2H_5)_3PAuBr_3$ . *Journal of the American Chemical Society* **109**:3810 - 3811.
117. **Welters, M. J., A. M. Fichtinger-Schepman, R. A. Baan, A. J. Jacobs-Bergmans, A. Kegel, W. J. van der Vijgh & B. J. Braakhuis.** 1999. Pharmacodynamics of cisplatin in human head and neck cancer: correlation between platinum content, DNA adduct levels and drug sensitivity in vitro and in vivo. *British Journal of Cancer* **79**:82-88.
118. **Whittaker, J. L., P. J. Byrd, R. J. Grand & P. H. Gallimore.** 1984. Isolation and characterisation of four adenovirus type 12-transformed human embryo kidney cell lines. *Molecular and Cellular Biology* **4**:110-116.
119. **Willingham, M. C.** 1999. Cytochemical methods for the detection of apoptosis. *Journal of Histochemistry & Cytochemistry* **47**:1101-1109.
120. **Wilson, M., K. Kannangarra, G. Smith, M. Simmons & B. Raguse.** 2002. Nanotechnology basic science and emerging technology. Chapman & Hall/CRC, Sydney.
121. **Wilson, N. T. & R. L. Johnston.** 2000. Modelling gold clusters with an empirical many-body potential. *The European Physical Journal D* **12**:161-169.
122. **Wong, E. & C. M. Giandomenico.** 1999. Current status of platinum-based antitumor drugs. *Chemical Reviews* **99**:2451-2466.
123. **Yang, P. & M. P. Guo.** 1999. Interactions of organometallic anticancer agents with nucleotides and DNA. *Coordination Chemistry Reviews* **185-186**:189-211.

## 10. Appendix

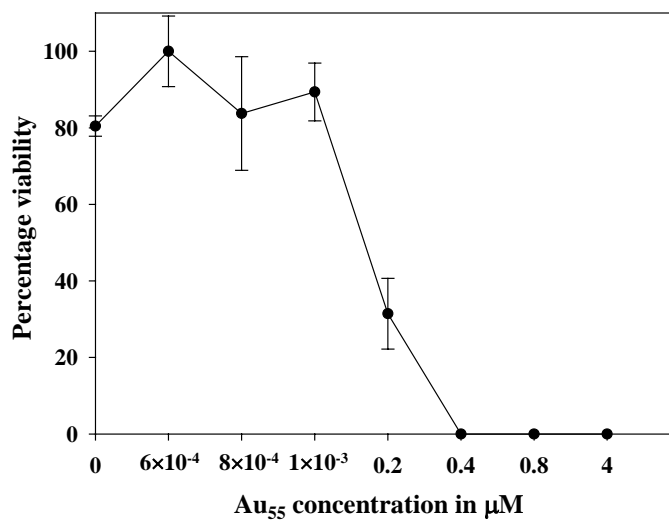
---

### 10.1 Additional *in vitro* cytotoxicity assays

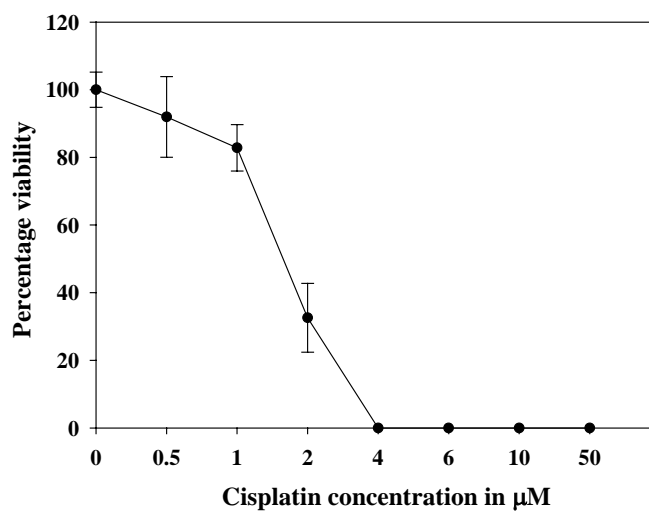
MC3T3-E1 cells exposed to various concentrations of Au<sub>55</sub> for 24 hours



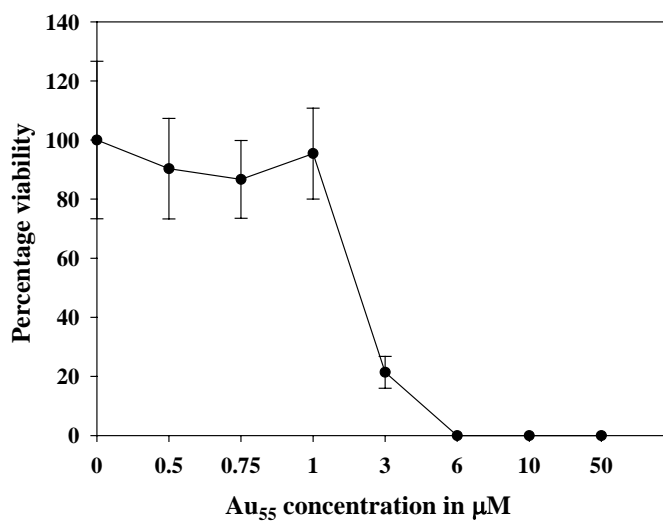
MC3T3-E1 exposed to various concentrations of Au<sub>55</sub> for 72 hours



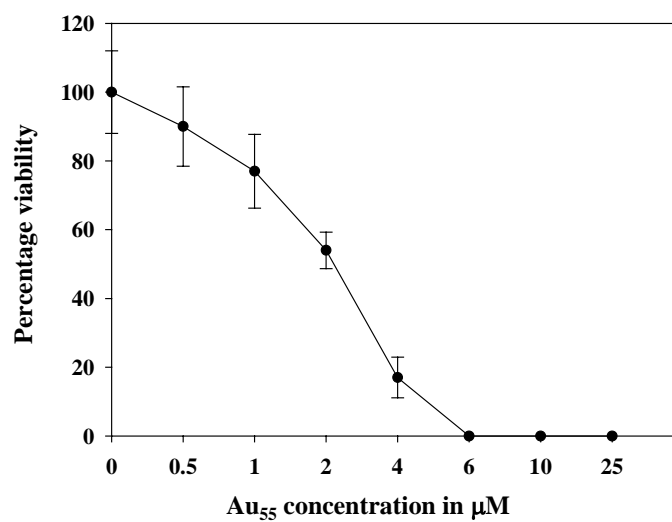
MC3T3-E1 exposed to various concentrations of cisplatin for 72 hours



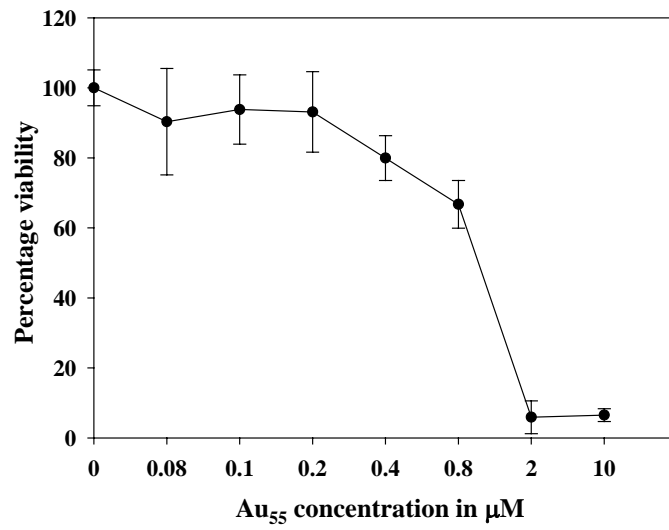
MOR/P cells exposed to various concentrations of Au<sub>55</sub> for 24 hours



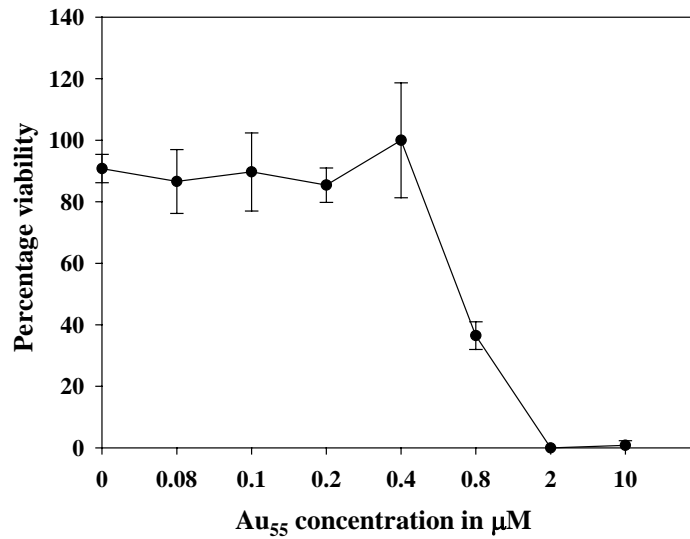
MOR/CPR cells exposed to various concentrations of Au<sub>55</sub> for 24 hours



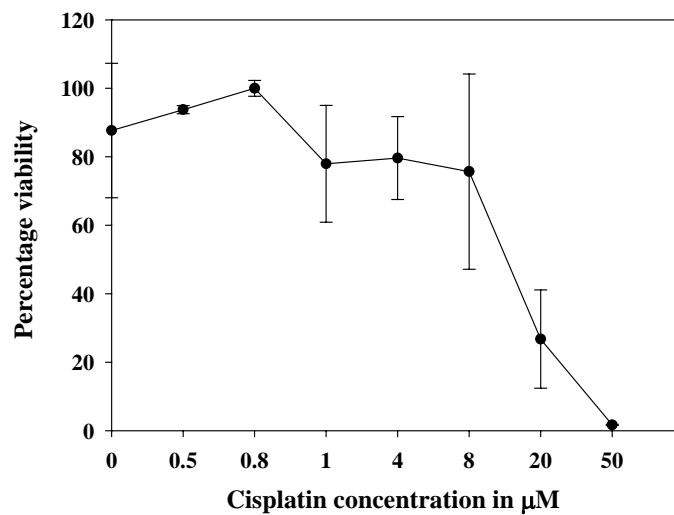
SK-Mel-28 cells exposed to various concentrations of Au<sub>55</sub> for 24 hours



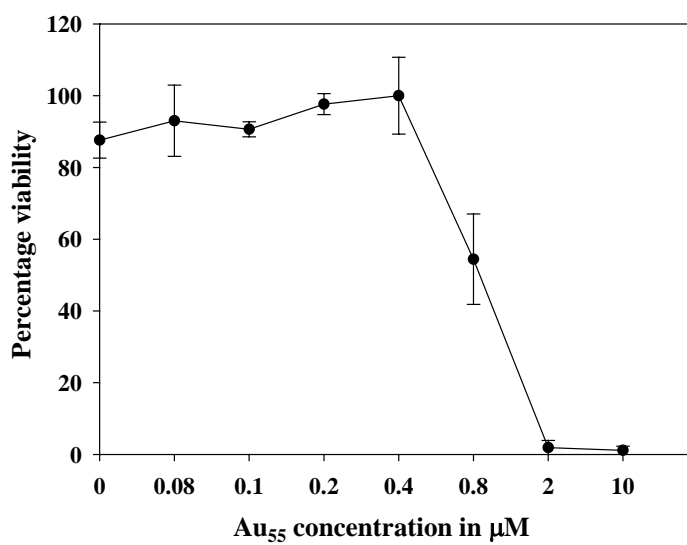
SK-Mel-28 cells exposed to various concentrations of Au<sub>55</sub> for 72 hours



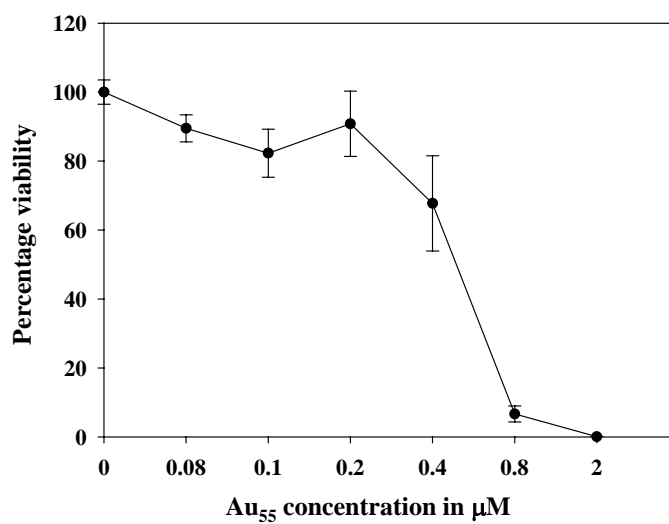
SK-Mel-28 cells exposed to various concentrations of cisplatin for 72 hours



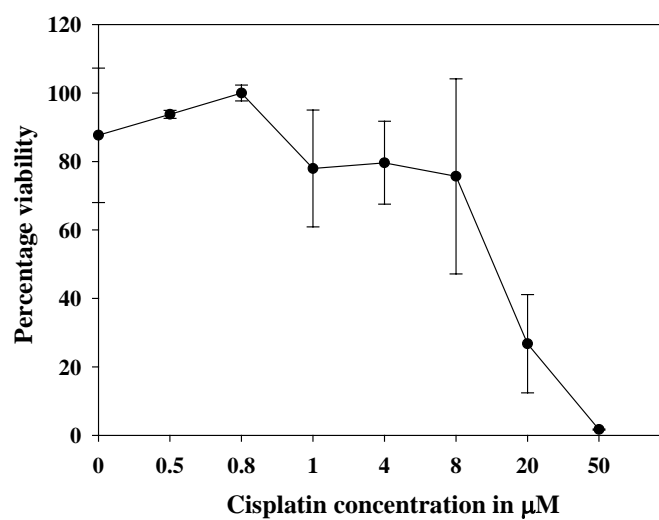
SK-ES-1 cells exposed to various concentrations of Au<sub>55</sub> for 24 hours



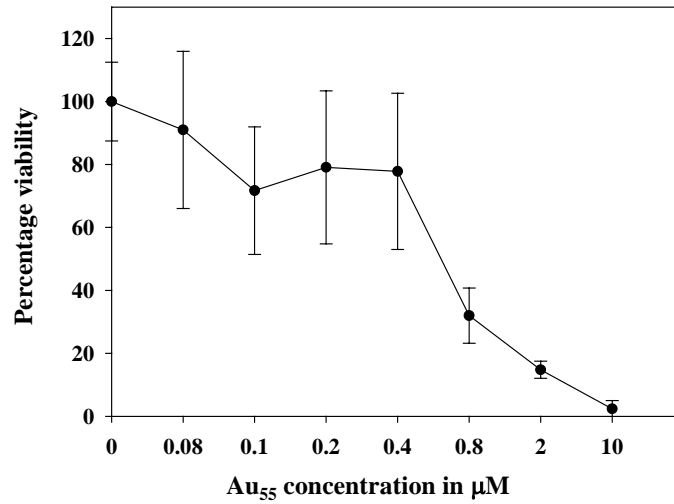
SK-ES-1 cells exposed to various concentrations of Au<sub>55</sub> for 72 hours



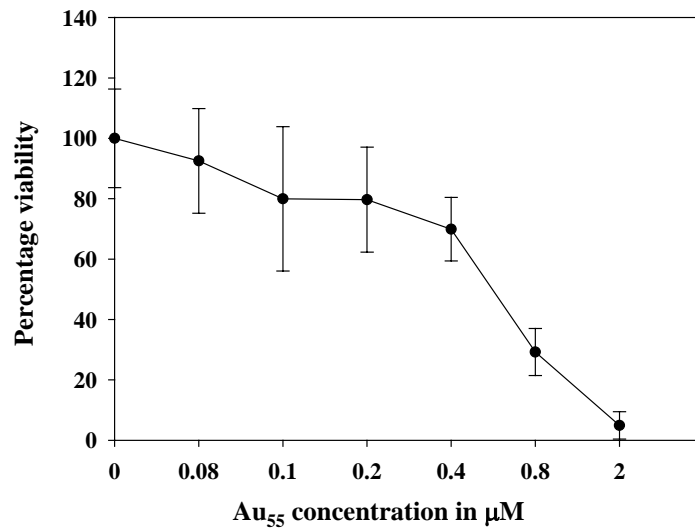
SK-ES-1 cells exposed to various concentrations of cisplatin for 72 hours



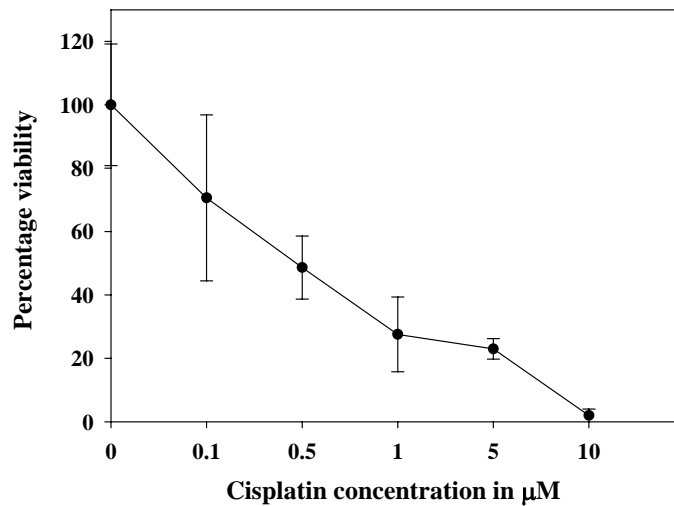
CCD-919Sk cells exposed to various concentrations of Au<sub>55</sub> for 24 hours



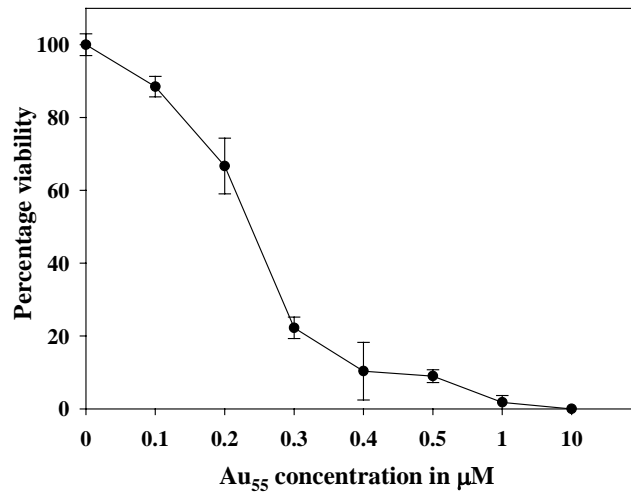
CCD-919Sk cells exposed to various concentrations of Au<sub>55</sub> for 72 hours



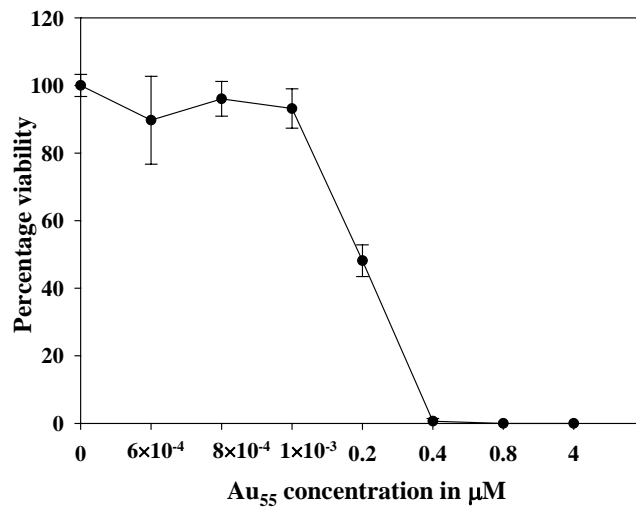
CCD-919Sk cells exposed to various concentrations of cisplatin for 72 hours



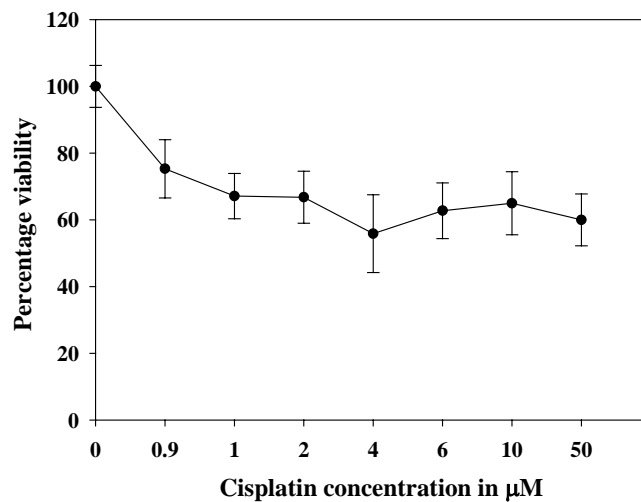
MV3 cells exposed to various concentrations of Au<sub>55</sub> for 24 hours



MV3 cells exposed to various concentrations of Au<sub>55</sub> for 72 hours

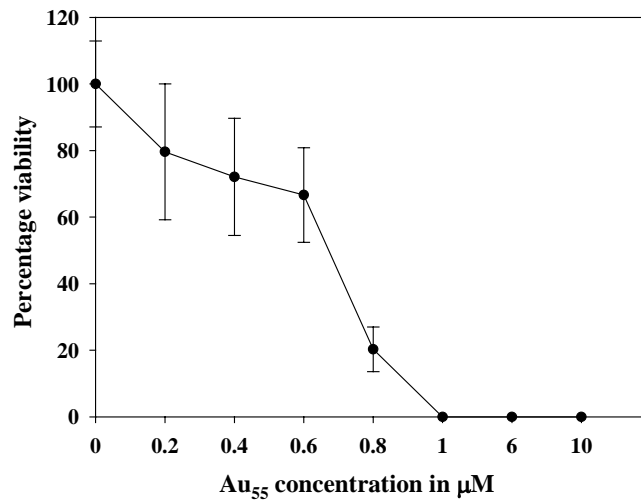


MV3 cells exposed to various concentrations of cisplatin for 72 hour

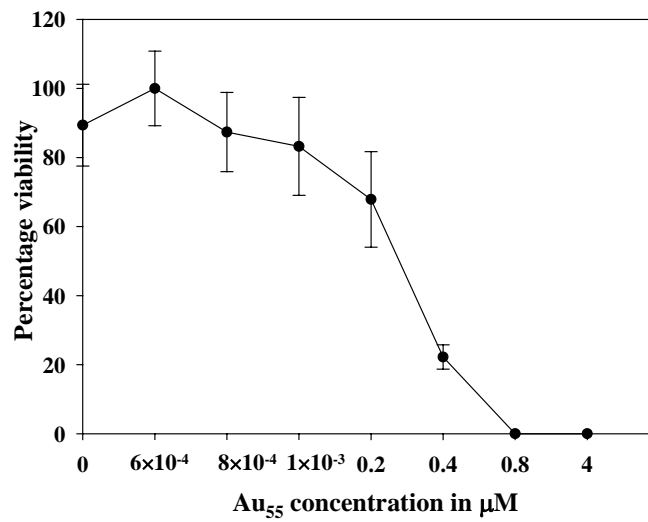




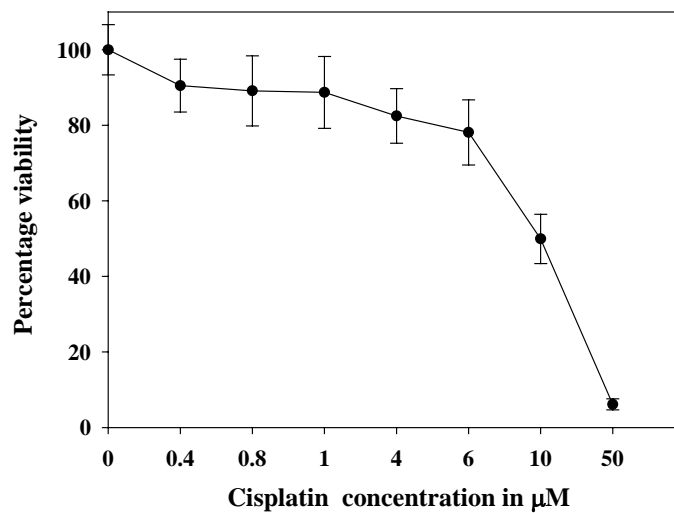
U-2OS cells exposed to various concentrations of Au<sub>55</sub> for 24 hours



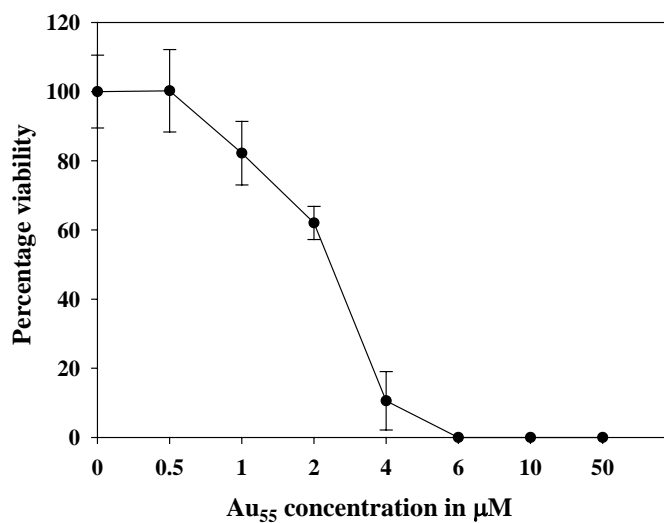
U-2OS cells exposed to various concentrations of Au<sub>55</sub> for 72 hours



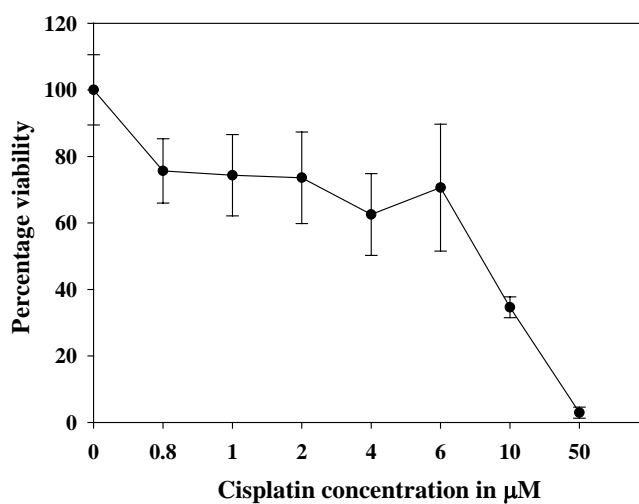
U-2OS cells exposed to various concentrations of cisplatin for 72 hours



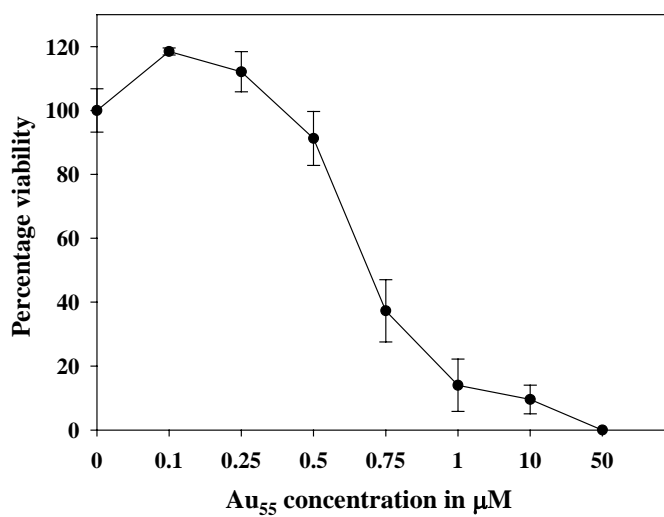
HeLa cells exposed to various concentrations of Au<sub>55</sub> for 24 h.



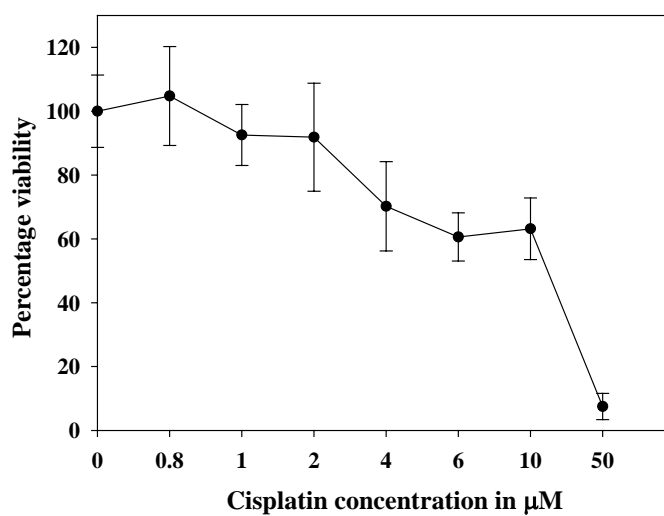
HeLa cells exposed to various concentrations of cisplatin for 72 h.



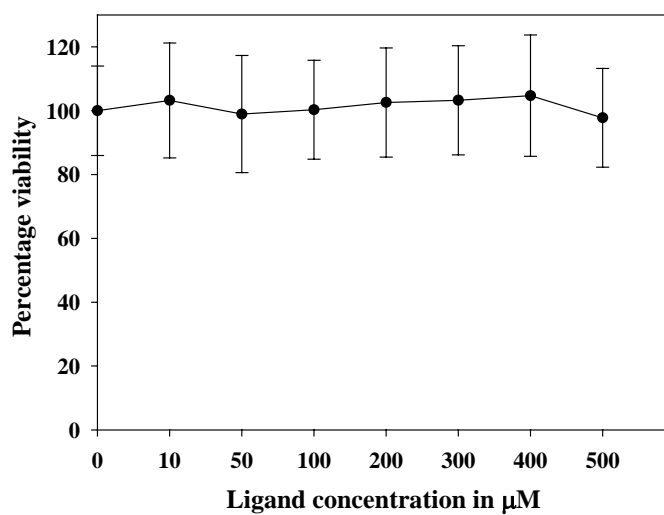
Hek-12 cells exposed to various concentrations of Au<sub>55</sub> for 24 h.



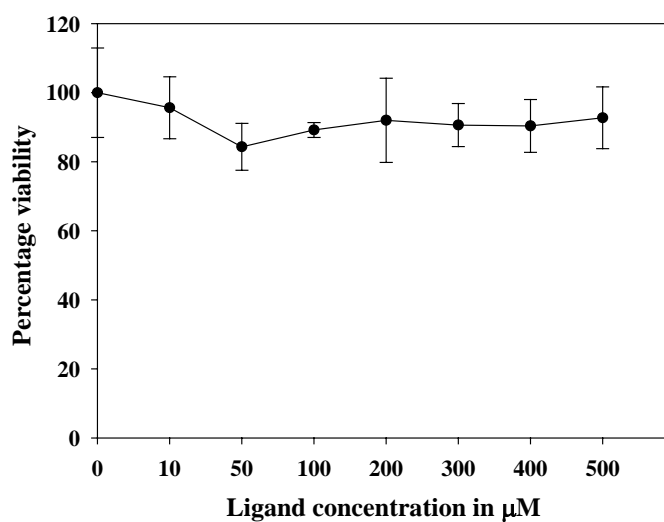
Hek-12 cells exposed to various concentrations of cisplatin for 72 h



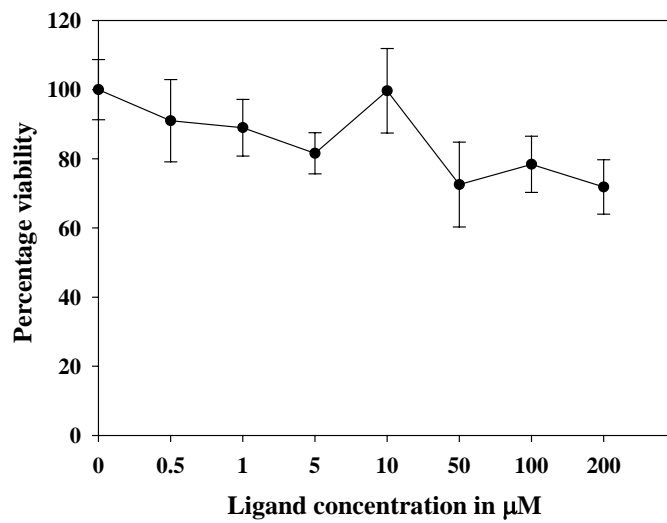
BLM cells exposed to various concentrations of ligand for 24 hours



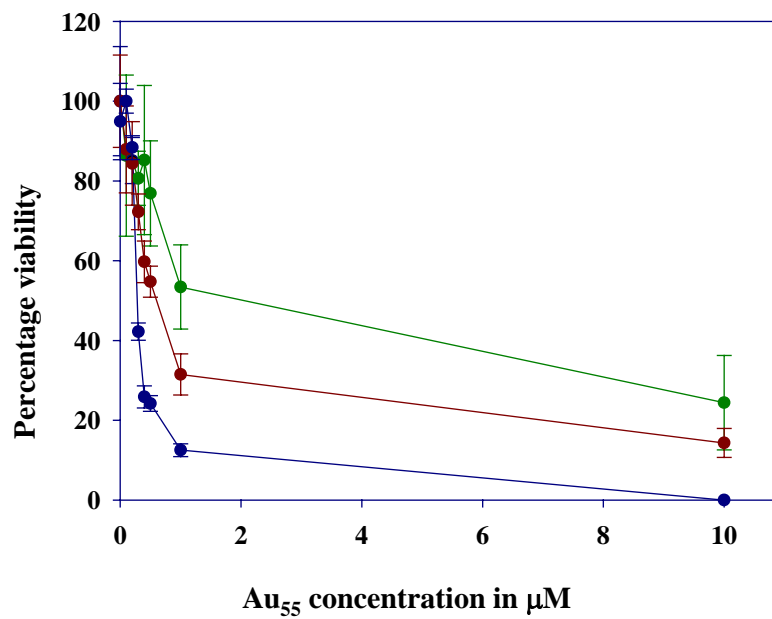
MC3T3-E1 cells exposed to various concentrations of ligand for 24 h.



MOR/CPR cells exposed to various concentrations of ligand for 24 h.

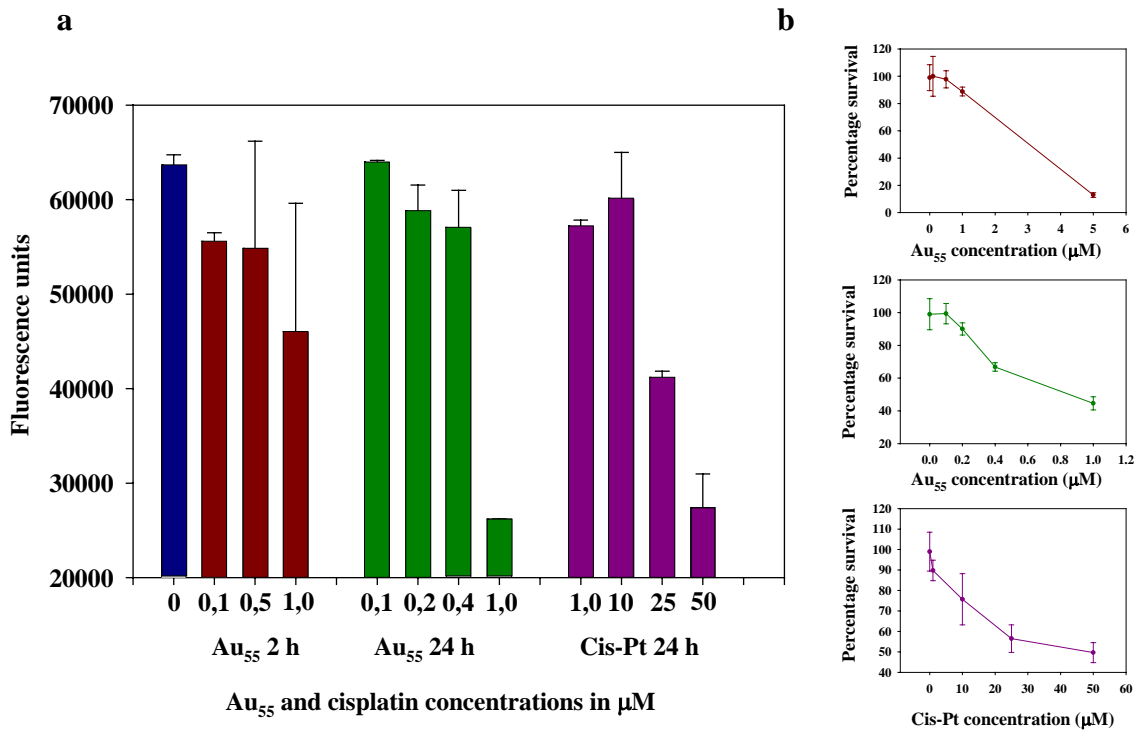


In vitro cytotoxicity assay performed in BLM cells exposed to various concentrations of  $\text{Au}_{55}$  in 10 % FCS (blue) 20 % FCS (green) and 30  $\mu\text{g}/\text{mL}$  albumin (red).

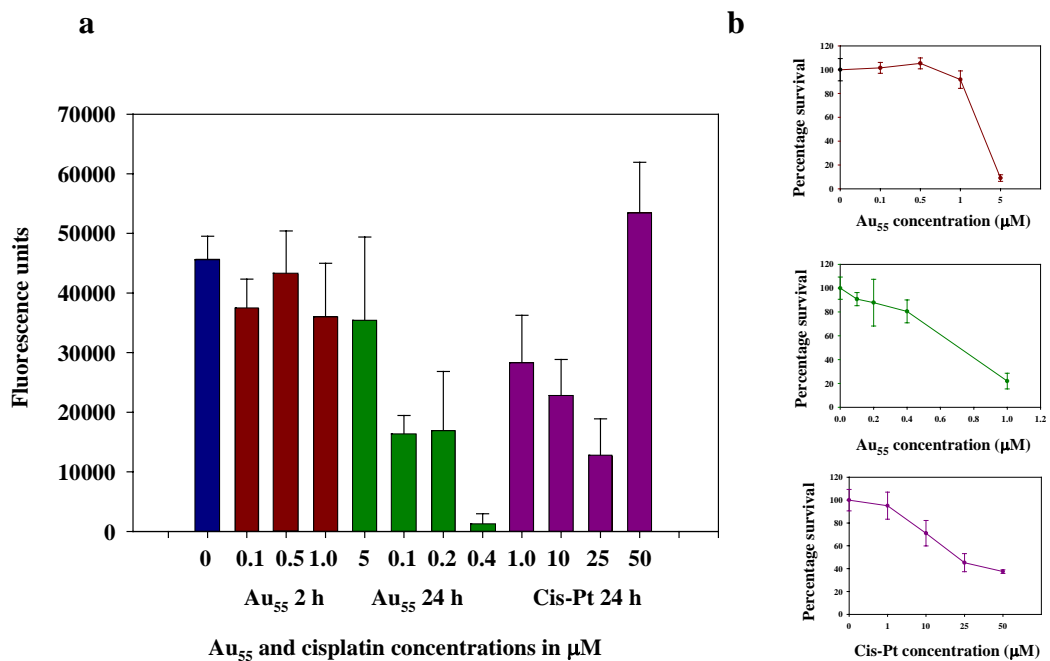


## 10.2 Caspase 3/7 assays

Caspase 3/7 assay (a) and respective (b) MTT assay for the healthy cell line MC3T3-E1 incubated for different periods in the presence of various concentrations of Au<sub>55</sub> clusters and cisplatin.

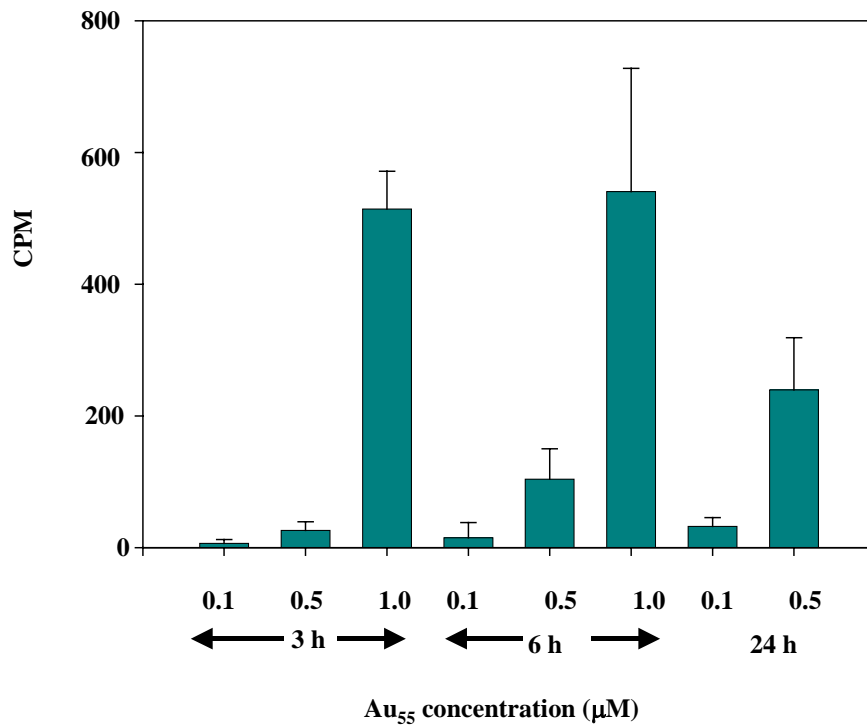


Caspase 3/7 assay (a) and respective (b) MTT assay for the melanoma cell line SK-Mel-28 incubated for different periods in the presence of various concentrations of Au<sub>55</sub> clusters and cisplatin.

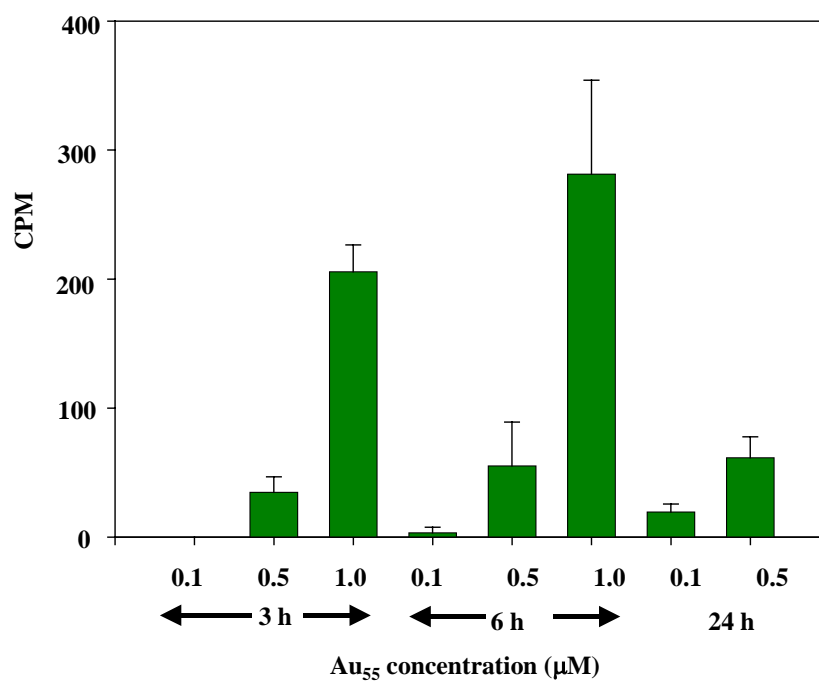


### 10.3 Additional results obtained from cellular fractionation experiments

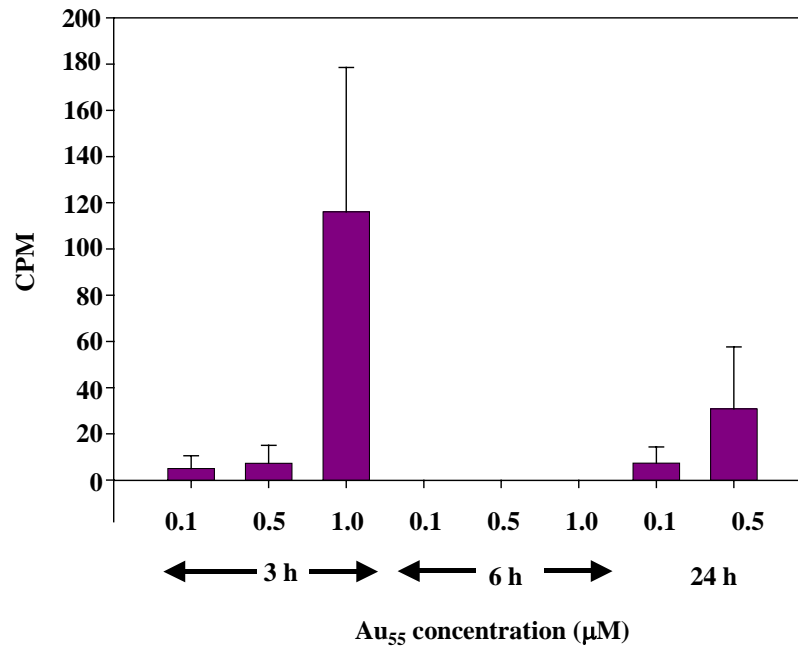
Extracts containing cytoplasmic and nuclear membrane proteins. These extracts are obtained after the first washing step with 50 mM NaCl.



Extracts obtained from the treatment of the nuclear pellet with Buffer S04. Buffer S04 was used to remove any nuclear proteins from the DNA.

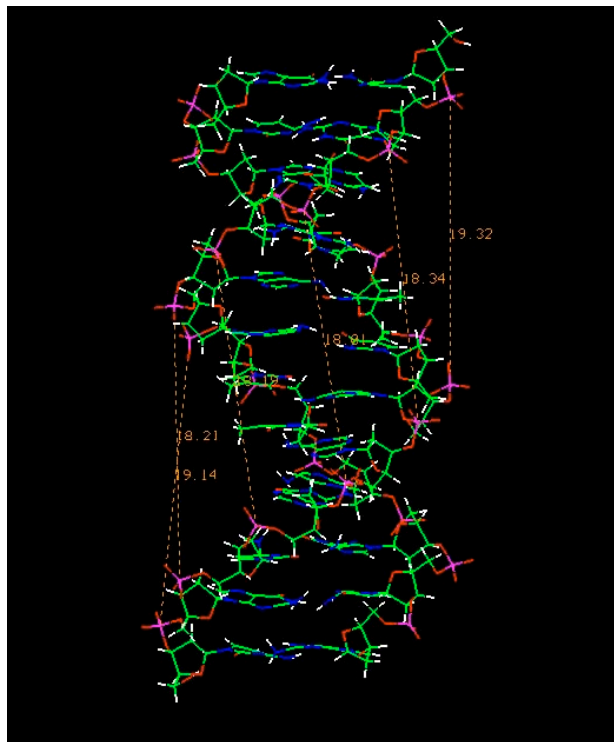


Extracts obtained from the treatment of the nuclear pellet with Buffer S08. Buffer S08 was used to remove from the nuclear pellet any nuclear proteins such as histones from the genomic DNA. It should be noted that for the treatment of the BLM cells with radioactive  $Au_{55}$  for 6 h the DNA pellet was not treated with the buffer S08.



### 11.4 Additional molecular modelling structures

B-DNA structure with distances between almost perpendicularly opposite phosphates indicated in orange color and in Å.





# 11 Curriculum Vitae

---

<b>Name</b>	Maria Tsoli
<b>Contact Details</b>	Meistersingerstr 48b, D-45307, Essen-Kray, Germany
<b>Date of Birth</b>	13-12-1975
<b>Nationality</b>	Greek

## Academic Degrees

- 2001-2004: **PhD**  
**Department of Inorganic Chemistry, University of Duisburg-Essen**  
**Essen, Germany**  
Thesis Title: Molecular modelling and experimental studies of the interactions between biomolecules and inorganic nanostructured materials.  
Supervisor: Prof. Dr. Günther Schmid. Professor of Inorganic Chemistry
- 1992-1999: **Bachelor of Science, Microbiology Honours Class 1**  
**Department of Microbiology & Immunology,**  
**The University of New South Wales, Sydney, Australia**  
Honours Title: Signal responsive of C-starvation genes of *Vibrio angustum* S14.  
Supervisor: Prof. Dr. Steffan Kjelleberg, Professor of Microbiology

## Previous Research Positions

- 2000: • Department of Microbiology, University of Bochum, Germany  
Short Project: Directed evolution of aldolases.  
Supervisor: Prof. Dr. Karl-Erich Jäger Professor of Microbiology
- 1996: • Department of Microbiology, The University of New South Wales  
Short Project: Site-directed mutagenesis of elongation factor -2 (EF-2) of *Escherischia coli*.  
Supervisor: Dr. Paul March, Senior Lecturer.

## Refereed Publications

- Liu Y., Meyer-Zaika W., Franzka S., Schmid G., Tsoli M. & H., Kuhn**, Gold cluster degradation by transition of B-DNA into A-DNA and formation of nanowires, 2003, *Angewandte Chemie*, **42**: 2853-2857.
- Tsoli M., Kuhn H. & G. Schmid**, Molecular docking simulations of the interactions between DNA molecules and a gold cluster. *Proceedings of the Materials Research Society Fall Meeting*, Boston 2003.

**Tsoli M., Kuhn H. & G. Schmid**, Molecular modelling simulations of the interactions between albumin and gold nanocluster Au<sub>55</sub>. Submitted to *Journal of Computational and Theoretical Nanoscience*.

**Tsoli M., Kuhn H., Schmid G., Brandau W., & H. Esche**, Gold clusters: a new anticancer compound, In preparation.

### **Presentations and Posters**

- *Molecular docking simulations of the interactions between biomolecules and a Au<sub>55</sub> cluster*. Poster presented at Materials Research Society Fall Meeting, December 2003, Boston, USA.
- *Gold clusters a potential anticancer drug*. Poster presented at the 11<sup>th</sup> International Conference on Platinum Coordination Compounds, October 2003, New York, USA.
- *Molecular docking studies of the interactions between dystrophin and  $\beta$ -dystroglycan peptides*. Presentation at the 17. Darmstädter Molecular Modelling Workshop, May 2003, Erlangen Germany.
- *Molecular modelling studies of the interactions between dystrophin and  $\beta$ -dystroglycan*. Poster presented at the Biomaterials: Fundamentals and Clinical Applications Conference, October 2002, Essen, Germany.
- *Molecular modelling studies of the interactions between DNA and gold clusters*. Poster presented at the 6<sup>th</sup> World Congress of Theoretically Oriented Chemists (WATOC 2002), August 2002, Lugano, Switzerland.

### **Conferences, Exhibitions and Workshops Attended**

- Materials Research Society Fall Meeting 2003, December 2003, Boston, USA.
- 11<sup>th</sup> International Conference on Platinum Coordination Compounds, October 2003, New York, USA.
- 17<sup>th</sup> Darmstädter Molecular Modelling Workshop, May 2003, Erlangen Germany.
- 27<sup>th</sup> International exhibition congress on chemical engineering, environmental protection and biotechnology (ACHEMA 2003), May 2003, Frankfurt am Main, Germany.
- NanoMed 2003, February 2003, Berlin, Germany
- Interdisciplinary Materials Science Seminars, January 2003, Geldern Germany.
- Biomaterials: Fundamentals and Clinical Applications Conference, October 2002, Essen, Germany.
- Interdisciplinary workshop: Organometallics in the Environment, October, 2002, Essen, Germany.
- International Congress of Mycology, International Congress of Virology, International Congress of Bacteriology and Applied Microbiology (IUMS 2002), July-August 2002, Paris, France.
- 6<sup>th</sup> World Congress of Theoretically Oriented Chemists (WATOC 2002), August 2002, Lugano, Switzerland.
- Interdisciplinary Materials Science Workshop Reactivity at the near surfaces, January 2002, Geldern Germany.

**Prizes and Scholarships**

- 2001-2004: -Deutsche Forschung Gemeinschaft Stiftung  
(DFG Graduate School scholarship)  
WATOC Conference 2002 2<sup>nd</sup> best explanation of poster  
Biomaterials Conference 2002 2<sup>nd</sup> best poster
- 1999: - Australian Postgraduate Award